UNIVERSITY OF CRETE

DOCTORAL THESIS

Effect of the finiteness of the atom number on the superfluid properties of Bose-Einstein condensed gases

Author:
Alexandra Roussou

Supervisors:
Prof. Georgios Kavoulakis [a]
Prof. Nikolaos Efremidis [b]

[a] TECHNOLOGICAL EDUCATION INSTITUTE OF CRETE
[b] UNIVERSITY OF CRETE

A thesis submitted in fulfillment of the requirements for the degree of Doctor of Philosophy

in the

Department of Mathematics and Applied Mathematics

April 3, 2019

Declaration of Authorship

I, Alexandra Roussou, declare that this thesis titled, "Effect of the finiteness of the atom number on the superfluid properties of Bose-Einstein condensed gases" and the work presented in it are my own. I confirm that:

- This work was done wholly or mainly while in candidature for a research degree at this University.
- Where any part of this thesis has previously been submitted for a degree or any other qualification at this University or any other institution, this has been clearly stated.
- Where I have consulted the published work of others, this is always clearly attributed.
- Where I have quoted from the work of others, the source is always given. With the exception of such quotations, this thesis is entirely my own work.
- I have acknowledged all main sources of help.
- Where the thesis is based on work done by myself jointly with others, I have made clear exactly what was done by others and what I have contributed myself.

Signed:

Date:

COMMITTEE

Prof.	Georgios Kavoulakis	-	TECHNOLOGICAL EDUCATION INSTITUTE OF CRETE
Prof.	Nikolaos Efremidis	-	UNIVERSITY OF CRETE
Prof.	Wolf von Klitzing	-	INSTITUTE OF ELECTRONIC STRUCTURE AND LASER (IESL) FOUNDATION OF RESEARCH AND THECHNOLOGY (FORTH)

UNIVERSITY OF CRETE

Abstract

Department of Mathematics and Applied Mathematics

Doctor of Philosophy

Effect of the finiteness of the atom number on the superfluid properties of Bose-Einstein condensed gases

by Alexandra Roussou

In the present thesis I have studied problems which are related to the behaviour of bosonic atoms at zero temperature and as a result they are Bose-Einstein condensed. Quite generally my thesis explores some of the effects which belong to the collection of phenomena that constitute "superfluidity".

In all my projects I have assumed one-dimensional motion of the atoms, and I have also imposed periodic boundary conditions, which is suitable for a ring potential. A substantial part of my thesis focuses on the corrections due to the finiteness of the atom number. These corrections come from correlations which show up beyond the mean-field approximation. The derived results are based mostly on the method of diagonalization of the many-body Hamiltonian, while I have also used the mean-field approximation.

The novelty of my results relies on the combined effect of one-dimensional motion, the imposed periodic boundary conditions, and the small atom numbers that I considered. As shown below, all of these give rise to effects which have not been investigated so far.

The experimental motivation for my studies comes from numerous experiments which have created and observed persistent currents in atomic Bose-Einstein condensates in topologically-nontrivial traps, i.e., annular and toroidal. In addition, the advances in atom detection has allowed experimentalists to lower the number of atoms and even work with just a few of them.

In the first project of my thesis I investigated two questions. The first was the phenomenon of hysteresis, i.e., the hysteresis loop and the corresponding critical frequencies. The second question was the critical coupling for stability of persistent currents, paying particular attention to the effect of the finiteness of the atom number on it.

In the second project of my thesis I studied the effect of the finiteness of the atom number on the solitary-wave solutions, going beyond the mean-field approximation. To attack this problem, I developed a general strategy, and considered a linear superposition of the eigenstates of the many-body Hamiltonian, with amplitudes that I extracted from the mean field approximation. The resulting many-body state has all the desired features and is lower in energy than the corresponding mean-field state.

In the third project I studied the rotational properties of a two-component Bose-Einstein condensed gas of distinguishable atoms. I demonstrated that the angular momentum may be given to the system either via single-particle, or “collective" excitation. Finally, despite the complexity of this problem, under rather typical conditions the excitation spectrum has a remarkably simple and regular form.

Acknowledgements

Firstly and mainly, I would like to express my sincere gratitude to my supervisor Prof. Georgios Kavoulakis for the continuous support of my Ph.D study and related research, for his patience, motivation, and immense knowledge. His guidance helped me all the time of research and writing of this thesis. I could not have imagined having a better advisor and mentor for my Ph.D study. To me, he consists an icon figure of how a person should be and I keep him in my mind as an example. Therefore, a "thank you" is not enough in this case.

Together with my supervisor, Prof. Nikolaos Efremidis is the one to whom I owe great part of my Ph.D, since he was the supervisor who continuously provided me with valuable feedback and supported me in every step of my studies. Our discussions, together with Prof. Georgios Kavoulakis, always motivated me to view my research from various perspectives.

Furthermore I would like to express my gratitude to Prof. Wolf von Klitzing and his laboratory members for their insightful comments and encouragement, but also for the oppurtunity to interact with them and for making me feel like being a part of their wonderful team.

My sincere thanks also go to Prof. Manolis Magiropoulos, and Prof. Giannis Smyrnakis, who were always willing to check the validity of our studies and gave me insight to work more, search in different directions, compare among various research areas. I am more than pleased to consider them as my research team, since without their arguments and precious support it would be incomparably harder to conduct this research.

I would like to thank my friends, Dr. Joniald Shena for the stimulating discussions and Mr. Stergios Kyanidis for the gradual support even without his natural presence. My special thanks goes to my brother, friend and roomate, Dr. Tsatrafyllis Nikos for all the sleepless nights that we shared our anxiety and all the fun we have had in the last four years. I am also grateful to Mr. Mastorakis Yannis for enlightening me with his remarkable programming skills in the first project of my research.

Last but not least, I would like to thank my family: my mother, in whom I owe the most, since without her I couldn't stay in Heraklion and work in science. All of her efforts and personal achievements is her great way to help me find who I am and keep me inspired in life. My sister for supporting me spiritually throughout writing this thesis and my life in general. My uncle together with my aunt and cousin are the three members of my family that are always there for me, no matter the distance that separates us, no matter the time passed. Thank you all for your love and patience!

Contents

Dedicated to my (grand)mother, who made me who I am.

Chapter 1

Introduction

1.1 General overview

Boiling and freezing water are perhaps the most well-known examples of a phase transition. The investigation of the phases of matter, as well as the transitions between them is a very interesting question which has been studied within many diverse fields of physics.

The problems I study in my thesis are all related with the phenomenon of "Bose-Einstein condensation". In 1924, Einstein [1], extending Bose's work on photons [2] argued that in a gas of massive bosonic particles there is a phase transition to a "Bose-Einstein condensed" state, Fig. (1.1). While in the normal phase the average occupancy of all single-particle states of the system are of order unity, in the condensed phase there is a *macroscopic* occupancy of a single-particle state of the system. As a result, quantum, microscopic, effects show up on a macroscopic scale, which give rise to fascinating phenomena [3, 4, 5, 6].

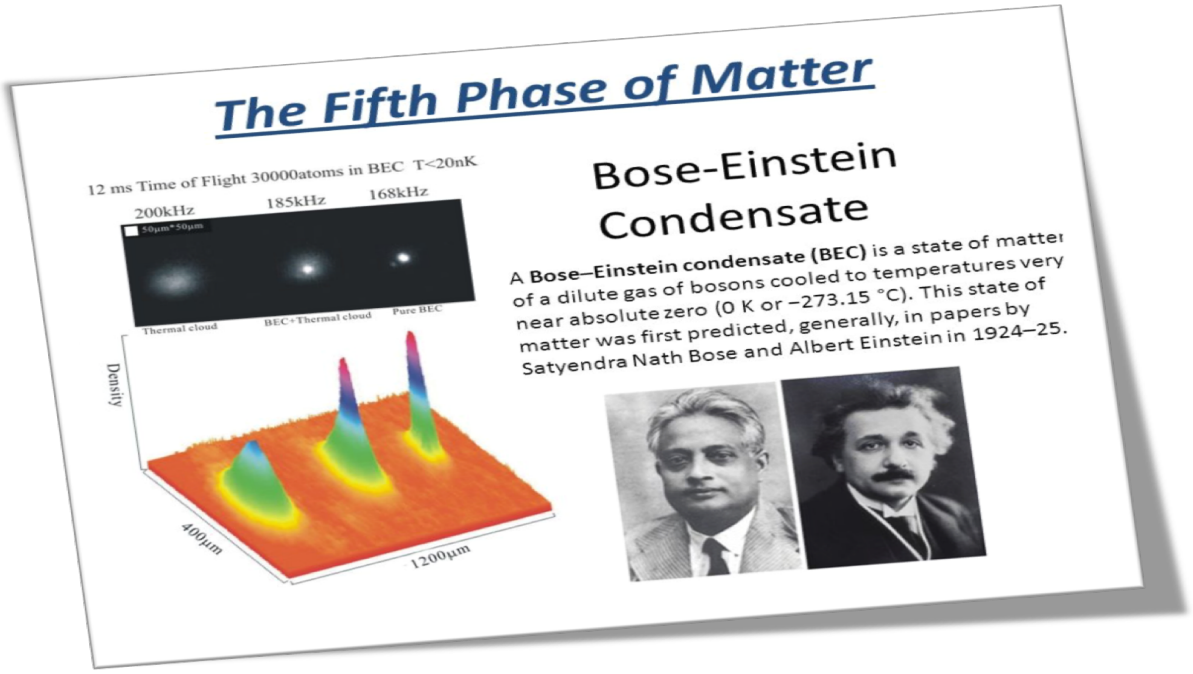

FIGURE 1.1: Satyendra Bose and Albert Einstein, the two pioneers in the phenomenon of condensation [7].

More generally, the class of problems that I have studied in my thesis go back to 1908, when Helium was liquified by Heike Kamerlingh Onnes [8] (which occurs at a temperature of around 2.17 K). In 1937 this, in turn, led Kapitza [9] and (independently) Allen and Misener [10] to the observation of the fascinating properties which nowadays constitute the collection of phenomena that we call "superfluidity" [11], i.e., peculiar rotational properties – vortex states, reduced moment of inertia – persistent currents, transport properties, collective effects (e.g., first and second sound), the Hess-Fairbank effect, the Josephson effect, etc. Actually, F. London [12] was the first one who argued in 1938 about the connection between the superfluidity of liquid Helium and Bose-Einstein condensation.

Another closely-related problem is "superconductivity" [13], which was also discovered by Heike Kamerlingh Onnes in 1911 [14] due to the very low temperatures that he had achieved 3 years earlier with liquid Helium. More specifically, in 1911 Onnes observed that the resistivity of mercury drops to zero below some critical temperature.

Ever since scientists have been studying the properties of superconducting materials, even up to now. Actually, a more recent breakthrough in this field took place in 1986, when high-temperature superconductivity was discovered [15]. In addition to the persistent currents that arise due to the drop of resistivity, other effects have also been discovered in superconductors, including the Meissner effect, the Josephson effect, etc.

Closely-related physical systems where superfluidity and superconductivity take place include Helium III, atomic nuclei, neutron stars, positronium atoms, photons in cavities, excitons in semiconductors, exciton polaritons, etc. [16, 17, 18, 19, 20, 21]. Other fascinating, quantum phenomena, which have been observed more recently and require low temperatures include the quantum Hall effect [22], the Kosterlitz-Thouless transition [23, 24], etc.

1.2 The general field of the present thesis – cold atomic gases

The field of my own thesis is that of cold atomic gases. This field is closely linked to the areas of superfluidity and superconductivity. On the other hand, it also has some serious differences compared with the "traditional" superfluids/superconductors, and, more importantly, it stands on its own.

This field really started to develop in 1995 when the first Bose-Einstein condensates in atomic vapors Fig. (1.2) were realized experimentally [25, 26, 27]. Remarkably, Eric Cornell with Carl Wieman, and Wolfgang Ketterle were awarded the Nobel prize in Physics in 2001 [25, 26, 28] for this achievement.

A few years earlier the combination of evaporative cooling with laser cooling had allowed us to achieve ultra-low temperatures. Equally important were the advances in trapping atoms. Combination of these techniques was necessary for the creation of a confined and sufficiently cold gas of atoms. These developments had given Steven Chu, Claude Cohen-Tannoudji, and William D. Phillips the Nobel prize in Physics a few years earlier, in 1997 [29, 30, 31, 32].

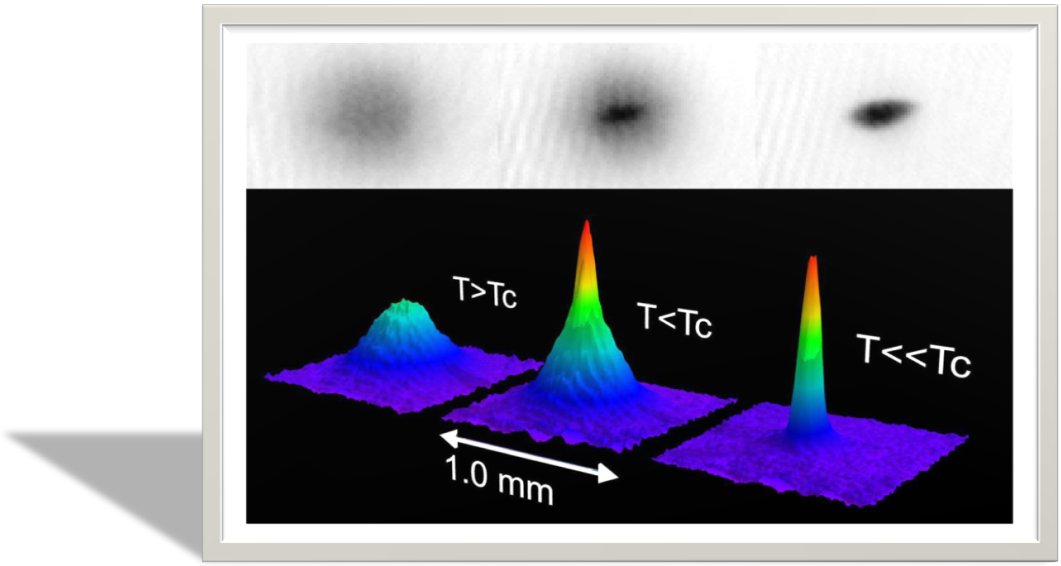

FIGURE 1.2: The experimental realization of Bose-Einstein condensation in an atomic vapour, from the group of W. Ketterle [26].

By now, after more that 20 years, this field has given rise to the observation of an impressive collection of phenomena. It is remarkable that it brings together various diverse fields of physics, including condensed-matter, atomic and molecular, nonlinear and nuclear physics, statistical mechanics, particle physics, quantum optics, quantum information, etc.

1.3 Some general remarks on cold atomic systems and some characteristic scales

Two characteristic length scales which enter this problem are the inter-particle spacing and the de-Broglie wavelength. Under typical conditions the de-Broglie wavelength is much smaller than the inter-particle spacing. In this case the atoms behave as classical particles, obeying Maxwell-Boltzmann statistics. Under sufficiently low temperatures and/or high densities these two length scales become comparable to each other, in which case interesting, quantum effects, show up.

Under these conditions, one has to distinguish between two cases. If the atoms are bosons – i.e., if their total spin is integer – they obey Bose-Einstein statistics, while if they are fermions – i.e., if their total spin is half integer – they obey Fermi-Dirac statistics, Fig. (1.3).

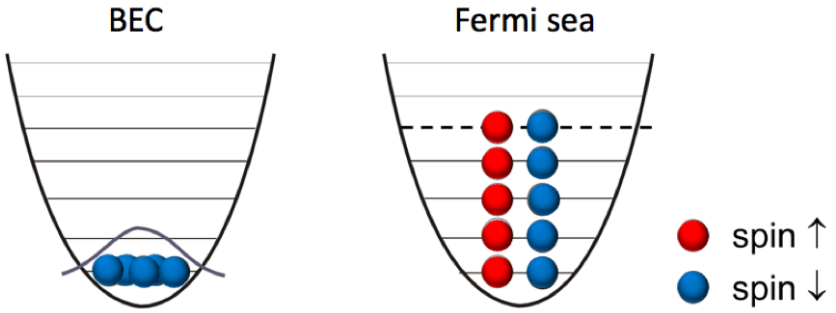

FIGURE 1.3: Occupancy of the single-particle energy levels of a harmonic potential at zero temperature, for bosonic (left) and fermionic (right) particles (with spin 1/2), due to their different statistics.

A serious problem that one has to overcome is the solidification of the atoms. This may be prevented by lowering the density, which suppresses three-body collisions. In order to reach the quantum regime this requires going to even lower temperatures. This has become possible with the combination of the laser and evaporative cooling techniques mentioned above.

Under typical conditions, the atom number is around 10^5 (varying between a few thousands, to a few million), the typical spatial dimensions of the clouds (in harmonic traps, where most of the experiments have been performed up to now) is 10 μm, the typical densities are 10^{14} cm^{-3}, while the typical temperatures are around 100 nK. In addition, the typical lifetime of these gases is on the order of a few minutes.

The zero-temperature limit of these systems thus leads to the formation of either a Bose-Einstein condensate in the case of bosonic atoms, or a Fermi sphere in the case of fermionic atoms (with the interesting possibility of pairing between the fermionic atoms, very much like the BCS pairing in superconductors).

In the Bose-Einstein condensed phase there is a macroscopic number of bosonic atoms occupying a single-particle state of the system. In more precise terms, there is at least one eigenvalue of the single-particle density matrix which is of order of the total number of particles in the system, N.

A major advantage of the atomic gases is that – contrary to both liquid Helium, which is a strongly interacting liquid, as well as superconductors, which are solids – under typical conditions they are dilute (roughly 10^5 times more dilute than air), in the sense that the inter-particle spacing is much larger than the scattering length for zero-energy atom-atom collisions (as a result, the critical transition temperature is roughly 10^7 times smaller than that of liquid Helium.) Furthermore, they can be manipulated easily, they have very low thermal velocities (as low as mm/sec), they have an adjustable coupling constant and an adjustable effective dimensionality, and even the functional form of the atom-atom interaction can be controlled.

As a result, cold and trapped atoms provide an ideal laboratory for confirming basic principles of physics and also for studying experimentally and theoretically a wide variety of problems including coherence, quantum phase transitions, nonlinear effects, superfluidity and quantized vortex states, many-body effects, etc.

1.4 Novel effects investigated in this thesis: Going beyond the mean-field approximation

The field of cold atoms has been expanding with an impressive rate, especially after 1995 (when, as mentioned above, the first atomic Bose-Einstein condensates were achieved experimentally) [25, 26, 27]. The main goals of the initial experiments, as well as of the corresponding theoretical studies, were to confirm some fundamental effects on superfluidity and superconductivity. One of the main and interesting aspects of these systems is the spatial confinement. As a result, while most studies which had been performed until then had investigated homogeneous systems, the confinement introduced novel effects.

More recently this field has followed various different directions. One direction is when the atom number N is reduced to the extent that finite-N corrections are important [33]; in this limit atomic systems resemble atomic nuclei. A crucial development that has allowed scientists to perform such experiments is the improvement in the experimental techniques on atom detection. All the three (theoretical) projects that I worked on in this thesis involved Bose-Einstein condensed atoms at zero temperature, with a finite atom number N.

Some of the most interesting and novel aspects of the problems I considered in this thesis include the following.

• The first one is the assumed spatial confinement. All the problems I attacked have the common feature that they assume (quasi-) one dimensional motion under periodic boundary conditions. The corresponding physical model is that of atoms which are confined in a toroidal/annular potential, with the transverse degrees of freedom frozen out due to the assumed tight confinement along this direction. In more simple terms, the atoms were assumed to move in a "ring" potential.

The finiteness of the radius of the ring, combined with the imposed periodic boundary conditions is another interesting and non-trivial effect which played an important role in the problems I considered. More specifically, the two relevant length scales are the circumference of the ring and the coherence length. Typically, in "large" systems, the coherence length is much smaller than the circumference of the ring and the problem reduces to that of an infinite system. Here, however, the two length scales were allowed to be also comparable to each other and thus novel effects showed up.

Finally, the spatial confinement has the effect of a discrete energy spectrum, which also introduces novel effects compared to the traditional "infinite" systems.

• The second novel aspect that is investigated in this thesis is the finiteness of the number of atoms. Typically the atom number is much larger than unity and in this case the mean-field approximation is valid. Actually, the vast majority of theoretical studies of these systems relies on the mean-field approximation. Within this approximation the many-body state is assumed to have a product form, and is remarkably successful because of the diluteness of these systems.

Still, for the problems that I studied this approximation is not as accurate: For the small systems that I considered, there are correlations between the atoms which are not captured by the mean-field approximation. In this case the finite-N corrections

are significant and introduce corrections, which are not captured by the mean-field approximation. A major part of my thesis was to identify such effects.

Since the mean-field approximation is not valid, I used the method of diagonalization of the many-body Hamiltonian, which does not make any assumption about the functional form of the many-body state and in that respect is exact. In addition, I also used the mean-field approximation. Since these two approaches have to converge to the same results for any observable in the appropriate limit of large N, the mean-field approximation provides the asymptotic limit of the solution derived from the numerical diagonalization.

I describe these two approaches in detail below. For the moment I just mention that within the diagonalization approach very often the atom number has to be rather low, because of the correspondingly (very) large dimensionality of the Hamiltonian matrix.

1.5 The three projects which were investigated in my thesis

In my thesis I worked on three different problems, which I describe briefly below.

Paper I: *Hysteresis and metastability of Bose-Einstein-condensed clouds of atoms confined in ring potentials*

In my first project [34] I investigated the rotational response of a Bose-Einstein condensate in a ring potential, focusing on the effects of the finiteness of N. This work was up to a certain extent motivated by an experiment which was performed by G. K. Campbell [35] and her group, which studied the effect of hysteresis in a Bose-Einstein condensate that is trapped in an annular potential and set into rotation.

In this problem I first evaluated the critical frequencies associated with the effect of hysteresis, starting with the mean-field approximation and then using the method of diagonalization. This allowed me to extract the effect of a finite number of atoms on the critical frequencies which are associated with the phenomenon of hysteresis.

Then, from the derived energy spectrum that I evaluated from the diagonalization, I also studied problems associated with the stability of the persistent currents, including the critical coupling for stability of the currents in a system with a small atom number N. I performed a detailed analysis of the effect of a finite N on the critical value of the coupling for stability of the currents.

Finally, introducing a single-particle operator that induces transitions from the current-carrying states to the zero-momentum state, I studied the matrix element which enters the decay mechanisms of these currents and concluded that this decreases very rapidly with increasing atom numbers.

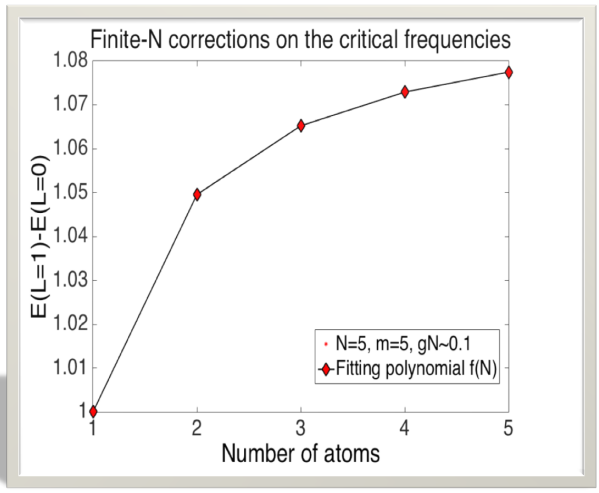
Finite-N corrections on the critical frequencies
E(L=1)-E(L=0)
Number of atoms
N=5, m=5, gN~0.1
Fitting polynomial f(N)

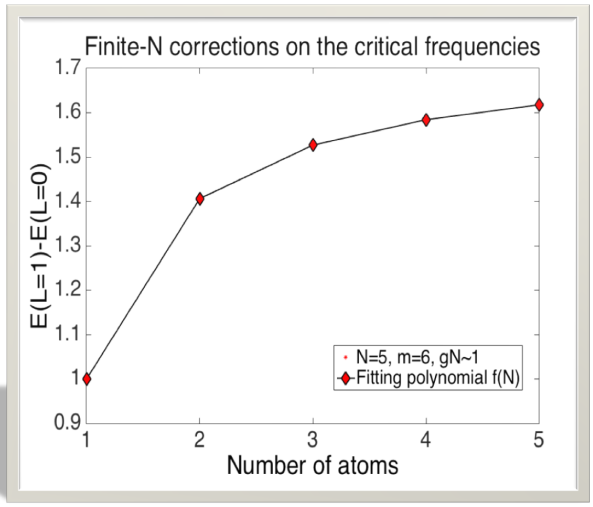
Finite-N corrections on the critical frequencies
E(L=1)-E(L=0)
Number of atoms
N=5, m=6, gN~1
Fitting polynomial f(N)

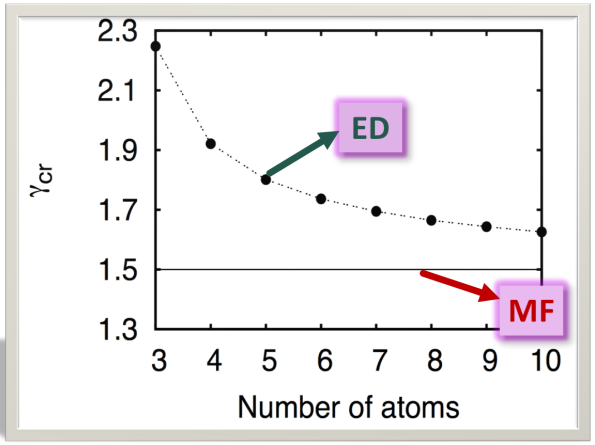
γcr
ED
MF
Number of atoms

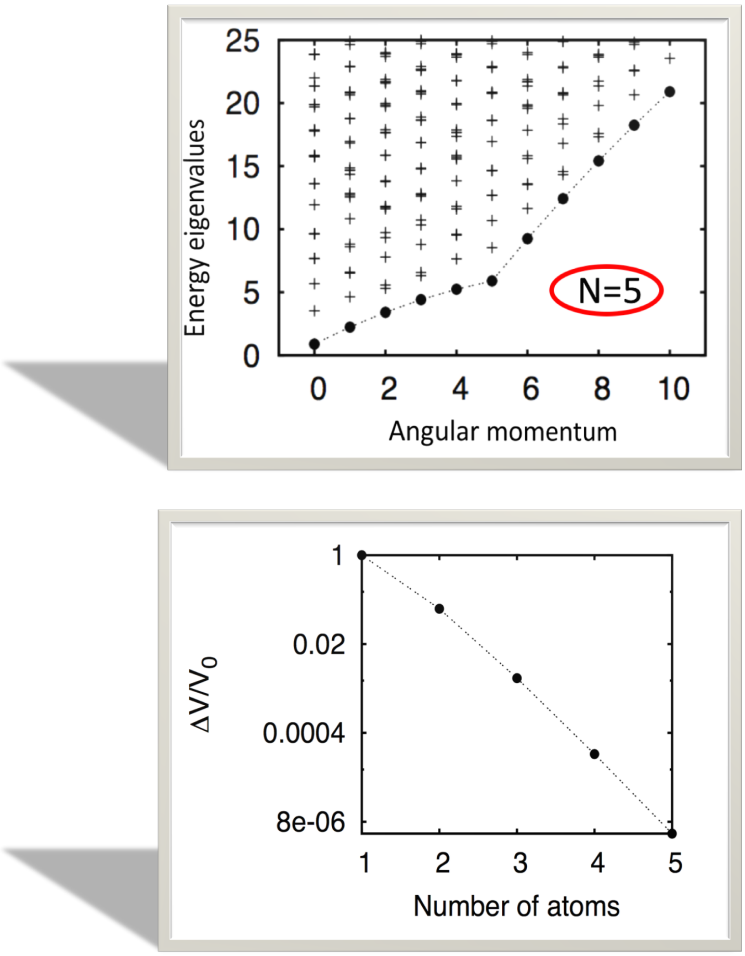

FIGURE 1.4: Some of the main results of Paper I, i.e., of the hysteresis problem.

Paper II: *Rotating Bose-Einstein condensates with a finite number of atoms confined in a ring potential: Spontaneous symmetry breaking beyond the mean-field approximation*

In my second project [36] I studied the limit of solitonic solutions for a finite (and small) number of atoms N. This problem was motivated by numerous experiments which have observed solitary-wave solutions in elongated traps, as well as in toroidal /annular traps.

The basic question that I had in mind was the fact that the solitary-wave solutions result as solutions of the non-linear Gross-Pitaevskii equation [37, 38], which is intimately connected/linked with the mean-field approximation. Still, for the small atom numbers that I considered, the validity of the mean-field approximation is questionable, and thus so is the accuracy/validity of the mean-field solitonic solutions.

To attack this problem, I again started with the diagonalization of the many-body Hamiltonian. I developed a general strategy, considering a linear superposition of the eigenstates of the many-body Hamiltonian, with amplitudes that I extracted from the mean-field approximation.

The derived many-body state that I constructed thus breaks the (assumed axial) symmetry of the Hamiltonian. Interestingly enough, it has the same energy to leading order in N as the mean-field state and the corresponding eigenstate of the Hamiltonian, however, it has a lower energy to subleading order in N. This many-body state thus has a lower energy, and is inherently energetically favorable, with the energy difference being more pronounced in small systems.

A "side" result of this study is that it also provides insight into the question of spontaneous symmetry breaking, since the Hamiltonian is axially symmetric (and so are its eigenvectors), while the mean-field solutions break the axial symmetry of the problem. Finally, it introduces a well-defined strategy which allows us to link the eigenstates of the many-body problem with the mean-field states of broken symmetry.

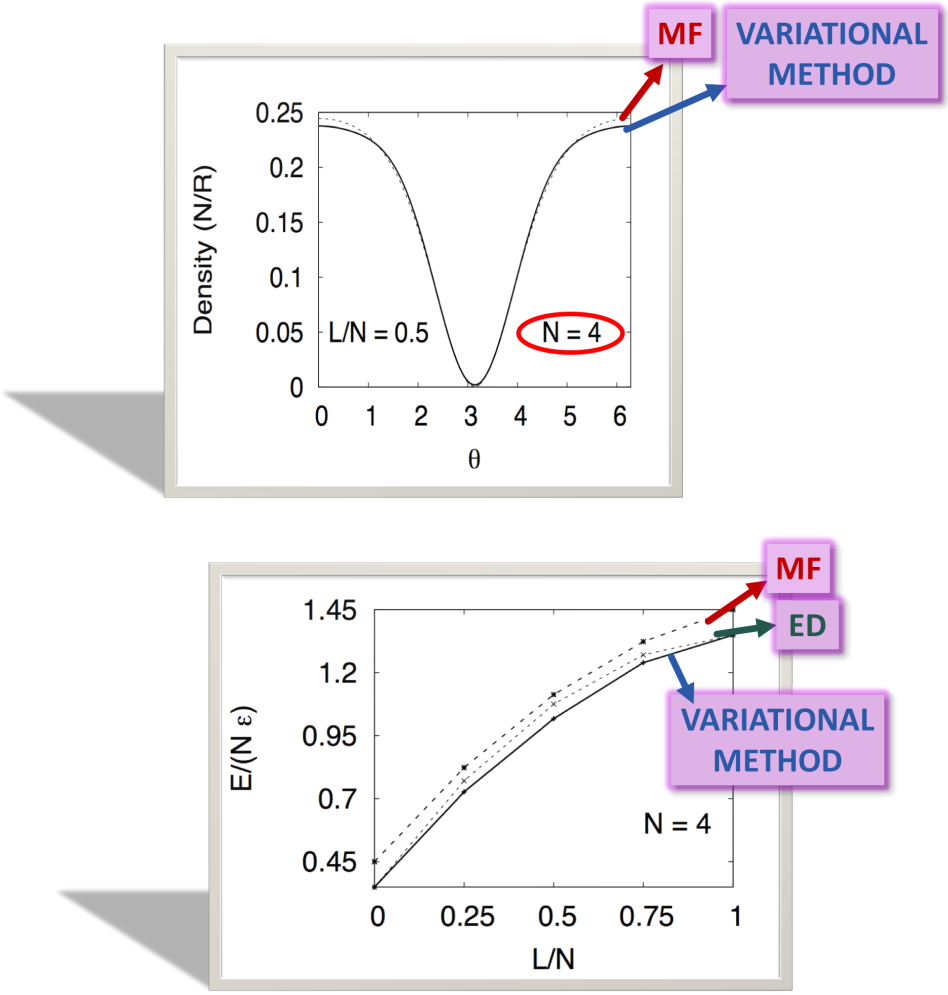

FIGURE 1.5: Some of the main results of Paper II, i.e., of the "quantum soliton" problem.

Paper III: *Excitation spectrum of a mixture of two Bose gases confined in a ring potential with interaction asymmetry*

In my third project [39] I investigated the rotational properties of a two-component Bose-Einstein condensed gas of distinguishable atoms. Again, numerous experiments have studied this question, where the extra degrees of freedom associated with the existence of a second component introduce novel effects.

Considering again a ring potential, with the two species coexisting along the ring (I assumed repulsive interactions), I investigated the rotational properties of this system. More specifically, one of the main questions that I examined is how the angular momentum is distributed between the two components. As I demonstrated, the angular momentum may be given to the system either via single-particle, or "collective" excitation.

When the angular momentum is carried by single-particle excitation, an important conclusion is that under typical conditions it is the minority component that carries the angular momentum for small values of the angular momentum. This fact has serious consequences on the more general structure of the dispersion relation, which takes a remarkably simple and regular form, despite the complexity of this problem. I stress that this regularity goes well beyond the one dictated by the periodic boundary conditions, i.e., by Bloch's theorem.

The angular momentum may also be carried by collective excitation (under certain conditions). Interestingly enough, in this case the corresponding many-body state, which, in addition to the interaction energy minimizes also the kinetic energy, is dictated by elementary number theory. As a result, the spectrum shows a form of "quantum chaos", where changes in the atom number of even one unit may change it dramatically.

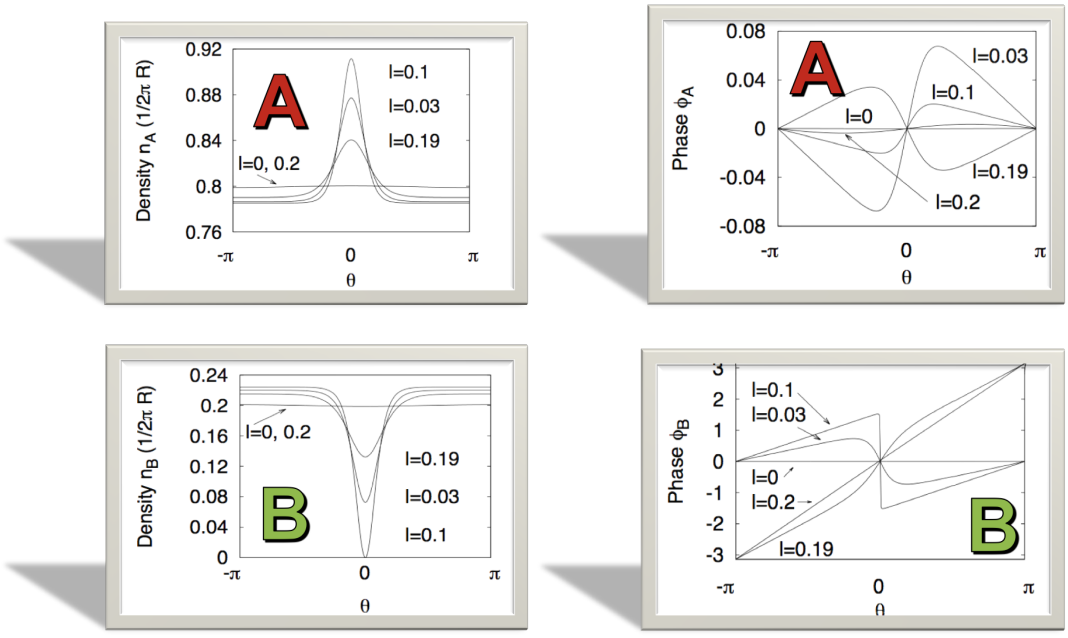

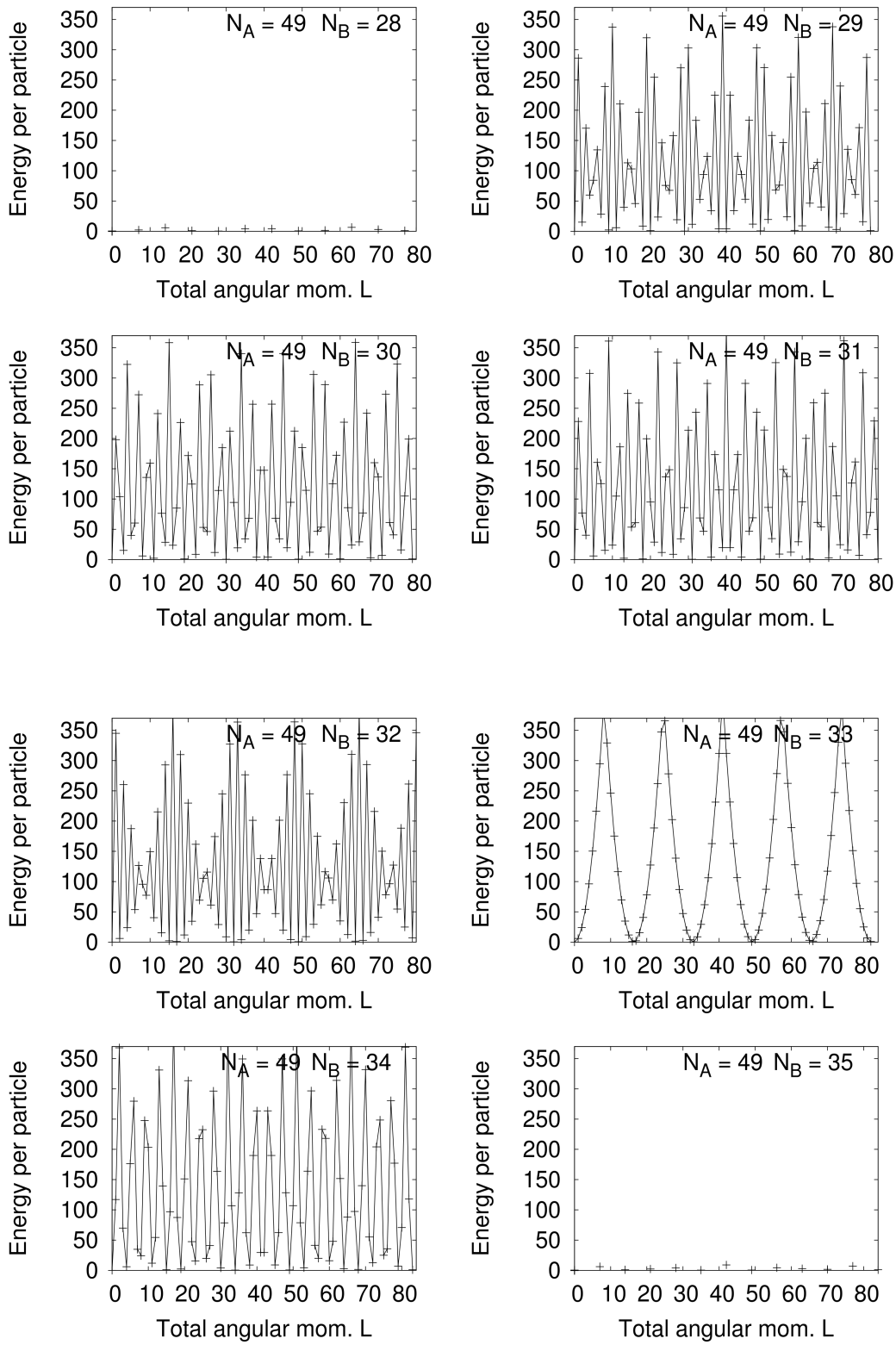

FIGURE 1.6: Some of the main results of Paper III, i.e., of the problem with mixtures.

1.6 Outline of the thesis

In what follows below, I start in Chap. 2 with the theoretical background, where I describe some fundamental concepts and I also describe the theoretical methods/tools I have used in my studies.

I start with the definition of Bose-Einstein condensation via the eigenvalues of the density matrix. I then present briefly the results for the critical temperature of an ideal Bose gas, the effect of the (effective) dimensionality on this phase transition, and the effect of the finiteness in the atom number, as well the presence of a trapping potential. I also present some well-known results for the irrotational nature of the superfluid velocity and the quantization of the circulation.

I then turn to the mean-field approximation, which makes the assumption of a product form for the many-body state and leads to the nonlinear Gross-Pitaevskii equation. I focus on the case of a ring geometry, presenting some results on solitary-wave excitation, Bloch's theorem, and the variational approach. Then I present a toy model, which demonstrates some of the effects that I have studied in my thesis (solitary waves, persistent currents etc). Finally, I give the mean-field equations for a two-component system.

A major part of this section also includes the alternative method that I have used in my thesis, namely the method of diagonalization of the many-body Hamiltonian. Since this is central in my thesis, after describing this approach, I give an explicit example of this method and I also comment on its advantages and disadvantages as compared to the mean-field approximation. Finally, I comment on the comparison between the two methods, and how they link.

In the following three chapters, Chaps. 3, 4, and 5, I turn to the three projects I have worked on within my thesis, namely the hysteresis, the "quantum solitons", and the problem of mixtures.

Finally, in Chap. 6 I give some general conclusions and an overview of my work.

Chapter 2

Relevant theoretical background

In this chapter I present the relevant theoretical background for the three main chapters of my thesis (i.e., the three different projects I worked on), which follow below.

As it was mentioned already in the previous chapter, the most common method that is adopted in these problems is the mean-field approximation [37, 38], which assumes a product form for the many-body state. This is very convenient, since the many-body problem reduces to a non-linear equation, of only one variable. This equation may vary from the standard nonlinear Schrödinger equation, with a quadratic nonlinear term, depending on the effective dimensionality, the trapping potential and the interaction strength. Still, standard numerical methods allow us to derive solutions of this equation.

The mean-field approximation has been tested and under “typical" conditions it is very successful, providing accurate answers. However, especially under certain conditions (e.g., when the atom number is small, as in the problems that I considered) this approximation fails. An alternative approach that I have used in my thesis is the method of diagonalization of the many-body Hamiltonian. The main advantage of this approach is that it does not make any assumption about the form of the many-body state, and thus it goes beyond the mean-field approximation, capturing correlations between the atoms.

Within the diagonalization of the Hamiltonian, one starts from a suitably chosen single-particle basis, and writes down the Hamiltonian in this basis (the more sparse the matrix, the better, as the numerical diagonalization becomes faster). Apparently, truncation of the Hamiltonian is necessary, as in general the dimensionality of the Hamiltonian is infinite.

Special care has to be taken in order to make sure that the derived results have converged with respect to the truncated space. While exact, this method may be applied to relatively small systems only — actually, it is a challenge to extract the behaviour of a large system (i.e., with a realistically large number of atoms) within this approach. Interestingly, the method of diagonalization gives the whole energy spectrum without any extra effort (contrary to the mean-field approximation), however it is reliable mostly for the lowest-energy state, as well as for the low-lying excited states, depending on the imposed truncation.

2.1 Definition of Bose-Einstein condensation

Penrose and Onsager [40] provided a rigorous criterion for the existence of Bose-Einstein condensation. Starting from the N-particle wave function $\Psi(\mathbf{r}_1, \mathbf{r}_2, \ldots, \mathbf{r}_N)$ of a system, one determines the eigenvalues of the (Hermitian) one-body density matrix,

$$\rho(\mathbf{r}, \mathbf{r}') = N \int d\mathbf{r}_2 \ldots d\mathbf{r}_N \Psi^*(\mathbf{r}, \mathbf{r}_2, \ldots \mathbf{r}_N)\Psi(\mathbf{r}', \mathbf{r}_2, \ldots, \mathbf{r}_N) \equiv \langle \psi^\dagger(\mathbf{r})\psi(\mathbf{r}')\rangle, \quad (2.1)$$

where $\psi(\mathbf{r})$ is the operator that annihilates a particle at point $\mathbf{r}$.

Since $\rho(\mathbf{r}, \mathbf{r}')$ is Hermitian it is always possible to find a complete orthonormal basis of single-particle eigenfunctions $\phi_i(\mathbf{r})$, such that

$$\rho(\mathbf{r}, \mathbf{r}') = \sum_i n_i \phi_i^*(\mathbf{r})\phi_i(\mathbf{r}'). \quad (2.2)$$

If none of the eigenvalues n_i is of order N, then we do not have Bose-Einstein condensation. If only one of the eigenvalues, say n_0, is of order N, we have single Bose-Einstein condensation, with the corresponding eigenvector $\phi_0(\mathbf{r})$ being the order parameter,

$$\rho(\mathbf{r}, \mathbf{r}') = n_0 \phi_0^*(\mathbf{r})\phi_0(\mathbf{r}') + \sum_{i\neq 0} n_i \phi_i^*(\mathbf{r})\phi_i(\mathbf{r}'). \quad (2.3)$$

Finally, if more than one eigenvalues is of order N, then the condensate is said to be fragmented [6].

Here are some remarks:

• Setting $\mathbf{r} = \mathbf{r}'$ in the density matrix, we get the single-particle density.

• The off-diagonal components of the density matrix also contain the information about the momentum distribution

$$n(\mathbf{p}) = \langle \psi^\dagger(\mathbf{p})\psi(\mathbf{p})\rangle, \quad (2.4)$$

where $\psi^\dagger(\mathbf{p})$ is the Fourier transform of $\psi^\dagger(\mathbf{r})$, i.e., it is the field operator in momentum space.

• Within the mean-field approximation, where the many-body state is a product state, according to the above criterion, the system is Bose-Einstein condensed, while the order parameter is the corresponding single-particle state.

2.2 Bose-Einstein condensation in an ideal gas

Let us start with an infinite system in three dimensions, and then we will see the effect of both the finiteness of a system in the particle number N, as well as of the dimensionality.

The well-known Bose-Einstein distribution is

$$f(E, \mu, T) = \frac{1}{e^{(E-\mu)/k_B T} - 1}, \quad (2.5)$$

where E is the energy, μ is the chemical potential and T is the temperature. In three spatial dimensions (in a volume V) the density of states $g(E)$ is given by

$$g(E) = \frac{VM^{3/2}}{\sqrt{2}\pi^2\hbar^3}E^{1/2}, \tag{2.6}$$

while the number of particles at the excited states is

$$N_{\rm exc} = \int_0^\infty g(E)f(E,\mu=0)\,dE = \frac{VM^{3/2}}{\sqrt{2}\pi^2\hbar^3}\int_0^\infty \frac{E^{1/2}}{e^{E/k_BT}-1}\,dE. \tag{2.7}$$

The corresponding density is thus:

$$n_{\rm exc} = \zeta(3/2)\left(\frac{Mk_BT}{2\pi\hbar^2}\right)^{3/2}, \tag{2.8}$$

where $\zeta(x)$ is the zeta function. The above is the well-known result that along the phase boundary of a Bose-Einstein condensation $n_{\rm exc} \propto T^{3/2}$. This is equivalent to the condition that the de-Broglie wavelength $\lambda = 2\pi\hbar/\sqrt{2Mk_BT}$ is comparable with the inter-particle spacing, $n_{\rm exc}^{-1/3}$. Setting in Eq. (2.8) $n_{\rm exc} = n_0$, i.e., the density of the (homogeneous) gas, this equation gives the critical temperature T_c for some given density n_0.

Finally, for $T < T_c$ the number of atoms in the condensate $N_0(T)$ is given by

$$N_0(T) = N\left[1-\left(\frac{T}{T_c}\right)^{3/2}\right]. \tag{2.9}$$

2.2.1 Bose-Einstein condensation in lower dimensions

For arbitrary spatial dimensions, the density of states $g(E) \propto E^{d/2-1}$, where d is the dimensionality (this holds for $d = 3$, 2, and 1).

An important consequence of this is that for $d = 2$ and $d = 1$ the integral that appears above has a divergence which is not integrable. This is the well-known result that there is no "true" Bose-Einstein condensation in two dimensions, or in one dimension for finite temperatures, in the thermodynamic limit.

2.2.2 Bose-Einstein condensation in a finite/confined system

In a system with finite number of atoms, or in a trapped system the above conclusions about the absence of "true" Bose-Einstein condensation in lower spatial dimensions do not hold (see, e.g., Refs. [41, 42, 43]). Another subtle point is that "real" phase transitions occur only in the thermodynamic limit.

The main observation here is that in a system with a finite number of atoms (as in a ring potential that we have considered), and for some set of excited states E_i, Eq. (2.7) should be replaced by the sum [41]

$$N_{\rm exc} = \sum_{i=1}^{\infty}\frac{1}{e^{E_i/k_BT}-1}, \tag{2.10}$$

which does not suffer from the problems of divergence described above. Alternatively, if one uses an integral representation instead, a cut-off has to be used in the lower bound of integration.

In addition, if there is a confining potential the density of states is also affected and Bose-Einstein condensation is present, even in lower dimensions [42]. For example, in a harmonic potential in d spatial dimensions the density of states $g(E)$ scales as E^{d-1}.

The main conclusion from the above remarks is that the statement about the absence of Bose-Einstein condensation in one-dimensional and two-dimensional systems in the thermodynamic limit is irrelevant in the problem of cold atomic gases, due to the finiteness of the atom number and their spatial confinement.

2.3 Rotational response of a Bose-Einstein condensate

Most of the problems that I have studied in my thesis involve Bose-Einstein condensates under rotation. Let me thus examine the rotational response of a Bose-Einstein condensed gas. As we saw earlier, the density matrix was examined, in the heart of Bose-Einstein condensation is the macroscopic occupancy of a single-particle state $\phi_0(\mathbf{r})$, see Eq. (2.3). This fact has serious consequences, as discussed below.

Since $\phi_0(\mathbf{r})$ is a complex field in general, it may be written as

$$\phi_0(\mathbf{r}) = \sqrt{n(\mathbf{r})}\, e^{i\varphi(\mathbf{r})}, \tag{2.11}$$

where $n(\mathbf{r})$ is the density and $\varphi(\mathbf{r})$ is the phase.

Evaluating the current density

$$j(\mathbf{r}) = \frac{\hbar}{2i}[\phi^*(\mathbf{r})\nabla\phi(\mathbf{r}) - \phi(\mathbf{r})\nabla\phi^*(\mathbf{r})] = n(\mathbf{r})\frac{\hbar}{M}\nabla\varphi(\mathbf{r}) \equiv n(\mathbf{r})v_s(\mathbf{r}), \tag{2.12}$$

from which it follows that the superfluid velocity $v_s(\mathbf{r})$ is

$$v_s(\mathbf{r}) = \frac{\hbar}{M}\nabla\varphi(\mathbf{r}). \tag{2.13}$$

The above equation implies that the rotational response of a condensate is very peculiar, since the curl of its velocity field consists of singularities, which correspond to vortex states located at the positions $\varrho = \varrho_i$ (assuming motion on a plane),

$$\nabla \times \mathbf{v_s} \propto \hat{z}\sum_i \delta^2(\varrho - \varrho_i). \tag{2.14}$$

Furthermore, the fact that the energy has to be finite, and since the velocity field diverges at $\varrho = \varrho_i$, the density vanishes at these points.

Finally, the line integral of the velocity field around a closed loop – i.e., the circulation – is quantized,

$$\oint v_s(\mathbf{r}) \cdot d\mathbf{l} = k\frac{2\pi\hbar}{M}, \tag{2.15}$$

where k is an integer.

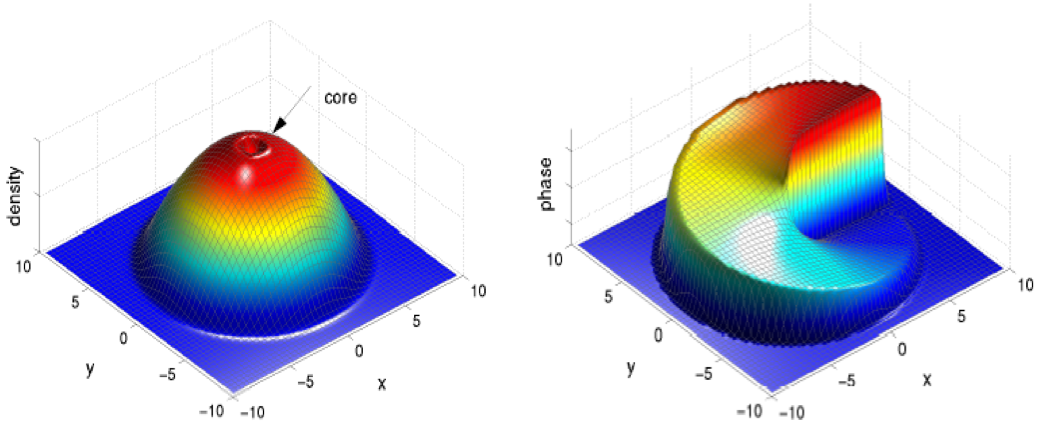

(A) Density of the wave function

(B) Phase of the wave function

FIGURE 2.1: Density and phase of a Bose-Einstein condensate with a single vortex state.

For example, if there is a single vortex state at $\varrho_i = 0$,

$$v_s(\mathbf{r}) = \hat{\theta}\frac{\hbar}{M\rho}. \tag{2.16}$$

Figure (2.1) shows such an example, of a single vortex state located at $(x, y) = (0, 0)$.

It should be stressed that vortex states also appear in classical fluids, however the difference here is the quantization of circulation, Eq. (2.15), as well as the possibility of persistent currents, which will be examined below.

2.4 Mean-Field approximation – Gross-Pitaevskii equation

Starting from the Schrödinger equation for the many-body wavefunction $\Psi(\mathbf{r}_1, \mathbf{r}_2, \ldots, \mathbf{r}_N)$,

$$\sum_{i=1}^{N}\left(-\frac{\hbar^2}{2M}\nabla_i^2 + V(\mathbf{r}_i) + \frac{1}{2}\sum_{j=1, j\neq i}^{N} V_{\text{int}}(\mathbf{r}_i - \mathbf{r}_j)\right)\Psi(\mathbf{r}_1, \mathbf{r}_2, \ldots, \mathbf{r}_N) = E\Psi(\mathbf{r}_1, \mathbf{r}_2, \ldots, \mathbf{r}_N), \tag{2.17}$$

where $V(\mathbf{r})$ is the external potential, and $V_{\text{int}}(\mathbf{r}_i - \mathbf{r}_j)$ is the potential due to two-body interactions.

Making the assumption of a product many-body state,

$$\Psi(\mathbf{r}_1, \mathbf{r}_2, \ldots, \mathbf{r}_N) = \prod_{i=1}^{N}\phi_0(\mathbf{r}_i), \tag{2.18}$$

the expectation value of the energy is

$$\begin{aligned}\langle H\rangle = -N\int \frac{\hbar^2}{2M}\phi_0^*(\mathbf{r})\nabla^2\phi_0(\mathbf{r})\,d\mathbf{r} + N\int V(\mathbf{r})|\phi_0(\mathbf{r})|^2 + \\ +\frac{1}{2}N(N-1)\int d\mathbf{r}\int d\mathbf{r}' V_{\text{int}}(\mathbf{r}-\mathbf{r}')|\phi_0(\mathbf{r})|^2|\phi_0(\mathbf{r}')|^2.\end{aligned} \tag{2.19}$$

Minimizing the above energy functional while respecting the condition of particle normalization,

$$\int |\phi_0(\mathbf{r})|^2 \, d\mathbf{r} = 1, \tag{2.20}$$

we end up with the following equation,

$$-\frac{\hbar^2}{2M}\nabla^2\phi_0(\mathbf{r}) + V(\mathbf{r})\phi_0(\mathbf{r}) + (N-1)\left(\int V_{\text{int}}(\mathbf{r}-\mathbf{r}')|\phi_0(\mathbf{r}')|^2 \, d\mathbf{r}'\right)\phi_0(\mathbf{r}) = \mu\phi_0(\mathbf{r}). \tag{2.21}$$

Here μ is a Lagrange multiplier associated with the normalization of $\phi_0(\mathbf{r})$ and it corresponds to the chemical potential. When the interaction potential is assumed to be a contact potential,

$$V_{\text{int}}(\mathbf{r}-\mathbf{r}') = g_{3D}\,\delta(\mathbf{r}-\mathbf{r}'), \tag{2.22}$$

and for $N-1 \approx N$ (for large N), then Eq. (2.21) takes the more familiar form

$$-\frac{\hbar^2}{2M}\nabla^2\phi_0(\mathbf{r}) + V(\mathbf{r})\phi_0(\mathbf{r}) + Ng_{3D}|\phi_0(\mathbf{r})|^2\phi_0(\mathbf{r}) = \mu\phi_0(\mathbf{r}), \tag{2.23}$$

which is the Gross-Pitaevskii equation [37, 38]. Here g_{3D} is the matrix element for elastic atom-atom s-wave collisions and is equal to $4\pi\hbar^2 a_{\text{sc}}/M$, where a_{sc} is the scattering length.

The validity of the mean-field approximation, i.e., Eq. (2.18), relies on the condition $na_{\text{sc}}^3 \ll 1$, where n is the typical atom density. In other words, this is a good approximation when the scattering length is much smaller than the mean distance between the atoms, $n^{-1/3}$. Under typical conditions a_{sc} is on the order of 100 Å$= 10^{-8}$ cm, while for $n \approx 10^{15}$ cm^{-3}, $n^{-1/3} \approx 10^{-5}$ cm.

To conclude this subsection, the corresponding time-dependent Gross-Pitaevskii equation follows directly from Eq. (2.23),

$$-\frac{\hbar^2}{2M}\nabla^2\phi_0(\mathbf{r},t) + V(\mathbf{r})\phi_0(\mathbf{r},t) + Ng_{3D}|\phi_0(\mathbf{r},t)|^2\phi_0(\mathbf{r},t) = i\hbar\frac{\partial\phi_0(\mathbf{r},t)}{\partial t}. \tag{2.24}$$

2.4.1 Bose-Einstein condensed atoms confined in a ring potential

In all the problems that I considered I assumed one-dimensional motion with periodic boundary conditions, as in a ring potential. This corresponds to experiments where the atoms are confined in either toroidal, or annular potentials, where the transverse degrees of freedom are frozen out. This condition is fulfilled when the quantum of energy of the trapping potential in the transverse direction is much higher than the interaction energy and thus these degrees of freedom are effectively frozen.

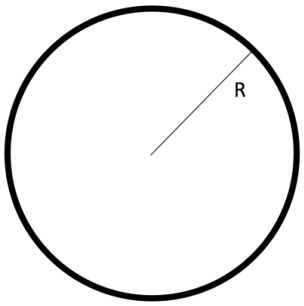

FIGURE 2.2: Ring potential

Mean-field, Gross-Pitaevskii equation

Under these conditions the order parameter $\phi_0(\mathbf{r})$ depends on the angle θ only. Assuming that the transverse profile of the cloud is constant, then $\phi_0(\mathbf{r}) = \phi(\theta)/\sqrt{RS}$, where R is the radius of the ring and S is the cross section of the torus/annulus. Then, the Gross-Pitaevskii equation, Eq. (2.23), takes the form

$$-\frac{\hbar^2}{2MR^2}\frac{\partial^2}{\partial\theta^2}\phi(\theta) + V(\theta)\phi(\theta) + 2\pi N g|\phi(\theta)|^2\phi(\theta) = \mu\phi(\theta), \tag{2.25}$$

where $g = g_{3D}/(2\pi RS)$. The corresponding time-dependent equation is in this case

$$-\frac{\hbar^2}{2MR^2}\frac{\partial^2}{\partial\theta^2}\phi(\theta,t) + V(\theta)\phi(\theta,t) + 2\pi N g|\phi(\theta,t)|^2\phi(\theta,t) = i\hbar\frac{\partial\phi(\theta,t)}{\partial t}. \tag{2.26}$$

Eigenvalue problem

In the absence of interactions and $V(\theta) = 0$ the above equation reduces to the well-known problem of a single particle moving on a ring. The eigenfunctions are

$$\psi_m(\theta) = \frac{e^{im\theta}}{\sqrt{2\pi}}, \tag{2.27}$$

where m corresponds to the quantum number of the angular momentum and is an integer. The corresponding eigenenergies are

$$E_m = \frac{\hbar^2 m^2}{2MR^2}. \tag{2.28}$$

Solitary-wave solutions

Solitary-wave solutions of Eq. (2.26) are self-localized solutions, which correspond to density waves that propagate around the ring without any change in their shape (I set the external potential $V(\theta)$ equal to 0).

These will have the form $\phi(\theta,t) = \phi(z)e^{-i\mu t/\hbar}$, where $z = \theta - \Omega t$, with Ω being the angular velocity of propagation of the wave, and μ the chemical potential. Equation

(2.26) then becomes time-independent,

$$-\frac{\hbar^2}{2MR^2}\frac{\partial^2}{\partial\theta^2}\phi(z)+(2\pi Ng|\phi(z)|^2-\mu)\phi(z)=-i\hbar\Omega\frac{\partial\phi(z)}{\partial z}. \tag{2.29}$$

Obviously the solutions of the above equation have to satisfy periodic boundary conditions and may be expressed in terms of Jacobi elliptic functions [44, 45].

Before I examine this more general problem let me start with the well-known problem of an "infinite" ring, i.e., the limit $N\to\infty$ and $R\to\infty$, with N/R finite. The density far away from the center of the wave approaches the constant density, $n_{1D}=N/(2\pi R)$. The solution then takes the form [47, 48]

$$\phi(z)=\frac{1}{\sqrt{2\pi}}\left(i\frac{u}{c}+\sqrt{1-\frac{u^2}{c^2}}\tanh\left[\frac{z}{\xi}\sqrt{1-\frac{u^2}{c^2}}\right]\right), \tag{2.30}$$

where $u=\Omega R$ is the velocity of propagation of the wave, c is the sound speed, and ξ is the coherence (or healing) length that corresponds to the density n_{1D}. This is defined as $\hbar^2/(2M\xi^2)=n_{1D}g$ and it gives the characteristic width of the solitary wave. In the above solution

$$\frac{u^2}{c^2}=\frac{n_{\min}}{n_{1D}}. \tag{2.31}$$

When $n_{\min}=0$, the solitary wave has a node in the density (i.e., we have a "dark" solitary wave, which is the well-known "pi-kink" solution), then $u=0$, i.e., the wave is also static. As we see below, in a ring with a finite radius this is no longer true.

I stress that this solution does not satisfy periodic boundary conditions (for example, the pi-kink solution has a phase difference of π). Still, in this limit this is a valid solution, since it is possible to impose periodic boundary conditions [46] by matching the phase at the interval where the density is homogeneous, i.e., "far" from the center of the solitary wave.

I turn now to the more interesting case of a ring with a finite radius. The two relevant length scales which enter the problem are the radius of the ring R and the coherence length ξ.

When $\xi\ll R$ then one goes to the limit of a "large" ring and the solitary-wave solutions are the ones given in Eq. (2.30). In this limit the wave is localized within a length scale that is set by the coherence length, and the density is constant elsewhere.

Depending on the phase difference at the edges of the system (which is either zero, or some integer multiple of 2π), two different situations can arise [45]. For zero phase difference, the minimum possible value of the density is zero, and the velocity of propagation varies between a lowest nonzero value, and a maximum velocity, which is set by the speed of sound. In the case of a nonzero phase difference, the velocity of propagation can be zero, but the corresponding density cannot vanish. Again, when $N\to\infty$ and $R\to\infty$, with N/R finite, one finds agreement with known results.

In the opposite limit of "small" rings, $\xi\gg R$, the density becomes sinusoidal with a length scale given by R itself. Furthermore, the velocity of propagation saturates to a constant value, which scales as $1/R$, and the minimum density of the wave can become zero.

A final remark that I should mention is that Eq. (2.29) may also be viewed as the equation that results from extremizing (minimizing) the energy under two constraints:

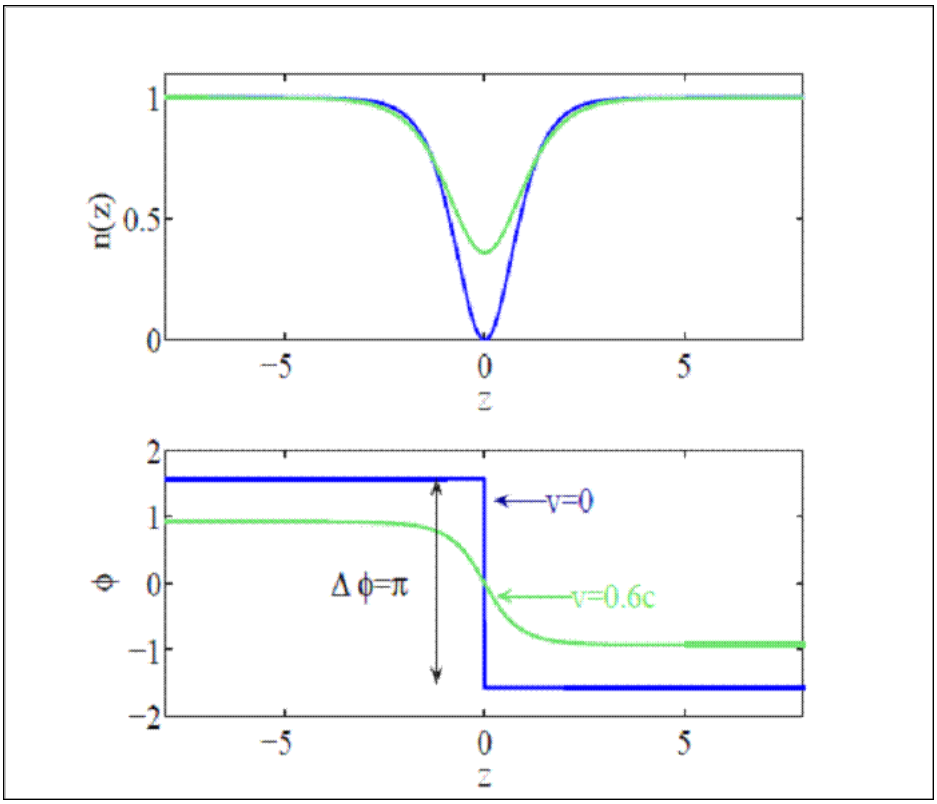

FIGURE 2.3: The density and the phase of a solitary-wave solution for two values of the velocity of propagation (denoted as v here), $v = 0$ and $v/c = 0.6$. The case $v = 0$ is the "dark" solitary-wave, i.e., the pi-kink solution.

fixing the angular momentum (term with the first derivative) and the atom number (term with the chemical potential). In other words, the equation for solitary-wave excitation coincides with the equation for rotational excitation [50] (obviously for the same boundary conditions). This observation is useful in what follows below.

Dispersion relation and Bloch's theorem

Another interesting aspect of this problem is the dispersion relation, i.e., the energy of the system, for some given angular momentum. The assumed one-dimensional motion, in combination with the periodic boundary conditions imply that the energy spectrum is quasi-periodic, i.e., it is a periodic function, on top of a parabola, as described by Bloch's theorem [49]. As we will see below, this behaviour affects all three problems which are examined in the following chapters.

More specifically, let us denote as $\ell = L/N$ the units of angular momentum given to the system where $L\hbar$ is the total angular momentum. If ℓ_0 is the value of ℓ in the interval between zero and unity, according to Bloch's theorem, the energy per particle $E(\ell)/N$ of the system may be written as

$$E(\ell)/N = \frac{\hbar^2}{2MR^2}\ell^2 + e(\ell_0), \tag{2.32}$$

where $e(\ell_0) = e(\ell_0 + n)$, with $n = 1, 2, \ldots$, i.e., $e(\ell_0)$ is a periodic function, with a period equal to unity. The function $e(\ell_0)$ is also even, $e(-\ell_0) = e(\ell_0)$. In other words, if one evaluates $e(\ell_0)$ for $0 \leq \ell_0 < 1$, then from Eq. (2.32) the whole excitation spectrum follows, for any value of ℓ.

Furthermore, if any eigenstate $\Psi_{\ell_0}(\theta_1, \ldots, \theta_N)$ of the many-body Hamiltonian (not necessarily the lowest-energy state) is known for any value of ℓ_0 between zero and unity, then the many body state for $\ell = \ell_0 + n$, with $n = 1, 2, \ldots$ is

$$\Psi_{\ell_0+n}(\theta_1, \ldots, \theta_N) = e^{in(\theta_1+\ldots+\theta_N)}\Psi_{\ell_0}(\theta_1, \ldots, \theta_N). \tag{2.33}$$

The general structure of the dispersion relation $E(L)$ is shown in the following plot, Fig. (2.4).

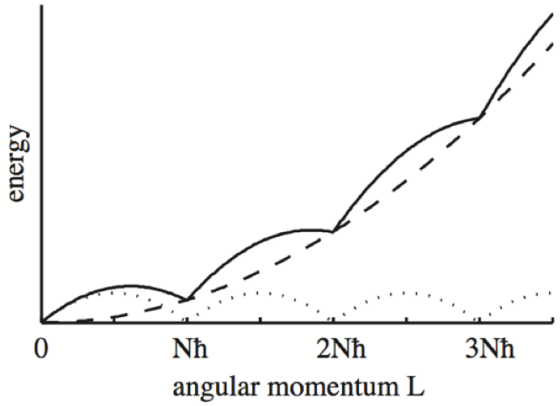

FIGURE 2.4: Schematic figure of the dispersion relation for N bosons in a ring potential. The dashed line is the envelope part, proportional to L^2, and the dotted line is the periodic part; the solid line is their sum i.e., the dispersion relation. The local minima give rise to persistent currents.

Variational approach

Alternatively Eq. (2.25) may also be solved numerically, or variationally. For example, if one wants to follow the variational approach, one may expand the order parameter in the (complete) basis of the plane-wave eigenfunctions of the non-interacting problem, Eq. (2.27),

$$\phi_0 = \sum_m c_m \psi_m. \tag{2.34}$$

Then, the energy has to be minimized under two constraints, namely normalization,

$$\sum_m c_m^2 = 1, \tag{2.35}$$

and a fixed expectation value of the angular-momentum operator,

$$\sum_m m c_m^2 = \ell, \tag{2.36}$$

where $\ell = L/N$ is the angular momentum per particle. This constraint minimization determines the amplitudes c_m.

Weak interactions – a toy model

An easy and instructive limit, which allows us to derive analytic expressions for various observables, is that of weak interactions, where $n_{1D}g \ll \hbar^2/(2MR^2)$ and one may work with two modes only, using the variational approach. Given that there are two constraints, these determine the two variational amplitudes (up to a phase, as we discuss below).

When the expectation value of the angular momentum is in the range $m\hbar \leq \ell\hbar \leq (m+1)\hbar$ (I take m to be positive for simplicity), the order parameter is, due to the limit of weak interactions,

$$\phi_m = \sqrt{1-\ell_0}\,\psi_m + \sqrt{\ell_0}\,e^{-i\lambda}\,\psi_{m+1}. \tag{2.37}$$

Here $0 \leq \ell_0 \leq 1$ and λ is a real number and constant (to be explained below).

The energy per particle is

$$\frac{E_m}{Ne_0} - \frac{\gamma}{2} = \ell^2 + (1+\gamma)\ell_0(1-\ell_0), \tag{2.38}$$

where $e_0 = \hbar^2/(2MR^2)$, $\gamma = n_{1D}g/e_0$ and $\ell = \ell_0 + m$ is the angular momentum per atom. From the above expression we see that indeed, the energy is periodic (last term) on top of a parabola (first term on the right side of the equation), in agreement with Bloch's theorem [49].

Furthermore, the density (in the rotating frame) is given by

$$n_m(\theta) = n_{1D}[1 + 2\sqrt{\ell_0(1-\ell_0)}\cos(\theta - \lambda)]. \tag{2.39}$$

We see that in this limit of weak interactions the density is sinusoidal, as mentioned also above. The parameter λ determines the center of the wave and is arbitrary because of the rotational invariance of the problem. We also see that $n_m(\theta)$ is the same at any interval $m\hbar \leq \ell\hbar \leq (m+1)\hbar$, and is independent of m, due to Bloch's theorem.

Equation (2.39) minimizes the energy for a fixed expectation value of the angular momentum. As mentioned above, this is actually equivalent to a nonlinear travelling-wave – i.e., a solitary-wave – solution [50], and it represents a density wave that propagates around the ring with a velocity v_m. This propagation velocity is given by the derivative of the energy with respect to the angular momentum and is equal to

$$v_m = \frac{\hbar}{MR}[1 + \gamma + 2(m - \gamma\ell_0)]. \tag{2.40}$$

From this equation we also observe that for $\ell_0 = 1$, i.e., for $\ell = m+1$, its slope vanishes for the critical coupling

$$\gamma_m = 2m + 1. \tag{2.41}$$

This equation implies that persistent currents – i.e., local minima in the dispersion relation – appear at these critical values of the coupling, at $\ell = m + 1$. Of course, we should not forget that self consistence requires that γ has to be small within this trial wavefunction. Actually, the exact result for the critical coupling is $\gamma_m = (2m+1)(2m+3)/2$ [51].

A mixture with two components

In my thesis I have also considered the case of a mixture of two, distinguishable bosonic species. Equation (2.25) is generalized for the two order parameters, say $\phi_A(\theta)$ and $\phi_B(\theta)$, as

$$\begin{aligned} -\frac{\hbar^2}{2MR^2}\frac{\partial^2}{\partial\theta^2}\phi_A(\theta) + V(\theta)\phi_A(\theta) + 2\pi(N_A g_{AA}|\phi_A(\theta)|^2 + N_B g_{AB}|\phi_B(\theta)|^2)\phi_A(\theta) \\ = \mu_A\phi_A(\theta), \\ -\frac{\hbar^2}{2MR^2}\frac{\partial^2}{\partial\theta^2}\phi_B(\theta) + V(\theta)\phi_B(\theta) + 2\pi(N_B g_{BB}|\phi_B(\theta)|^2 + N_A g_{AB}|\phi_A(\theta)|^2)\phi_B(\theta) \\ = \mu_B\phi_B(\theta), \end{aligned} \tag{2.42}$$

where we now have the atom numbers N_A and N_B in each component, the parameters g_{AA} for $A-A$ collisions, g_{BB} for $B-B$ collisions, and g_{AB} for $A-B$ collisions, and the chemical potential μ_A and μ_B for each species. Finally, the atom mass M of the two species is assumed to be the same.

The above coupled equations also support solitary-wave solutions, the so-called "vector solitons", as I analyze in detail in Chap. 5. In this case both the periodic boundary conditions – in connection with the finiteness of the radius of the ring – as well as the additional degrees of freedom associated with the second component introduce novel effects [52].

2.5 Diagonalization of the many-body Hamiltonian

2.5.1 General remarks

I turn now to the alternative approach mentioned earlier, i.e., to the solutions of the many-body Schrödinger equation, which in matrix notation takes the form

$$H|\Psi\rangle = E|\Psi\rangle. \tag{2.43}$$

To solve this problem one starts with a single-particle basis of states and expresses the Hamiltonian matrix in this basis. For example, one may choose the eigenstates of the non-interacting problem – a "suitably" chosen basis of states will make the corresponding matrix more sparse and will speed up the diagonalization, or equivalently it will allow us to handle matrices of a larger dimensionality.

In general the dimensionality of the Hamiltonian matrix is infinite. Given that typically we are interested in either the lowest-energy state, or the low-lying excited states, the space of single-particle states is truncated, since states of higher energy contribute very little to the low-energy many-body states.

It is a challenge to make sure that the observables we evaluate from the diagonalization have converged with respect to the truncation. One of my achievements is that I developed a dynamic algorithm, which allowed me to perform the diagonalization in a space with a tuned truncation, and thus I managed to check the convergence of my results.

Furthermore, the dimensionality of the Hamiltonian matrix increases rapidly with the atom number N, as well as with the units of angular momentum L (in the problems that involve rotational properties that I have considered). As a result, within this approach both N and L are very limited (compared to the ones in current, typical experiments).

I stress that the many-body states that result from the diagonalization have all the information that is needed for the evaluation of any observable. On the other hand, the only observables that follow immediately from the diagonalization are the eigenenergies (actually not only the lowest one, but the whole excitation spectrum). For any other observable that one may need (e.g., single-particle density, pair-correlation function, etc.), extra effort is required.

2.5.2 Atoms confined in a ring potential

Let me now consider the problem of atoms confined in a ring potential. The single-particle basis states that I choose are the plane-wave states, Eq. (2.27). The Hamiltonian H that I use is, in second-quantized form,

$$H = \frac{\hbar^2}{2MR^2} \sum_{m=m_{\min}}^{m_{\max}} m^2 a_m^\dagger a_m + \frac{g}{2} \sum_{m,n,k,l} a_m^\dagger a_n^\dagger a_k a_l \, \delta_{m+n,k+l}, \tag{2.44}$$

where a_m annihilates an atom with angular momentum $m\hbar$. The first term on the right corresponds to the kinetic energy, while the second to the interaction energy (the interaction is assumed to be a contact potential). Also $m_{\min}$ denotes the minimum (integer) value of the quantum of angular momentum that we choose in our space, and $m_{\max}$ the maximum one. We consider only the single particle states ϕ_m, with $m_{\min} \leq m \leq m_{\max}$.

In order to proceed with the diagonalization, we have to construct the many-body basis states. Since the Hamiltonian operator is axially symmetric, it commutes with the angular momentum operator,

$$[H, \hat{L}] = 0, \tag{2.45}$$

and also with the number operator,

$$[H, \hat{N}] = 0. \tag{2.46}$$

The many-body basis states

$$|\phi_{m_{\min}}^{N_{m_{\min}}}, \ldots, \phi_0^{N_0}, \ldots, \phi_{m_{\max}}^{N_{m_{\max}}}\rangle \tag{2.47}$$

will thus be eigenstates of both $\hat{L}$ and $\hat{N}$. Here the upper index denotes the occupancy of the single-particle state.The constraints due to fixing N and L take the form

$$\sum_{m=m_{\min}}^{m=m_{\max}} N_m = N, \tag{2.48}$$

and

$$\sum_{m=m_{\min}}^{m=m_{\max}} m N_m = L. \tag{2.49}$$

Therefore, after the construction of the many-body basis states of some fixed N and L, the Hamiltonian matrix is written in this basis and diagonalized. The derived eigenstates are also expressed in terms of these many-body basis states, while the corresponding eigenenergies follow immediately.

A mixture with two components

If there are two distinguishable components, the Hamiltonian takes the form (assuming equal masses for the two species)

$$\begin{aligned} H = \frac{\hbar^2}{2MR^2} \sum_{m=m_{\min}}^{m_{\max}} m^2 (a_m^\dagger a_m + b_m^\dagger b_m) + \frac{g_{AA}}{2} \sum_{m,n,k,l} a_m^\dagger a_n^\dagger a_k a_l \, \delta_{m+n,k+l} \\ + \frac{g_{BB}}{2} \sum_{m,n,k,l} b_m^\dagger b_n^\dagger b_k b_l \, \delta_{m+n,k+l} + g_{AB} \sum_{m,n,k,l} a_m^\dagger b_n^\dagger a_k b_l \, \delta_{m+n,k+l}, \end{aligned} \tag{2.50}$$

where a_m destroys an atom of species A with angular momentum $m\hbar$, and b_m destroys an atom of species B with angular momentum $m\hbar$.

2.5.3 An explicit example

Let me consider $N = 4$ atoms, $L = 3$ units of angular momentum, $g = 0.1$, and truncate to the space with $m_{\min} = -2$, and $m_{\max} = 2$.

Starting with the many-body basis states which satisfy the two constraints for N and L, these are

$$\begin{aligned} |1\rangle &= |(-2)^0, (-1)^0, 0^1, 1^3, 2^0\rangle \\ |2\rangle &= |(-2)^0, (-1)^0, 0^2, 1^1, 2^1\rangle \\ |3\rangle &= |(-2)^0, (-1)^1, 0^0, 1^2, 2^1\rangle \\ |4\rangle &= |(-2)^0, (-1)^1, 0^1, 1^0, 2^2\rangle \\ |5\rangle &= |(-2)^1, (-1)^0, 0^0, 1^1, 2^2\rangle. \end{aligned} \tag{2.51}$$

Here in the notation "m^{N_m}" the lower index denotes the quantum number m of the single-particle state ϕ_m and the upper index denotes the occupancy of this single-particle state.

If H_1 is the kinetic-energy operator and H_2 the interaction-energy operator, the corresponding matrices are the following two, which lead to the total Hamiltonian matrix H,

H_1	$\|1\rangle$	$\|2\rangle$	$\|3\rangle$	$\|4\rangle$	$\|5\rangle$
$\|1\rangle$	3	0	0	0	0
$\|2\rangle$	0	5	0	0	0
$\|3\rangle$	0	0	7	0	0
$\|4\rangle$	0	0	0	9	0
$\|5\rangle$	0	0	0	0	13

H_2	$\|1\rangle$	$\|2\rangle$	$\|3\rangle$	$\|4\rangle$	$\|5\rangle$
$\|1\rangle$	0.9000	0.3464	0.3464	0	0
$\|2\rangle$	0.3464	1.1000	0.2000	0.4000	0.2000
$\|3\rangle$	0.3464	0.2000	1.1000	0.2000	0.4000
$\|4\rangle$	0	0.4000	0.2000	1.1000	0.2000
$\|5\rangle$	0	0.2000	0.4000	0.2000	1.1000

H	$\|1\rangle$	$\|2\rangle$	$\|3\rangle$	$\|4\rangle$	$\|5\rangle$
$\|1\rangle$	3.9000	0.3464	0.3464	0	0
$\|2\rangle$	0.3464	6.1000	0.2000	0.4000	0.2000
$\|3\rangle$	0.3464	0.2000	8.1000	0.2000	0.4000
$\|4\rangle$	0	0.4000	0.2000	10.1000	0.2000
$\|5\rangle$	0	0.2000	0.4000	0.2000	14.1000

Diagonalizing this matrix implies that the eigenenergies are

Eigenenergies
3.8227
6.0859
8.0999
10.1468
14.1447

and the corresponding eigenvectors are

Eigenstates
$-0.9864\|1\rangle + 0.1460\|2\rangle + 0.0741\|3\rangle - 0.0115\|4\rangle - 0.0055\|5\rangle$
$0.1381\|1\rangle + 0.9800\|2\rangle - 0.1087\|3\rangle - 0.0914\|4\rangle - 0.0168\|5\rangle$
$-0.0882\|1\rangle - 0.0854\|2\rangle - 0.9843\|3\rangle + 0.1090\|4\rangle + 0.0648\|5\rangle$
$0.0109\|1\rangle + 0.1001\|2\rangle + 0.0955\|3\rangle + 0.9882\|4\rangle - 0.0647\|5\rangle$
$0.0033\|1\rangle + 0.0294\|2\rangle + 0.0689\|3\rangle + 0.0555\|4\rangle + 0.9956\|5\rangle$

Chapter 3

Hysteresis in a Bose-Einstein condensate

The phenomenon of hysteresis appears in various physical systems. One of the most well-known examples of hysteretic behaviour is magnetism: When a ferromagnetic material is subjected to an external magnetic field, it becomes a magnet, and then, even in the absence of the field, it remains a magnet. In order for the material to become non-magnetic, an opposite field has to be applied, or to be heated. Therefore, quite generally, hysteresis refers to the fact that the state of a system depends on its history.

Hysteresis is in the heart of the collection of phenomena associated with superfluidity (and superconductivity). In this chapter, I examine the phenomenon of hysteresis in a Bose-Einstein condensed cloud of atoms which rotate in a toroidal/annular potential [49, 53, 54, 55, 56, 57]. Assuming one-dimensional motion, I evaluate the critical frequencies associated with the effect of hysteresis and the critical coupling for stability of the persistent currents [6, 66], as well as their decay mechanisms.

I perform these calculations using both the mean-field approximation (where the implicit assumption of a large atom number has been made), as well as the method of numerical diagonalization of the many-body Hamiltonian (considering, in this approach, a small atom number), thus identifying the corrections due to the finiteness of the atom number.

3.1 Experimental motivation

Over the last years, scientists have managed to trap and manipulate Bose-Einstein condensed clouds of atoms in a wide variety of trapping potentials of different topologies. Numerous experiments have been performed in topologically-nontrivial trapping potentials, namely in annular/toroidal traps [58, 59, 60, 61, 62, 63, 64, 65]. More recently the phenomenon of hysteresis was also observed in an annular potential [35].

In this experiment – see Fig. (3.1) and Fig. (3.2)– a Bose-Einstein condensate of sodium atoms, which was trapped in an annular trap and it was initially at rest, was stirred. As the rotational frequency of the stirring potential increased, the cloud was observed to make a transition to a state with one unit of circulation at a critical frequency, Ω_1. On the other hand, in the reverse process (i.e., starting with the gas

having one unit of circulation and decreasing the frequency of the stirrer) the system was observed to return to the state with zero circulation at a different critical frequency, Ω_2. This is indeed a clear indication of hysteresis.

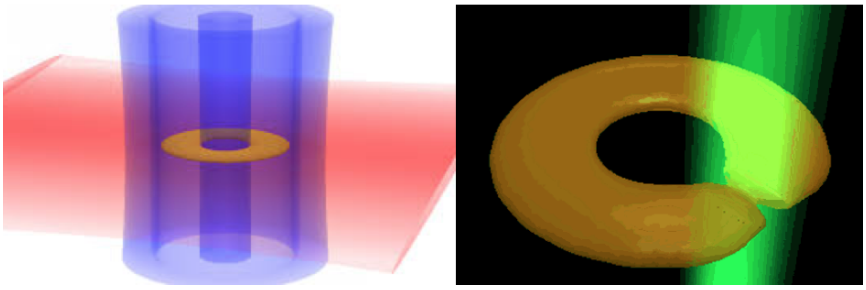

FIGURE 3.1: Schematic picture from the experiment of Ref. [35], where the phenomenon of hysteresis was observed. A combination of magnetic fields trapped the atoms (left), resulted into a cloud of atoms which were confined in the annulus (right). A green laser beam was applied locally, reducing the atom density, and forcing the atoms to rotate.

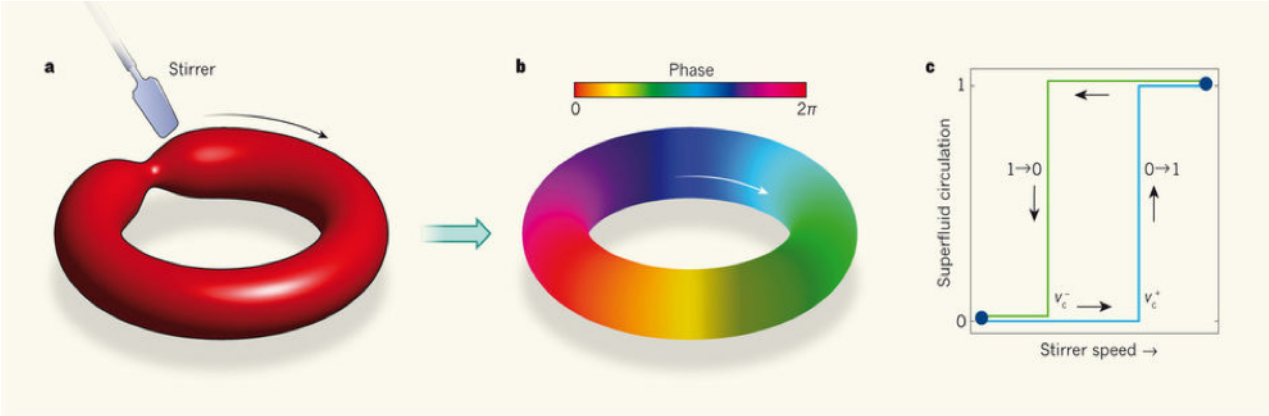

FIGURE 3.2: Schematic picture from the experiment of Ref. [35]. The left and the middle plots show the density and the phase of the condensate, respectively. The right shows the hysteresis loop.

In what follows below I first present the model in Sec. 3.2 and comment on the phenomenon of hysteresis in Sec. 3.3. Then, I evaluate in Sec. 3.4 the relevant critical frequencies within the mean-field approximation. In Sec. 3.5 I perform the same calculation beyond the mean-field approximation, where I consider corrections of order $1/N$ (and lower), which result due to the finiteness of the atom number N. I also investigate in Sec. 3.6 the corresponding finite-N corrections on the critical coupling for metastability and the matrix element for the decay rate of persistent currents. Finally in Sec. 3.8 I present some conclusions of the results of the present chapter.

3.2 Hysteresis in a system with a finite number of atoms in a ring potential

3.2.1 Model

Contrary to the mean-field approximation - which makes the implicit assumption of a large particle number - the diagonalization approach includes corrections due to a finite number of atoms. In addition, it avoids the assumption of a simple product state for the many-body wavefunction that is central to the mean-field approach. As a result, this approach captures correlations that are built when the atom number is very low or when the diluteness condition is violated.

I stress that in various recent experiments it became possible to trap and detect very small numbers of atoms, which can even be of order unity. Indeed, there appears to be a more general tendency in the field of cold atoms to move towards the study of small systems. Interestingly, the vast majority of the theoretical studies which have been performed on the superfluid properties of cold atomic gases and on the phenomenon of hysteresis assume the opposite limit of large particle numbers, since they are based on the mean-field Gross-Pitaevskii approximation. As a result, very little is known about the effect of the finiteness of systems with a small number of atoms.

I assume one-dimensional motion of bosonic atoms under periodic boundary conditions, as in a ring potential. This model is expected to be valid in an annular/toroidal trap as long as the interaction energy is much smaller than the energy of the trapping potential in the transverse direction.

If a_m and $a_m^\dagger$ are annihilation and creation operators of an atom with angular momentum $m\hbar$, the Hamiltonian has the form of Eq. (2.44)

$$H = \frac{\hbar^2}{2MR^2} \sum_{m=m_{\min}}^{m_{\max}} m^2 a_m^\dagger a_m + \frac{g}{2} \sum_{m,n,k,l} a_m^\dagger a_n^\dagger a_k a_l \, \delta_{m+n,k+l}. \tag{3.1}$$

Here M is the atom mass, R is the mean radius of the torus/annulus, with $R \gg \sqrt{S}$, where S is the cross section of the torus/annulus in the transverse direction. Also $g = g_{3D}/(2\pi RS)$, where $g_{3D} = 4\pi\hbar^2 a_{\rm sc}/M$ is the matrix element for elastic s-wave atom-atom collisions, with a scattering length $a_{\rm sc}$.

3.3 The dispersion relation and its effect on hysteresis

In analysing the phenomenon of hysteresis and of the metastability of superflow [6, 66], the main feature to be considered is the dispersion relation [49, 53, 54, 55, 56, 57], i.e., the energy of the system as a function of the angular momentum.

Let $E(\ell)$ denote the total energy where $\ell\hbar \equiv L\hbar/N$ is the angular momentum per atom and $L\hbar$ is the total angular momentum. As we saw in the previous section, according to Bloch's theorem [49], $E(\ell)$ consists of a periodic part plus a quadratic part which comes from the motion of the center of mass. Thus, one needs to consider only $0 \leq L \leq N$ ($0 \leq \ell \leq 1$); the remainder of the spectrum follows trivially as a consequence of Bloch's theorem.

The periodic part has minima at $L = 0$ and $L = N\hbar$, and thus local minima in the dispersion relation may occur at these values of L. The dispersion relation is shown schematically in Fig. (2.4). We note that since only the periodic part is the one that can cause local minima, and only the periodic part depends on the internal motion of the atoms, it is the interactions that may cause local minima to appear. If interactions are sufficiently weak, there will be no local minima and the system will not support persistent currents.

3.3.1 Non-interacting problem

In the absence of interactions $E(\ell)$ consists of straight lines, see Fig. (3.3). In the intervals $m \leq \ell \leq m+1$, where m is an integer,

$$E(\ell)/Ne_0 = m^2 + (2m+1)\ell_0, \tag{3.2}$$

where $\ell = \ell_0 + m$ and $0 \leq \ell_0 \leq 1$. Obviously, at the end points of each interval the first derivative of $E(\ell)$ is discontinuous.

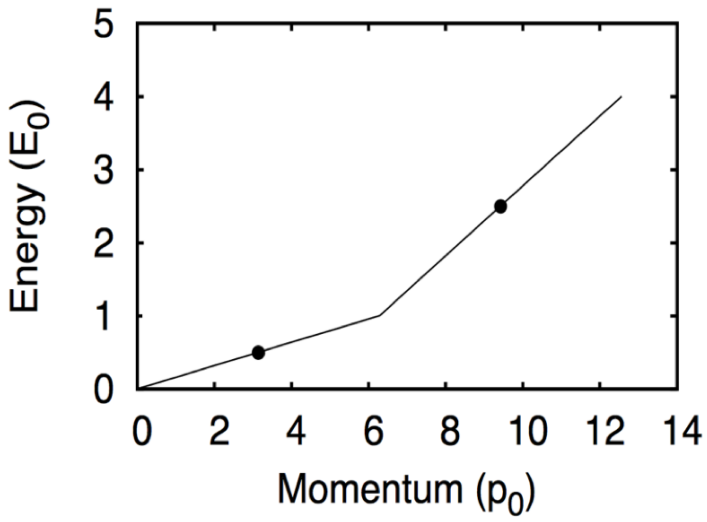

FIGURE 3.3: Dispersion relation in the absence of interactions.

3.3.2 Effect of the interactions

In the presence of repulsive/attractive interactions these discontinuities remain, while the curvature is negative/positive, respectively. Figures (3.4), (3.5) show a schematic picture of the dispersion relation $E(\ell)$ for the repulsive interactions which we consider here. Such a spectrum will give rise to hysteresis. If one goes to the rotating frame and considers $E_{rot}(\ell)/N = E(\ell)/N - \ell\Omega$, there are competing local minima as the rotational frequency of the trap Ω is varied. These competing minima give rise to discontinuous transitions and thus to hysteresis. The two critical frequencies Ω_1 and Ω_2 (see Fig. (3.5)) of the hysteresis loop correspond to the value of the slope of the dispersion relation $E(\ell)$ for $\ell \to 0^+$ and $\ell \to 1^-$, respectively.

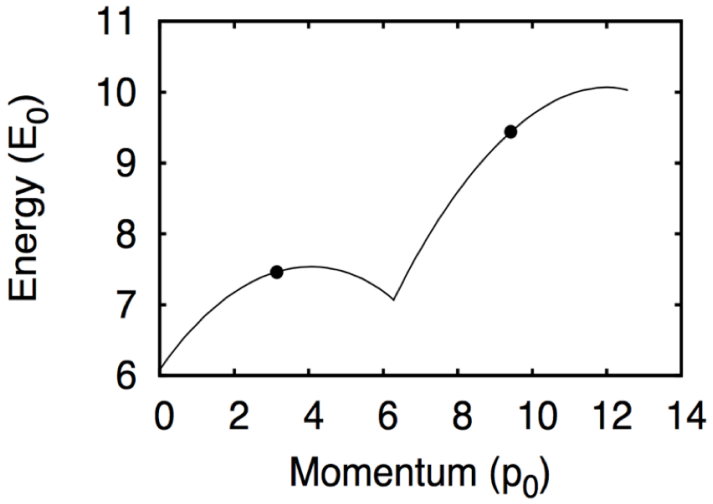

FIGURE 3.4: Dispersion relation for repulsive interactions.

The effect of hysteresis is thus a generic feature of this problem. On the other hand, for an effective attraction between the atoms, hysteresis is absent, since the curvature of $E(\ell)$ is positive, and thus there are no discontinuous transitions as the rotational frequency of the trap is varied.

It is convenient to write (in the interval $0 \leq \ell \leq 1$) the total energy per particle $E(\ell)/N$ as [1]

$$\frac{E(\ell)}{N} = \frac{\hbar^2}{2MR^2}\ell + \tilde{e}(\ell). \tag{3.3}$$

In the case of the non-interacting problem the first term on the right gives the kinetic energy, and $\tilde{e}(\ell)$ vanishes. Due to Bloch's theorem, $\tilde{e}(\ell)$ is symmetric around $\ell = 1/2$ and a periodic function with a period equal to unity. Expanding $\tilde{e}(\ell)$ for $\ell \to 0^+$, $\tilde{e}(\ell) = \tilde{e}(0) + \varepsilon\ell + \mathcal{O}(\ell^2)$. This implies that the slope of the dispersion relation for $\ell \to 0^+$ is $\hbar^2/(2MR^2) + \varepsilon$. On the other hand, for $\ell \to 1^-$, $\tilde{e}(\ell) = \tilde{e}(0) + \varepsilon(1-\ell) + \mathcal{O}(1-\ell)^2$, and thus the slope of the dispersion relation for $\ell \to 1^-$ is $\hbar^2/2MR^2 - \varepsilon$. In the hysteresis loop it is precisely these slopes that determine the two critical frequencies, $\hbar\Omega_1 = \hbar^2/(2MR^2) + \varepsilon$ and $\hbar\Omega_2 = \hbar^2/(2MR^2) - \varepsilon$ as seen in the schematic plot of Fig. (3.5).

Therefore, it is crucial to determine the value of ε. Interestingly, the difference $\hbar(\Omega_1 - \Omega_2)$ is equal to 2ε. Furthermore, the sign of Ω_2 determines the stability of persistent currents. Specifically, the condition $\Omega_2 = 0$ represents the critical value of the coupling for metastability of the currents, and metastability will be present if $\Omega_2 < 0$.

[1] I stress that this expression is consistent with Bloch's theorem, since the energy may also be written as $E(\ell)/N = [\hbar^2/(2MR^2)][\ell^2 + (\ell^2 - \ell)] + e(\ell)$, where the last term is periodic.

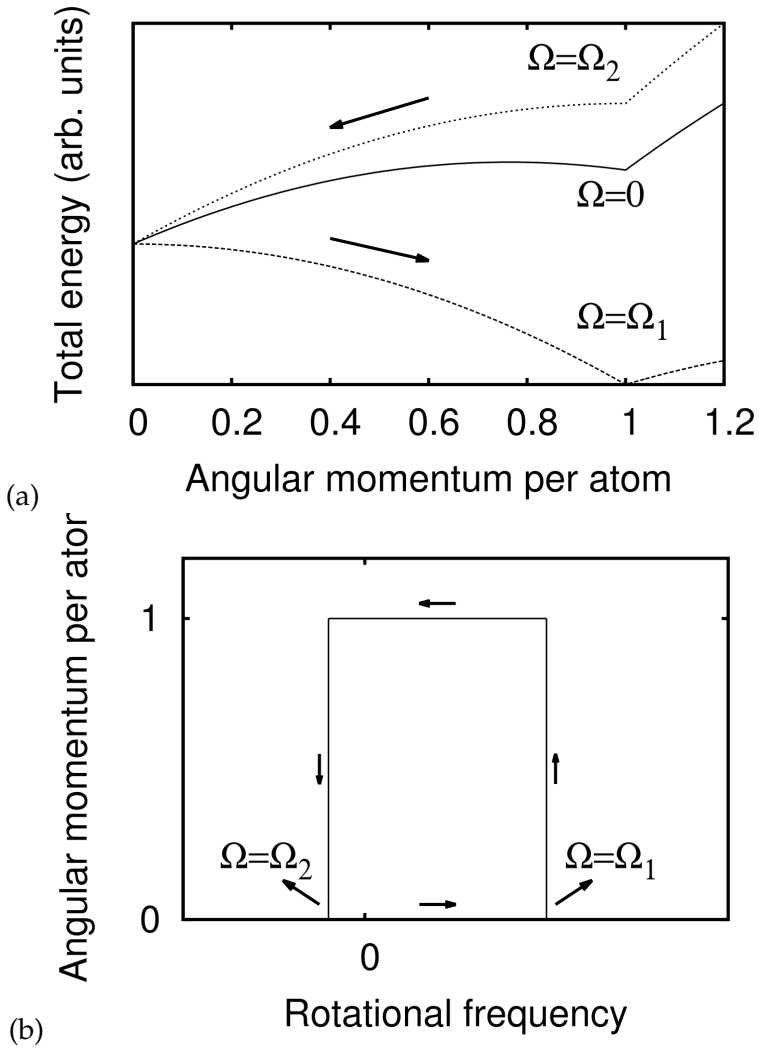

FIGURE 3.5: (a) Energy in the lab frame, $E(\ell)$, (middle curve) as well as in the rotating frame, $E_{rot}(\ell)/N = E(\ell)/N - \ell\Omega$. (b) The two critical frequencies Ω_1 and Ω_2 for which the slope of E_{rot} vanishes for $\ell \to 0^+$ and $\ell \to 1^-$, respectively. The arrows in the upper plot indicate the instability that results from the disappearance of the energy barrier; in the lower plot they indicate the hysteresis loop as the rotational frequency varies.

3.4 Hysteresis within the mean-field approximation

I begin with the mean-field approximation and consider the limit $\ell \to 1^-$. One can construct a Taylor-series expansion of the energy as a function of the small parameter $1 - \ell$. Since I am interested in the slope of the dispersion relation, we only need the linear term in the expansion for the energy. To get that, it suffices to consider only the dominant state in the order parameter Ψ, which is ϕ_1, with $\phi_m = e^{im\theta}/\sqrt{2\pi}$ as well as the neighbouring modes ϕ_0 and ϕ_2. This is due to the fact that there is a cross term in the energy that comes from the scattering of two atoms with $m = 1$ resulting an atom with $m = 0$ and $m = 2$. This term can be negative and thus lowers the

energy [67]. Therefore, I write the order parameter as

$$\Psi = c_0\phi_0 + c_1\phi_1 + c_2\phi_2, \tag{3.4}$$

where the coefficients are real variational parameters and also $|c_1|$ is of order unity, while $|c_0|$ and $|c_2|$ are both of order $1-\ell$. I stress that a completely analogous calculation holds for $\ell \to 0$, in which case one should assume that $\Psi = c_{-1}\phi_{-1} + c_0\phi_0 + c_1\phi_1$. We should also mention that one may work more generally with the three states $\phi_{1-\kappa}, \phi_\kappa$, and $\phi_{1+\kappa}$ with $\kappa = 2, 3, \ldots$, however the fact that the kinetic energy of the states ϕ_m scales as m^2 necessarily implies that $\kappa = 1$.

The coefficients appearing in Eq. (3.4) must satisfy the normalization condition, $c_0^2 + c_1^2 + c_2^2 = 1$, and the constraint of fixed angular momentum, $c_1^2 + 2c_2^2 = \ell$ or $c_0^2 - c_2^2 = 1-\ell$. The expectation value of the energy per particle in the above state is

$$\frac{E}{Ne_0} = c_1^2 + 4c_2^2 + \frac{\gamma}{2}(c_0^4 + c_1^4 + c_2^4 + 4c_0^2c_1^2 + 4c_1^2c_2^2 + 4c_0^2c_2^2 - 4|c_0|c_1^2|c_2|), \tag{3.5}$$

where c_0 and c_2 have been assumed to have opposite signs in order to minimize the energy. Here, $\gamma/2 = Ng/(2e_0) = 2NaR/S$ is the ratio between the interaction energy of the gas with a homogeneous density distribution and the kinetic energy $e_0 \equiv \hbar^2/(2MR^2)$. After linearization, the above expression may also be written as

$$\frac{E}{Ne_0} - \frac{\gamma}{2} \approx \ell + 2c_2^2 + \gamma(|c_0| - |c_2|)^2. \tag{3.6}$$

Writing $c_0 = \sqrt{1-\ell}\cosh\theta$, $c_2 = \sqrt{1-\ell}\sinh\theta$, the value of θ that minimizes the energy is $\theta_0 = (1/4)\ln(2\gamma+1)$. Therefore, the minimized energy is

$$\frac{E}{Ne_0} - \frac{\gamma}{2} \approx \ell + [\sqrt{2\gamma+1} - 1](1-\ell). \tag{3.7}$$

The derived value of ε is thus $\varepsilon/e_0 = \sqrt{2\gamma+1} - 1$ and therefore

$$\Omega_1/\omega = \sqrt{2\gamma+1}, \tag{3.8}$$

while

$$\Omega_2/\omega = 2 - \sqrt{2\gamma+1}, \tag{3.9}$$

where $\omega = e_0/\hbar$. We note here that Ω_2 will vanish if $\gamma = 3/2$. This is the well-known result for the stability of persistent currents in a single-component gas, see, e.g., Ref.[68].

One can generalize the above results (using Bloch's theorem) in the interval $m \le \ell \le m+1$, where

$$\Omega_1/\omega = 2m + \sqrt{2\gamma+1}, \tag{3.10}$$

and

$$\Omega_2/\omega = 2(m+1) - \sqrt{2\gamma+1}. \tag{3.11}$$

From the last equation it follows trivially that the critical value of the coupling for stability of persistent currents (for $\ell = m+1$) is $\gamma = (2m+1)(2m+3)/2$.

3.5 Hysteresis beyond the mean-field approximation

I now examine the same problem beyond the mean-field approximation. To do this, I use the method of diagonalization of the many-body Hamiltonian. The order parameter can be written as Eq. (3.4), although the actual space, consisting of the number of single-particle states, $|\phi_n\rangle$, is infinite. Therefore the eigenstates may be written in the form

$$|\Psi_n\rangle = \sum_p c_p^n |p\rangle, \tag{3.12}$$

where $n = 0, 1, 2, \ldots$ denotes the excited state with index n. Here the states $|p\rangle$ are defined as $|0^p, 1^{N-2p}, 2^p\rangle$, since we have only taken into account the three single-particle states of Eq. (3.4), meaning ϕ_0, ϕ_1 and ϕ_2.

The notation $|0^{N_0}, 1^{N_1}, 2^{N_2}\rangle$ indicates that N_0 atoms occupy the state ϕ_0, etc. Clearly, the states $|p\rangle$ are eigenstates of the number operator and of the angular momentum for a system of N atoms with angular momentum $L = N$.

Again, one can work more generally with the three states $\phi_{1-\kappa}, \phi_1$ and $\phi_{1+\kappa}$, with $\kappa = 2, 3, \ldots$, however the corresponding problem becomes block diagonal, with the triplet of the states with $\kappa = 1$ giving the slope we are looking for [68].

One can diagonalize the Hamiltonian in this truncated space using the Bogoliubov transformation to obtain the eigenvalues $E_n(L)$, which are

$$E_n(L = N)/e_0 - \gamma(N-1)/2 = N - (\gamma+1) + \sqrt{2\gamma+1}(1+2n). \tag{3.13}$$

Considering the states $|p'\rangle = |0^{p+1}, 1^{p-2m}, 2^{p-1}\rangle$ with N atoms and $L = N-2$ units of angular momentum, one can follow the same procedure as before to find that

$$E_n(L = N-2)/e_0 - \gamma(N-1)/2 = N - 4 - (\gamma+1) + \sqrt{2\gamma+1}(3+2n). \tag{3.14}$$

From the lowest eigenvalues of each of the last two equations it follows that $\Omega_2/\omega = 2 - \sqrt{2\gamma+1}$, in agreement with the result of the mean-field approximation, Eq. (3.9).

The approach considered above has assumed that N is $\gg 1$, while the expectation value of m [in Eq. (3.12)] is of order unity. To find the finite-N corrections for the critical values of Ω_1 and Ω_2, I have diagonalized the many-body Hamiltonian numerically without making any approximations beyond the truncation to some set of single-particle states ϕ_m with $-m_{\max} \le m \le m_{\max}$. Figure (3.6) shows the result of such a calculation for $N = 5$ atoms, $0 \le L \le 10$, $\gamma = Ng/e_0 = 0.5$, and $m_{\max} = 4$, where we plot a few eigenvalues for each value of L. The dispersion relation satisfies Bloch's theorem. The fact that the form of this figure is the same as that of the schematic plot of Fig. (3.5) indicates the presence of hysteresis. I stress that for the small values of N that we consider here one can easily reach the Tonks-Girardeau

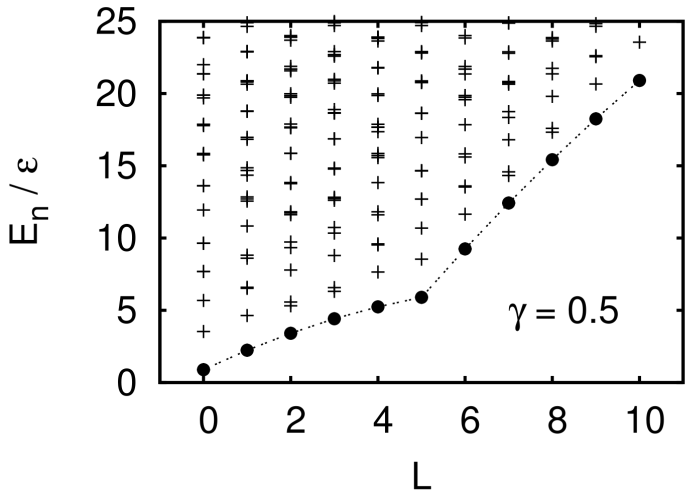

FIGURE 3.6: The lowest eigenvalues E_n of the Hamiltonian for $N = 5$ atoms as a function of L. The calculation was performed for $\gamma = Ng/e_0 = 0.5$, and $m_{\max} = 4$.

limit. In this limit γ is at least of order N^2. Thus, in order for the mean-field approximation to be valid, γ has to be much less than N^2.

3.5.1 Critical rotational frequencies of the hysteresis loop

Having diagonalized the Hamiltonian, I extract the slope of the dispersion relation from the difference $E_0(L = 1) - E_0(L = 0)$ to determine Ω_1. Finally, by varying the atom number, $2 \leq N \leq 5$ I find that Ω_1 can be approximated as

$$\Omega_1/\omega \approx 1.0953 - 0.8782/N - 0.7513/N^2, \tag{3.15}$$

for $\gamma = 0.1$. A subtle point in this calculation is the fact that the interaction strength increases with increasing N. This results in a greater depletion of the condensate. Thus, in order to extract the critical frequencies associated with the hysteresis, we keep γ fixed or equivalently allow g to scale like $1/N$.

In obtaining Eq. (3.15) $m_{\max}$ was set equal to 5. Clearly, $m_{\max}$ must be sufficiently large so that the fitting parameters have saturated. The differences in these parameters due to changing $m_{\max} = 4$ to $m_{\max} = 5$ are in the seventh, third, and second significant figures respectively. The value of the leading term is remarkably close to the value of $\sqrt{1+2\gamma} \approx 1.09544$ found in Eq. (3.8), which is the asymptotic value of Ω_1 for $N \to \infty$. Similar calculations for $\gamma = 1$ yield

$$\Omega_1/\omega \approx 1.7453 - 0.6101/N - 0.1353/N^2. \tag{3.16}$$

Although the leading term is still reasonably close to $\sqrt{1+2\gamma} \approx 1.73205$, the agreement is materially worse. This is presumably because of the larger depletion of the condensate due to the stronger interaction strength.

One general observation that emerges from the above analysis is that the effect of the finiteness of the system and of the correlations, captured by the method of diagonalization, is to decrease the value of Ω_1 from its asymptotic value (and thus to

increase the value of Ω_2). I comment on this observation in the following section.

Last but not least, we mention that the value of the angular momentum for which the winding number of the order parameter changes is exactly $\ell = 1/2$. In the equivalent language of solitary waves [69] the lowest-energy state with this value of the angular momentum corresponds to a "dark" solitary wave (i.e., a solitary wave with a node) which, although dark, still has a finite propagation velocity due to the finiteness of the ring [45, 69]. Assuming without loss of generality that the center of the solitary wave is located at $\theta = \pi$, the real part of the order parameter has a fixed sign. Its minimum value (at $\theta = \pi$) vanishes as $\ell \to (1/2)^-$. The imaginary part of the order parameter has sinusoidal behaviour and vanishes at $\theta = 0, \pi$, and 2π. This necessarily implies that the net phase change is zero. On the other hand, for $\ell \to (1/2)^+$, the minimum value of the real part of the order parameter, which remains $\theta = \pi$, is negative and approaches zero from below. This tiny change in the minimum value of the real part of the order parameter from slightly positive to slightly negative is sufficient to change the winding number of the phase. I stress that this tiny change can be described perturbatively and, although there is a violent rearrangement of the phase of the order parameter, this rearrangement can in no way prevent hysteresis.

3.6 Metastability of persistent currents in a small system

The dispersion relation can develop an energy barrier for sufficiently strong and repulsive interatomic interactions which separates the state with $L = N$ from the state with $L = 0$ [6]. While $E_0(L = N)$ will always have a higher energy than $E_0(L = 0)$ [in fact, $E_0(L = N) - E_0(L = 0) = Ne_0$], the state with $L = N$ is then metastable. As a result, if the system is prepared in the state $L = N$, it will require an exponentially long time for the system to decay, since this process must occur via quantum tunnelling. Furthermore, the energy and the angular momentum of the gas must be dissipated by small non-uniformities in the trapping potential.

In this section I investigate two different questions. The first is the critical value of the coupling required for the system to develop an energy barrier with particular concern for finite-N effects. The second question is how the matrix element of a symmetry-breaking single-particle operator ΔV, that can connect the two eigenstates of lowest energy, $|L = N\rangle$ and $|L = 0\rangle$, depends on the atom number N (for reasons explained below).

Starting with the first question, according to Eq. (3.9) the critical value of γ for the existence of a local minimum for $\ell \to 1^-$ is $\gamma_{\rm cr} = 3/2$. This is an asymptotic result, which does not include finite-N corrections. To find these corrections, I choose a fixed value of the atom number N and identify the critical value of g, $g_{\rm cr}$, which gives a zero slope in the dispersion relation for $\ell \to 1^-$, i.e., $E_0(L = N) = E_0(L = N - 1)$. The result of this calculation is given in Fig. (3.7) where I plot the number of atoms on the x axis and the product $Ng_{\rm cr} \equiv \gamma_{\rm cr}$ on the y axis, for $m_{\rm max} = 4$. These results can be fit as

$$\gamma_{\rm cr} \approx 1.5106 + 0.6020/N + 8.2820/N^2 - 34.8262/N^3 + 73.3879/N^4. \qquad (3.17)$$

The small deviation of the asymptotic value of $\gamma_{\rm cr}$ in the above expression from the expected value of $3/2$ is presumably due to the truncation, $m_{\rm max} = 4$, the limited

number of atoms we have considered, $N \leq 10$, and correlations which are absent in the calculation within the mean-field approximation. Interestingly, as seen from Fig. (3.7), the value of $\gamma_{\rm cr}$ for a finite number of atoms is higher than $3/2$. Since this is determined by the slope $E_0(L=N) - E_0(L=N-1)$, we conclude that the correlations which are captured within the present approach (but are absent within the mean-field approximation) lower the energy of the state with $L = N-1$ more than that of the state with $L = N$. Thus, a higher value of γ is necessary to stabilize the currents in the state with $L = N$. The same mechanism which increases $\gamma_{\rm cr}$ is also responsible for the decrease (increase) of $\Omega_1(\Omega_2)$ found in the previous section.

I turn now to the second question regarding the decay rate of the persistent current. In order for the energy barrier (which develops for sufficiently strong interatomic interactions) to prevent the decay of the currents and render them metastable with an exponentially long decay time, the matrix element of any symmetry-breaking single-particle operator ΔV connecting the states $|L = N\rangle$ and $|L = 0\rangle$ must be vanishingly small [2].

Otherwise the presence of the energy barrier becomes irrelevant and the currents will decay.

To investigate this problem, I consider a single-particle operator $\Delta V = V_0 \sum_{i=1}^{N} \delta(\theta_i)$, which is a sum of delta function potentials intended to mimic irregularities in the trap [54]. This potential breaks the axial symmetry of the Hamiltonian and induces transitions between the two states $|L = N\rangle$ and $|L = 0\rangle$. I thus evaluate the matrix element $\langle L = N|\Delta V|L = 0\rangle$, making use of the lowest-energy states $|L = 0\rangle$ and $|L = N\rangle$ that I got from the diagonalization of the axially-symmetric Hamiltonian. Clearly the only terms which give a nonzero contribution to this matrix element are those that raise the angular momentum by $L = N$ units when acting on $|L = 0\rangle$,

$$\langle L = N|\Delta V|L = 0\rangle = V_0 \sum_n \langle L = N|a_n a^{\dagger}_{n+N}|L = 0\rangle. \tag{3.18}$$

In the absence of interactions, when all the atoms are in the single-particle state ϕ_1 and ϕ_0, respectively, this matrix element vanishes for all $N > 1$. This is also the case in the mean-field approximation. To get a non-vanishing matrix element it is necessary to consider non-zero interactions that deplete the condensate and a finite number of atoms.

Figure (3.8) shows the value of $|\langle L = N|\Delta V|L = 0\rangle / V_0|$ as function of N. Again, I keep $\gamma = gN$ fixed for the reasons stated above. Here, I have chosen $\gamma = gN = 0.1$, while the states $|L = 0\rangle$ and $|L = N\rangle$ have been evaluated for $m_{\rm max} = 5$. As seen from this plot, this matrix element shows an exponential decay as function of N.

To get an understanding of this decay we recall that the operator ΔV excites atoms, increasing their angular momentum by N units. Furthermore, the amplitudes c_m in the expression of Eq. (3.12) decay very rapidly with m, as seen in Fig. (3.9) for $N = 50$ atoms with a rate that does not depend on N. This is a more general result that also holds in more extended spaces. The fact that the amplitudes of the states contributing to $|L = 0\rangle$ and $|L = N\rangle$ decrease rapidly as one moves away from $|0^N\rangle$ and $|1^N\rangle$ along with the nature of ΔV, which induces single-particle excitations by N units of angular momentum, combine to make this decay matrix element extremely sensitive to N.

[2] Processes due to perturbation theory of higher-order are allowed, but they are suppressed for weak irregularities.

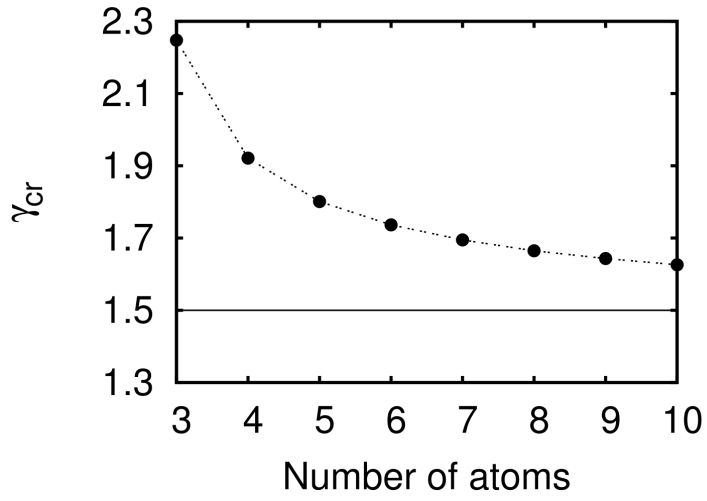

FIGURE 3.7: The value of γ_{cr} obtained with the method of diagonalization as a function of N for $m_{max} = 4$. The horizontal line shows the asymptotic value of $\gamma_{cr} = 3/2$.

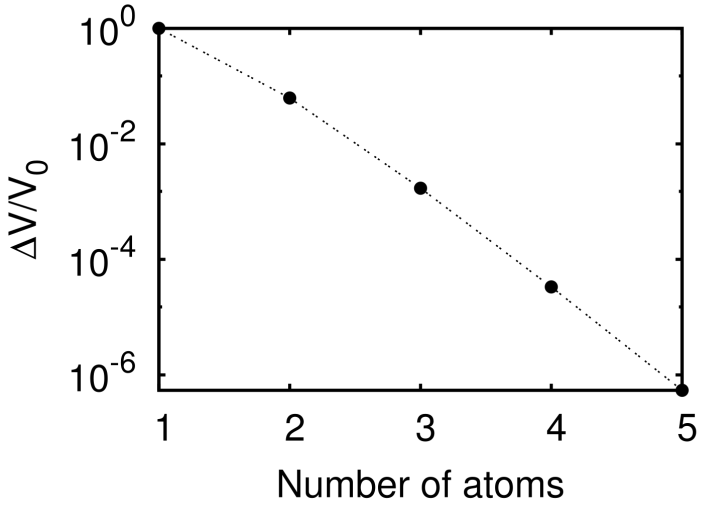

FIGURE 3.8: The matrix element of the operator ΔV between the states with $|L = N\rangle$ and $|L = 0\rangle$, $|\langle L = N|\Delta V|L = 0\rangle / V_0|$, as function of the atom number N, for a fixed value of $\gamma = gN = 0.1$. Here the states $|L = 0\rangle$ and $|L = N\rangle$ have been evaluated for $m_{max} = 5$.

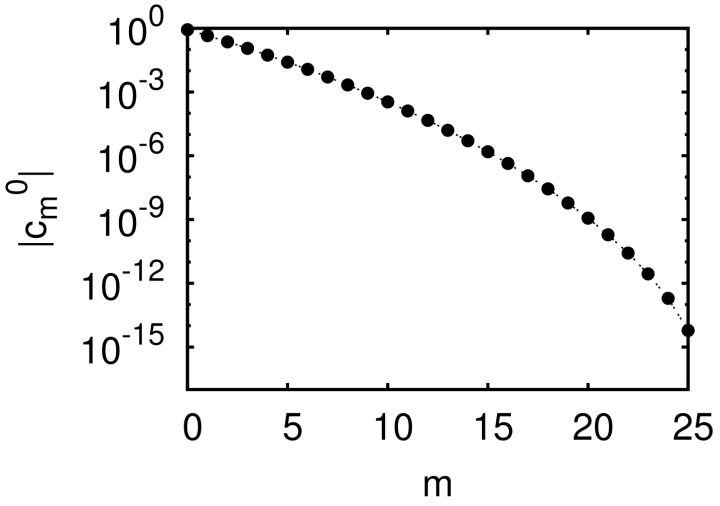

FIGURE 3.9: The amplitudes $|c_m^0|$ which appear in Eq. (3.12) as function of the index m, for $N = 50$ atoms, $L = 0$, $\gamma = 5$, and truncation within the single-particle states ϕ_{-1}, ϕ_0, and ϕ_1.

Thus, the main result of this section is, quite generally, that a combination of sufficiently strong interatomic interactions and a finite number of atoms enhances the size of the matrix element and thus reduces the timescale that is associated with the decay rate of the persistent currents. This result may be interesting to explore experimentally in small systems with an interaction whose strength can be tuned.

3.7 Connection with the experiments on hysteresis and metastability

In order for our assumption of one-dimensional motion to be valid, I stress that the interaction energy must be much smaller than the quantum of energy associated with the motion of the atoms in the transverse direction (or, equivalently, the coherence length must be much larger than the transverse dimensions of the annulus/torus). However, this assumption is violated under current typical conditions, and thus the motion is not quasi-one-dimensional.

For example, in the experiment of Ref. [35], where ^{23}Na atoms were used, the chemical potential is $\mu/\hbar \approx 2\pi \times 1.7$ kHz, while the frequencies of the annular-like trapping potential (in the transverse direction) are $\omega_1 \approx 472$ Hz and $\omega_2 \approx 188$ Hz. (As a result, it has been argued that vortex-antivortex pairs form in this experiment.) Thus, it is not possible to make neither a quantitative nor a qualitative comparison of the present theory and the experiment of Ref. [35]. An investigation of this problem using a more realistic model is underway and will be described in a future publication.

If one wants nonetheless to get an estimate for the critical frequencies of hysteresis for the parameters of Ref. [35] using the present theory, it follows for a radius of $R \approx 19.5$ μm, that $\omega = \hbar/(2MR^2) \approx 3.6$ Hz. Given that $a \approx 28$ Å, $N \approx 4 \times 10^5$, and $S = \pi a_1 a_2$ with $a_i = \sqrt{\hbar/(M\omega_i)}$, i.e., $a_1 \approx 2.42$ μm and $a_2 \approx 3.83$ μm, the dimensionless parameter $\gamma = 2NaR/S$ has the value $\gamma \approx 1500.0$. It then follows

from Eqs. (3.8) and (3.9) that $\Omega_1 \approx 197.2$ Hz and $\Omega_2 \approx -190.0$ Hz. Clearly, these large frequencies (as compared to the observed frequencies, which are on the order of 10 Hz) are due to the very large value of γ, which is the ratio between the interaction energy of a homogeneous cloud with a density $n_0 = N/(2\pi RS)$ and the kinetic energy associated with the motion in the ring, $\hbar^2/(2MR^2)$.

It is also interesting to make estimates for the case where the motion is quasi-one-dimensional. Consider, for example, the case where the experimental conditions are identical to those of Ref. [35] but where the number of atoms is reduced by, e.g., a factor of 4×10^4 to the value $N = 10$. This would reduce the interaction energy to the extent that the conditions for one-dimensional motion would be fulfilled. This reduction in N would also reduce the value of γ to ≈ 0.04. The corresponding critical frequencies would become $\Omega_1 \approx 3.7$ Hz and $\Omega_2 \approx 3.5$ Hz. While the difference between Ω_1 and Ω_2 is small, $\approx 2\gamma\omega$, it would still be of interest to investigate their dependence on N, which, according to the results of Sec. 3.5, is $1/N$ to leading order.

It would also be interesting to investigate the effect of finite system size on the critical value for stability of the persistent currents in such small systems. According to the results of Sec. 3.6, the value of $\gamma_{\rm cr}$ also scales as $1/N$ to leading order. Last but not least, the decay time of the currents would show a much more rapid – and thus more pronounced – decrease as N decreases.

3.8 Summary and conclusions

In this chapter I investigated the phenomenon of hysteresis and of metastability in a Bose-Einstein condensed cloud of atoms which are confined in a ring potential. Interestingly, this problem has recently been examined experimentally [35], while many other experiments have focused on the question of persistent currents in such topologically nontrivial potentials [58, 59, 60, 61, 62, 63, 64, 65].

In the phenomenon of hysteresis the main question is the evaluation of the critical frequencies. As I have shown, in a purely one-dimensional system these two frequencies are related as a consequence of Bloch's theorem. Further, I have evaluated those both within the mean-field approximation and beyond mean field (i.e., by numerical diagonalization of the many-body Hamiltonian) in order to determine finite-N corrections.

I also performed calculations of the critical coupling for the metastability of superflow and of the matrix element associated with the decay rate in a finite system of atoms. As I have argued, the depletion of the condensate due to the interaction combined with the finiteness of the atom number can cause the decay rate to increase exponentially with decreasing N. Thus, the general tendency is that the finiteness of a system makes the supercurrents more fragile, in the sense that it increases the decay rate of the currents, and it also increases the critical coupling for metastability.

Given the recent experimental activities on the problems of hysteresis and of metastability, and also given the more general tendency in the community of cold atoms to move to small systems (i.e., systems with a small atom number N) the present results, which I believe are of theoretical interest, may also become experimentally relevant in the near future.

Chapter 4

"Quantum solitons" in a Bose-Einstein condensate

The problem that is investigated in this chapter is motivated by recent experiments on Bose-Einstein condensed atoms which rotate in annular/toroidal traps. I study the effect of the finiteness of the atom number N on the states of lowest energy for a fixed expectation value of the angular momentum (yrast states[1]), under periodic boundary conditions. To attack this problem, I develop a general strategy, considering a linear superposition of the eigenstates of the many-body Hamiltonian, with amplitudes that I extract from the mean field approximation. This many-body state breaks the symmetry of the Hamiltonian, it has the same energy to leading order in N as the mean-field state and the corresponding eigenstate of the Hamiltonian, however it has a lower energy to subleading order in N and thus it is energetically favorable.

Therefore, this project offers a suitable framework for the investigation of the effect of the finiteness of the atom number N on the states of lowest energy for a fixed expectation value of the angular momentum, under periodic boundary conditions. Thus, the problem examined in the present chapter attacks the more general question of the relationship between the mean-field approximation - where one assumes a product many-body state and fixes the expectation value of the angular momentum - and the diagonalization of the many-body Hamiltonian - that is associated with eigenstates of the angular momentum and of the number operator.

As mentioned in the previous chapter, several recent experiments in the field of cold atomic gases have managed to rotate, and even create persistent currents in clouds of Bose-Einstein condensed atoms which are confined in annular/toroidal traps [58, 59, 60, 61, 62, 63, 64, 65, 70]. Furthermore, the phenomenon of hysteresis has also been observed in an annular trap [35], as presented in Chap. 3. Thus, a question which arises naturally from these experiments is what is the state of lowest energy of the atoms for a fixed expectation value of their angular momentum.

[1]The terminology of the “yrast" state that we use below refers to the eigenstate with the lowest eigenenergy, i.e., the state which minimizes the energy for some given eigenvalue of the angular momentum. The same term is used within the mean-field approximation, where one fixes the expectation value of the angular momentum, instead. We stress that these yrast states play a fundamental role in the rotational response of these systems, very much like the phonon-roton spectrum in the problem of liquid Helium.

4.1 The state of lowest energy for a fixed expectation value of the angular momentum

Within the mean-field, Gross-Pitaevskii, approximation the answer to this question is given by the well-known solitary-wave solutions [56, 69], which have been investigated thoroughly [71, 72, 73]. When a trapping potential is present – as in the case of cold atomic gases – interesting phenomena arise. The easiest problem is that of an infinite system in the longitudinal direction, with a very tight trapping potential in the transverse direction. In this case the transverse degrees of freedom are frozen and the problem essentially reduces to that of an infinite line. As the transverse trapping potential becomes less tight and/or the interaction strength increases, the transverse degrees of freedom start to play a role, and as a result deviations from the standard quadratic nonlinear Schrödinger equation [74] arise.

4.1.1 Dark and grey solitary-wave solutions

Another interesting possibility is that of a ring-like trap, where one has to impose periodic boundary conditions. As discussed also in Sec. (2.4.1), in this case the solutions are given by Jacobi elliptic functions [44, 45]. Depending on the ratio between the coherence length and the periphery of the ring the density of these solutions is either sinusoidal, or exponentially localized [45]. In an infinite system the “dark" solution (i.e., the one with a density notch) is also static. On the other hand – as a result of the periodic boundary conditions – in a ring of a finite length the dark solitary wave has a finite velocity, while the static solitary-wave solution is “grey" (i.e., the lowest value of the density is nonzero), however no solution exists which is both dark and static [45].

4.1.2 Experimental relevance of the finiteness in the atom number

The behavior becomes more complicated when correlations are introducted beyond the mean-field approximation [75, 76], which is actually the subject of the present study. More specifically, in what follows below, I investigate the effect of the finiteness of the atom number N (assumed to be of order unity) on the state of lowest energy, for a fixed expectation value of the angular momentum. I stress that this question is not only interesting theoretically, but also it is experimentally relevant, since recent experiments have managed to trap and detect very small numbers of atoms, see, e.g., Ref. [77] and also Ref. [78]. I should also mention that other studies [79, 80, 81, 82, 83, 84, 85, 86, 87] have investigated a closely-related question, i.e., the relationship between the “classical" and the “quantum" solitons, according to their terminology.

4.1.3 A problem with the symmetry of the many-body Hamiltonian

To go beyond the mean-field approximation the method of diagonalization of the many-body Hamiltonian may be used. The questions which are associated with the energy of the system (i.e., the dispersion relation, or the velocity of propagation of the waves, which is given by the slope of the dispersion relation) are examined in a straightforward way from the eigenvalues of the Hamiltonian.

On the other hand, extracting the density is much more challenging, since the eigenstates that one gets from the diagonalization of the many-body Hamiltonian are also eigenstates of the angular momentum and thus they are rotationally invariant. Still, the physically-relevant solutions are the ones which break the axial symmetry of the Hamiltonian and clearly are not eigenstates of the angular momentum.

To answer this question, it is instructive to recall that the energy of the mean-field state for some fixed expectation value of the angular momentum coincides to leading order in N with that of the corresponding "yrast" state [88, 89] (an "yrast" state is the lowest-energy eigenstate of the Hamiltonian and is also an eigenstate of the angular momentum, however, the yrast state has a lower energy to subleading order in N.

4.1.4 Adopted approach

Having all this in mind, I adopt the following strategy, which is based on the minimization of the energy: First of all, I evaluate the yrast states (diagonalizing the many-body Hamiltonian). Then, I evaluate the corresponding product, mean-field-like many-body state. Projecting this state on the yrast state of some given angular momentum, I evaluate the amplitude that corresponds to the yrast state of this specific value of the angular momentum. Using these amplitudes, I thus construct a many-body state which is a linear superposition of yrast states. This state has an energy which coincides to leading order in N with that of the corresponding yrast state, and of the mean-field state, but it has a lower energy to subleading order in N, even than the yrast state, provided that the effective interaction between the atoms is repulsive.

In what follows below I first describe the model in Sec. 4.2. In Sec. 4.3 I then present my results for the many-body state that I construct. I then apply this method to the case of weak interactions in Sec. 4.4, where I solve the (two-state) model analytically. In Sec. 4.5 I go beyond the two-state model, presenting my numerical results and the finite-N corrections that I am interested in. In Sec. 4.6 I investigate the asymptotic form of the many-body state, which reduces to the well-known state of the mean-field approximation in the appropriate limit of a large atom number. In Sec. 4.7 I discuss the experimental relevance of the results of this chapter. Finally, in Sec. 4.8 I give a summary of the main results of this chapter and some conclusions.

4.2 A variational many-body state

I assume for simplicity one-dimensional motion of bosonic atoms under periodic boundary conditions, as in a ring potential. This assumption is valid provided that the interaction energy is much smaller than the quantum of energy of the trapping potential in the transverse direction, in which case the transverse degrees of freedom are frozen.

If a_m and $a_m^\dagger$ are the annihilation and creation operators of an atom with angular momentum $m\hbar$, the Hamiltonian that I consider is the same as in Eq. (2.44)

$$H = \frac{\hbar^2}{2MR^2} \sum_{m=m_{\min}}^{m_{\max}} m^2 a_m^\dagger a_m + \frac{g}{2} \sum_{m,n,k,l} a_m^\dagger a_n^\dagger a_k a_l \, \delta_{m+n,k+l}. \tag{4.1}$$

Here $m_{\min}$ and $m_{\max}$ are the lowest and the highest values of m, M is the atom mass, R is the radius of the ring, and g is the matrix element for elastic s-wave atom-atom collisions (assumed to be positive).

There are thus two energy scales in the problem, namely the kinetic energy per particle $e_0 = \hbar^2/(2MR^2)$ associated with the motion of the atoms along the ring, and the interaction energy per particle, which for a homogeneous gas is equal to $(N-1)g/2$. It is convenient to introduce the dimensionless quantity γ as the ratio between the interaction energy $(N-1)g$ and the kinetic energy e_0, $\gamma = (N-1)g/e_0$.

4.2.1 Constructing the many-body state as a superposition of yrast states

The first step in this calculation is the evaluation of the yrast states $|\Phi_{\rm ex}(L)\rangle$, which are eigenstates of the Hamiltonian H, of the operator of the angular momentum L and of the number operator N. As mentioned above, the Hamiltonian is axially symmetric and thus the eigenstates respect this symmetry, which implies that the corresponding single-particle density distribution is axially symmetric. Indeed, if $\Psi(\theta)$ is the destruction operator of a particle at an angle θ, then the single-particle density is,

$$\begin{aligned} n(\theta) &= \langle\Phi_{\rm ex}(L)|\Psi^\dagger(\theta)\Psi(\theta)|\Phi_{\rm ex}(L)\rangle = \\ &= \frac{1}{2\pi R}\sum_{m,m'}\langle\Phi_{\rm ex}(L)|a_m^\dagger a_{m'}|\Phi_{\rm ex}(L)\rangle\, e^{i(m'-m)\theta} = \\ &= \frac{N}{2\pi R}, \end{aligned} \tag{4.2}$$

i.e., $n(\theta)$ is spatially independent and equal to the mean density for any value of L, since the matrix elements appearing above are diagonal.

On the other hand, the physically-relevant solutions are not axially symmetric (in general), and this is a major problem. Actually, this problem has a much more general aspect, namely the relationship between the mean-field solutions, which break the axial symmetry of the problem, and the eigenstates of the many-body Hamiltonian – where one is working with eigenstates of the angular momentum, too, and as a result they respect the axial symmetry of the problem. Here the general strategy that I develop allows us to extract the spatially-dependent single-particle density distribution from the yrast states, going beyond the mean-field approximation.

A widely-used method for breaking the symmetry

It should be mentioned that a method that is often used to overcome this difficulty of breaking of the axial symmetry is to introduce correlation functions, for example [90],

$$n^{(2)}(\theta,\theta_0) \propto \langle\Phi_{\rm ex}(L)|\Psi^\dagger(\theta)\Psi^\dagger(\theta_0)\Psi(\theta_0)\Psi(\theta)|\Phi_{\rm ex}(L)\rangle, \tag{4.3}$$

whre θ_0 is some reference point. While this method does indeed break the axial symmetry and allows to get a qualitative answer, it cannot be trusted quantitatively. The easiest example is that of weak interactions (examined in detail below), where

it turns out that

$$\begin{aligned} n^{(2)}(\theta,\theta_0) &\propto [N(N-1)+2L(N-L)\cos(\theta-\theta_0)] \\ &\propto (1-1/N)+2\ell(1-\ell)\cos(\theta-\theta_0), \end{aligned} \tag{4.4}$$

where $\ell = L/N$. The above expression cannot in any way be related to the density that results from the mean-field approximation,

$$n_{\rm MF}(\theta) = \frac{N}{2\pi R}(1+2\sqrt{\ell(1-\ell)}\cos\theta), \tag{4.5}$$

not even in the limit of large values of N. (In the above expression I have assumed that the arbitrary position of the minimum of the density is at $\theta = 0$.) Therefore, I conclude that $n^{(2)}(\theta,\theta_0)$ cannot be used for quantitative comparisons.

Breaking the symmetry

The way that I proceed is thus the following. I introduce an essentially variational many-body state, namely

$$|\Phi(\ell_0)\rangle = \mathcal{C}\sum_{L=L_{\rm min}}^{L_{\rm max}} \langle\Phi_{\rm ex}(L)|\Phi_{\rm MF}(\ell_0)\rangle\,|\Phi_{\rm ex}(L)\rangle, \tag{4.6}$$

where $\mathcal{C}$ is the normalization constant. In other words, I take the inner product between the mean-field state with some angular momentum per atom $\ell_0\hbar$, $|\Phi_{\rm MF}(\ell_0)\rangle$, and some yrast state with total angular momentum $L\hbar$, $|\Phi_{\rm ex}(L)\rangle$, to get the amplitudes $\langle\Phi_{\rm ex}(L)|\Phi_{\rm MF}(\ell_0)\rangle$. From these amplitudes I then construct a linear superposition of eigenstates $|\Phi_{\rm ex}(L)\rangle$, which constitute the many-body state $|\Phi(\ell_0)\rangle$.

This state has the following crucial features: (i) it has the desired expectation value of angular momentum, (ii) to leading order in N it has the same energy as the mean-field state, as well as the yrast state, but it has a lower energy to subleading order in N, (iii) it gives the same single-particle density distribution as the mean-field state for large values of N, and (iv) finally it is not fragmented.

Turning to $|\Phi_{\rm MF}(\ell_0)\rangle$, this is a product many-body state, which corresponds to the order parameter of the mean-field approximation; obviously we work in the same basis of single-particle states, with $m_{\rm min} \le m \le m_{\rm max}$, as in the method of diagonalization,

$$|\Phi_{\rm MF}(\ell_0)\rangle \;=\; \frac{1}{\sqrt{N!}}\left(\sum_{m=m_{\rm min}}^{m_{\rm max}} c_m a_m^\dagger\right)^N |0\rangle, \tag{4.7}$$

where $|0\rangle$ denotes the vacuum; also c_m are real, variational parameters, which I evaluate by minimizing the corresponding expectation value of the energy

$$E_{\rm MF}(\ell_0) = N\frac{\hbar^2}{2MR^2}\sum_{m=m_{\rm min}}^{m_{\rm max}} m^2c_m^2 + \frac{1}{2}N(N-1)g\int\left|\sum_{m=m_{\rm min}}^{m_{\rm max}} c_m\phi_m\right|^4 d\theta. \tag{4.8}$$

Here $\phi_m = e^{im\theta}/\sqrt{2\pi}$ are the single-particle eigenstates of the ring potential with an eigenvalue of the angular momentum equal to $m\hbar$ and an eigenenergy $E_m = m^2e_0$.

The normalization imposes the constraint $\sum c_m^2 = 1$, while there is the additional constraint that comes from the expectation value of the angular momentum being $\ell_0 = L_0/N, \sum m c_m^2 = \ell_0$.

4.3 Results of the method for weak interactions

I start with the limit of weak interactions, where I can solve this problem analytically, and then proceed with the more general problem of stronger interactions.

To define the limit of "weak"/"strong" interactions let us introduce quite generally the ratio between the interaction energy per particle of the homogeneous gas $(N-1)g/2$ and the kinetic energy $E_m = m^2\hbar^2/(2MR^2)$, which is $\gamma/(2m^2)$. For some given value of γ, setting $\gamma/(2m^2) \sim 1$, the maximum value of $|m|$ has to be (much) larger than $\sqrt{\gamma/2}$ in order to achieve convergence. In terms of length scales, the parameter $\sqrt{\gamma}$ gives the ratio between the radius of the ring R and the coherence length ξ (ignoring terms of order unity). The limit $\gamma \ll 1$ defines the regime of "weak" interactions, where $\xi \gg R$, while for $1 \ll \gamma \ll N^2$, then $R/N \ll \xi \ll R$, which is the "Thomas-Fermi" limit. When γ becomes of order N^2, then the system approaches the Tonks-Girardeau limit, where the coherence length ξ becomes comparable to the inter-particle spacing R/N and correlations play a crucial role.

4.4 The two-state model

When $\gamma \ll 1$ one may work with the single-particle states ϕ_0 and ϕ_1 only. In this case $|\Phi_{\rm ex}(L)\rangle$ has the very simple form (because of the two constraints)

$$|\Phi_{\rm ex}(L)\rangle = |0^{N-L}, 1^L\rangle. \tag{4.9}$$

In the above notation the state ϕ_0 has $N-L$ atoms, and the state ϕ_1 has L atoms.

The mean-field, many-body state is

$$\begin{aligned} |\Phi_{\rm MF}(\ell_0)\rangle &= \frac{1}{\sqrt{N!}}(c_0 a_0^\dagger + c_1 a_1^\dagger)^N|0\rangle \\ &= \sum_{L=0}^{N} \frac{\sqrt{N!}}{(N-L)!L!}\, c_0^{N-L} c_1^L (a_0^\dagger)^{N-L}(a_1^\dagger)^L|0\rangle \\ &= \sum_{L=0}^{N} \frac{\sqrt{N!}}{\sqrt{(N-L)!L!}}\, c_0^{N-L} c_1^L |0^{N-L}, 1^L\rangle \\ &\equiv \sum_{L=0}^{N} d_L(\ell_0)|0^{N-L}, 1^L\rangle. \end{aligned} \tag{4.10}$$

The actual value of c_0^2 is $1-\ell_0$, while $c_1^2 = \ell_0$.

The amplitudes of the above state of Eq. (4.10) have the interesting feature that

$$|d_L(\ell_0)|^2 \equiv \frac{N!}{(N-L)!L!}\, c_0^{2(N-L)} c_1^{2L}$$

$$\approx \frac{e^{-(L-N\ell_0)^2/[2N\ell_0(1-\ell_0)]}}{\sqrt{2\pi N\ell_0(1-\ell_0)}}\left[1+\mathcal{O}\left(\frac{1}{\sqrt{N}}\right)\right], \tag{4.11}$$

where the approximate expression holds for large N and $\ell_0(1-\ell_0)$ not close to zero. Therefore, $|d_L|^2$ is a Gaussian, with its peak at $L_0 = N\ell_0$ (scaling as N) and a width which is of order $\sqrt{N}$, which becomes a delta function in the limit of large N. The above observations are generic features and not specific to the two-state model and thus are central in the analysis that follows below.

In the final step of our calculation I evaluate $|\Phi(\ell_0)\rangle$, which is, as described earlier,

$$|\Phi(\ell_0)\rangle = \mathcal{C}\sum_{L=0}^{N} d_L(\ell_0)|0^{N-L},1^L\rangle. \tag{4.12}$$

In the two-state approximation, $|\Phi(\ell_0)\rangle$ coincides with $|\Phi_{\rm MF}(\ell_0)\rangle$. However, I stress that this is not a general result, as I explain below.

4.4.1 Calculating the observables in the two-state model: Energy spectrum and density profile

The single-particle density matrix of $|\Phi(\ell_0)\rangle$, $\rho_{ij} = \langle\Phi(\ell_0)|a_i^\dagger a_j|\Phi(\ell_0)\rangle$ (with $i,j = 0,1$), is

$$\rho = N\begin{pmatrix} c_0^2 & c_0c_1 \\ c_0c_1 & c_1^2 \end{pmatrix}.$$

The two eigenvalues are $\lambda = 0$ and $\lambda = 1$ (the determinant of the above matrix vanishes and thus one of the eigenvalues has to vanish). The state $|\Phi(\ell_0)\rangle$ is not fragmented, as one expects. The eigenvector that corresponds to $\lambda = 1$ is the expected one, namely $\psi = c_0\phi_0 + c_1\phi_1$. The single-particle density distribution in $|\Phi(\ell_0)\rangle$ is given by

$$\begin{aligned} n(\theta) &= \langle\Phi(\ell_0)|\Psi^\dagger(\theta)\Psi(\theta)|\Phi(\ell_0)\rangle = \\ &= \frac{N}{2\pi R}[1+2|c_0||c_1|\cos(\theta-\theta_0)] \\ &= \frac{N}{2\pi R}[1+2\sqrt{\ell_0(1-\ell_0)}\cos(\theta-\theta_0)], \end{aligned} \tag{4.13}$$

where θ_0 is the relative phase between c_0 and c_1. This phase is arbitrary reflecting the rotational invariance of the Hamiltonian; assuming that c_0 and c_1 are real, it is equal either to zero, or π. However, this degeneracy is lifted when the symmetry is broken (see more in the following paragraph). The result of Eq. (4.13) coincides with that of Eq. (4.5), and therefore in the two-state model the density that one gets from the many-body state $|\Phi(\ell_0)\rangle$ is the same as the one derived from the Jacobi (sinusoidal) solutions of the mean-field Gross-Pitaevskii approximation.

Furthermore, the expectation value of the energy $\mathcal{E}$ in the state $|\Phi(\ell_0)\rangle$ is

$$\mathcal{E} - \frac{g}{2}N(N-1) = \frac{\hbar^2 L_0}{2MR^2} + gL_0(N-L_0)(1-1/N), \tag{4.14}$$

where again the phase θ_0 does not appear in the energy due to the assumed axial symmetry of the Hamiltonian. When a "weak" symmetry breaking potential $\Delta V = V_0 \cos\theta$ is added to the Hamiltonian, then

$$\begin{aligned} \mathcal{E} - gN(N-1)/2 &= \frac{\hbar^2 L_0}{2MR^2} + gL_0(N-L_0)(1-1/N) + \\ &+ \cos\theta_0 N V_0 \sqrt{\ell_0(1-\ell_0)}/2. \end{aligned} \tag{4.15}$$

Here we see an explicit dependence of the energy on θ_0. Obviously θ_0 has to take the value π in order for the energy to be minimized. As a result, the single-particle density is $n(\theta) = N(1 - 2\sqrt{\ell(1-\ell)}\cos\theta)/(2\pi R)$, and thus the minimum of the density is at $\theta = 0$, where the value of the potential is maximum.

In Eqs. (4.14) and (4.15) above we observe that to leading order in N the interaction energy agrees with that of the eigenstates $|0^{N-L_0}, 1^{L_0}\rangle$, $\mathcal{E}_{\rm ex}$, which is

$$\mathcal{E}_{\rm ex} - \frac{g}{2}N(N-1) = \frac{\hbar^2 L_0}{2MR^2} + gL_0(N-L_0), \tag{4.16}$$

but is lower to subleading order. This result is due to the fact that the dispersion relation has a negative curvature and the fact that $|\Phi(\ell_0)\rangle$ samples other states – of order $\sqrt{N}$ – around the "pure" state $|\Phi_{\rm ex}(L_0)\rangle = |0^{N-L_0}, 1^{L_0}\rangle$. Actually, this lowering of the energy to subleading order in N of the state that breaks the axial symmetry reflects precisely this fact, namely that the curvature of the dispersion relation is negative (provided that the effective interaction is repulsive).

Indeed, quite generally, a distribution $P(L) \propto e^{-(L-L_0)^2/N}/\sqrt{N}$ [see Eq. (4.11)] gives an average of $gL(N-L)$ which differs from $gL_0(N-L_0)$ [see Eq. (4.16)] that is proportional to $-gN$, as in Eq. (4.14),

$$\begin{aligned} g\langle L(N-L)\rangle - gL_0(N-L_0) &\propto -gN\,\mathrm{erf}(L_0/\sqrt{N}) \\ &\approx -gN, \end{aligned} \tag{4.17}$$

where $\mathrm{erf}(x)$ is the error function.

4.5 Beyond the two-state model: Finite-N corrections and numerical results

The two-state model discussed above has the advantage that all the calculations may be performed analytically. In addition, it provides an accurate description of $|\Phi(\ell_0)\rangle$ in the limit of weak interactions, $\gamma \ll 1$. The results of the previous section demonstrate that in this limit the state $|\Phi(\ell_0)\rangle$ – even in a system with a finite number of atoms N – essentially coincides with the one of the mean-field approximation (which, in the limit of weak interactions, gives a sinusoidal density distribution).

On the other hand, as we also saw earlier, the very drastic restriction to the states ϕ_0 and ϕ_1 (only) forces the yrast states to have the trivial form $|0^{N-L}, 1^L\rangle$ and therefore all the angular momentum is carried by the single-particle state ϕ_1. It is thus necessary to work in a more extended space. In the interval $0 \leq \ell \leq 1$ and for relatively stronger interactions in addition to ϕ_0 and ϕ_1, ϕ_2 and ϕ_{-1} have the most significant

contribution, while if one wants to go even further ϕ_3 and ϕ_{-2} have to be included, too, and so on, as Bloch's theorem implies [49].

4.5.1 The three-state model

Before I turn to a higher truncation, it is instructive to examine the case with ϕ_0 and ϕ_1, and ϕ_2 only. In this subspace the yrast states have the form

$$|\Phi_{\rm ex}(L)\rangle = \sum_m (-1)^m b_m |0^{N-L+m}, 1^{L-2m}, 2^m\rangle, \tag{4.18}$$

where the amplitudes b_m are Gaussian distributed [88, 89]. The corresponding mean-field, product many-body state has the form

$$\begin{aligned} |\Phi_{\rm MF}(\ell_0)\rangle &= \frac{1}{\sqrt{N!}}(c_0 a_0^\dagger + c_1 a_1^\dagger + c_2 a_2^\dagger)^N |0\rangle \\ &= \sum_{k=0}^{N}\sum_{m=0}^{k} \frac{\sqrt{N!}\, c_0^{N-k} c_1^{k-m} c_2^m}{\sqrt{(N-k)!(k-m)!m!}} |0^{N-k}, 1^{k-m}, 2^m\rangle \\ &\equiv \sum_{k=0}^{N}\sum_{m=0}^{k} d_{m,k} |0^{N-k}, 1^{k-m}, 2^m\rangle. \end{aligned} \tag{4.19}$$

Taking the inner product between the states $|\Phi_{\rm ex}(L)\rangle$ and $|\Phi_{\rm MF}(\ell_0)\rangle$ forces the index "k" to be equal to $L-m$ and therefore the only non-zero amplitudes are $d_{m,L-m}$, which are also Gaussian distributed. When more single-particle states are included in the calculation the general picture is the same, with the only difference being that one has a multi-dimensional space; if r is the number of single-particle states, the dimensionality is $r-2$, because of the two constraints. In each direction in this space one still obtains Gaussian distributions and on a qualitative level the final result is essentially the same.

4.5.2 Results from an expanded Hilbert space

I proceed now with the calculation within the states $\phi_{-2}, \phi_{-1}, \phi_0, \phi_1, \phi_2$ and ϕ_3. I stress that γ has to be sufficiently large in order to have a significant occupancy of the states other than the ones with $m=0$ and $m=1$, since otherwise one goes back to the two-state model described earlier. In addition we have to make sure that we have reached convergence with respect to the number of single-particle states that are considered and finally we have to ensure that Bloch's theorem [49] is not violated. As described also above, I first evaluate the yrast states $|\Phi_{\rm ex}(L)\rangle$ for $-2N \le L \le 3N$, diagonalizing the many-body Hamiltonian. I also evaluate $|\Phi_{\rm MF}(\ell_0)\rangle$

$$|\Phi_{\rm MF}(\ell_0)\rangle = \frac{1}{\sqrt{N!}}\left(\sum_{m=-2}^{m=3} c_m a_m^\dagger\right)^N |0\rangle, \tag{4.20}$$

where $c_{-2}, c_{-1}, c_0, c_1, c_2$ and c_3 are evaluated from the constraint minimization of the energy. In the final step I evaluate $|\Phi(\ell_0)\rangle$ using Eq. (4.6), which then gives us the single-particle density distribution (or any other observable).

In Figs. (4.1) and (4.2) I plot the corrections of the density in a finite system of atoms for various values of the angular momentum. The solid curves show the single-particle density $n(\theta)$ that corresponds to $|\Phi(\ell_0)\rangle$, while the dashed ones show the density $n_{\rm MF}(\theta)$ that corresponds to the mean-field state $|\Phi_{\rm MF}(\ell_0)\rangle$. In Fig. (4.1) $N = 4$, and in Fig. (4.2) $N = 8$, while $\gamma = 0.9$ in both of them. Also ℓ_0 takes the three values $\ell_0 = 0.5, 0.75$, and 1. According to Bloch's theorem [49] for any $0 \leq \ell_0 \leq 1$, the density distribution is the same also for $\ell_0' = 1 - \ell_0$, as well as for $\ell_0' = \ell_0 + \kappa$, where κ is an integer. In other words, the three graphs for $\ell_0 = 1\,(L = 4)$, $\ell_0 = 3/4\,(L = 3)$, and $\ell_0 = 1/2\,(L = 2)$ shown in Fig. (4.1) cover all the possible values of the angular momentum of the whole spectrum (for $N = 4$).

For $\ell_0 = 1$ both $n_{\rm MF}(\theta)$, as well as $n(\theta)$ are constant, even for small values of N. I stress, however, that the two states are different, since $|\Phi(\ell_0)\rangle$ coincides with the yrast state for $L = N = 4$. For example, even within the space with $m = 0, 1$, and 2,

$$|\Phi_{\rm MF}(\ell_0 = 1)\rangle = |0^0, 1^4, 2^0\rangle, \tag{4.21}$$

while

$$|\Phi(\ell_0 = 1)\rangle = A_1|0^0, 1^4, 2^0\rangle + A_2|0^1, 1^2, 2^1\rangle + A_3|0^2, 1^0, 2^2\rangle, \tag{4.22}$$

where A_i are constants. As a result, the energy of the two states is also different, see Fig. (4.3), which shows the dispersion relation, that we discuss in the next section).

Returning to the density shown in Figs. (4.1) and (4.2), while for $\ell_0 = 1$ the situation is not interesting (at least with regards to the density), for $\ell_0 = 1/2$ and $\ell_0 = 3/4$ there are deviations (between the dashed and the solid curves). For $\ell_0 = 1/2$ within the mean-field approximation, the "dark" solitary wave forms and $n_{\rm MF}(\theta)$ has a node. As seen from Fig. (4.1), $n(\theta)$ still has a node. The most significant deviations appear at the maxima of the density. The state of lower energy flattens out within a larger interval compared to the mean-field density. These deviations (almost) disappear for $N = 8$, as shown in Fig. (4.2), where γ is still 0.9 (I discuss the asymptotic behavior of $|\Phi(\ell)\rangle$ in the following section). Finally, for $\ell_0 = 3/4$, there is still a significant deviation between $n(\theta)$ and $n_{\rm MF}(\theta)$, with roughly the same characteristics as the case $\ell_0 = 1/2$.

Although the difference between the density is small (due to the relatively small value of γ, which makes $|c_0|$ and $|c_1|$ to be much larger than all the other coefficients – for example, for $\ell = 1/2$, $|c_0| = |c_1|$ are roughly 7 times larger than $|c_{-1}| = |c_2|$), still these results are generic. Increasing γ will give more pronounced differences, however the problem becomes more demanding computationally, since we also need to make sure that convergence with respect to the single-particle states that we have considered has been achieved.

4.6 Asymptotic limit of the many-body state

It is crucial to confirm that the observables from the state that I have introduced coincide with the ones of the mean-field state in the appropriate limit of large N. The relevant limit is the one where N increases, with the ratio between the interaction energy and the kinetic energy kept fixed (which in our notation is γ).

As seen already in the previous section, the density indeed approaches that of the mean-field state. Turning to the energy, as argued in Sec. 4.4, in the above limit, the

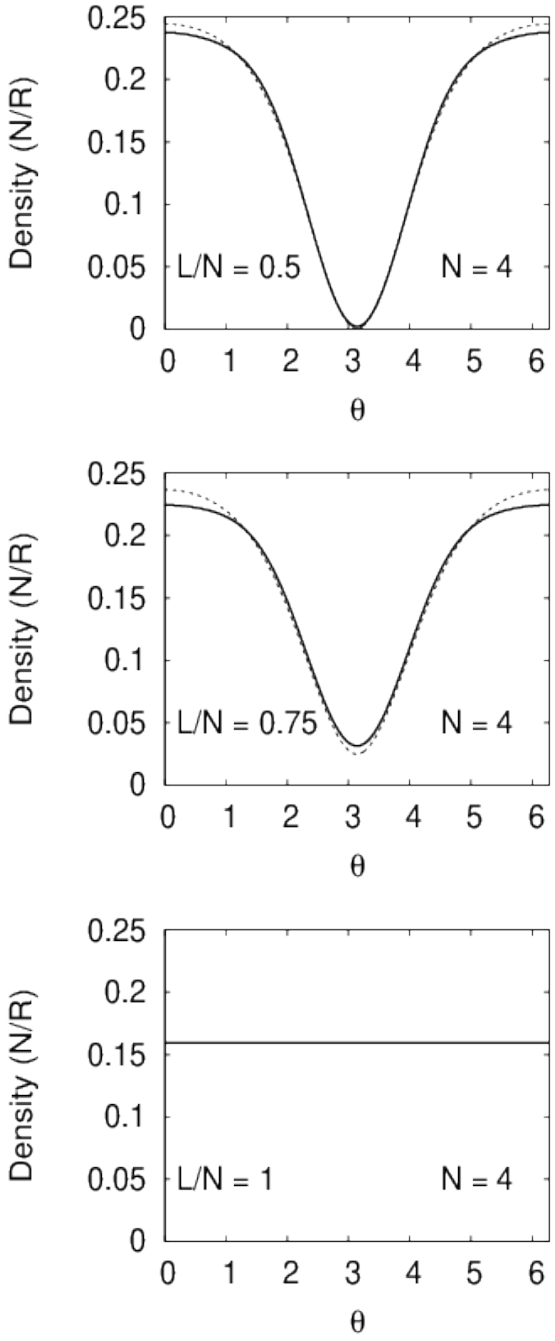

FIGURE 4.1: Solid lines: The single-particle density distribution $n(\theta)$ corresponding to $|\Phi(\ell)\rangle$ of a finite system of atoms, within the space of states with $m = -2, \ldots, 3$, for $N = 4$ atoms, $\gamma = (N-1)g/e_0 = 0.9$, and $\ell = L/N = 0.50, 0.75$, and 1.00, from top to bottom. Dashed lines: The single-particle density distribution $n_{\rm MF}(\theta)$, corresponding to $|\Phi_{\rm MF}(\ell)\rangle$, derived within the mean-field approximation, via the minimization of the energy, for the same set of parameters.

dominant amplitude in $|\Phi(\ell_0)\rangle$ is the one that corresponds to $L_0 = N\ell_0$, which is the yrast state $|\Phi_{\rm ex}(L_0)\rangle$ with this value of $L = L_0$. As shown in Ref. [88, 89] $|\Phi_{\rm ex}(L_0)\rangle$ has the same energy to leading order in N as the mean-field state $|\Phi_{\rm MF}(\ell_0)\rangle$, and the same result is true for $|\Phi(\ell_0)\rangle$. Therefore, all these three states have the same energy

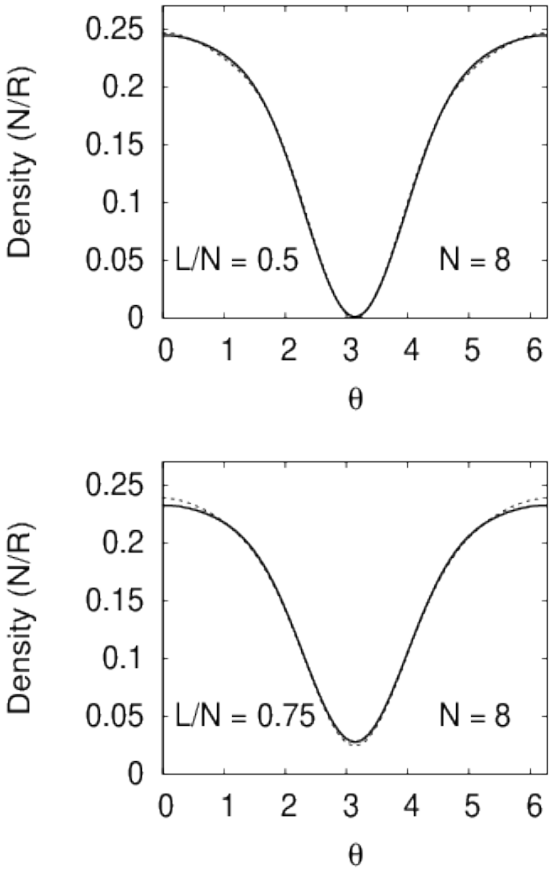

FIGURE 4.2: Same as Fig. (4.1), with $N = 8$ and $\gamma = 0.9$. The difference between the two curves is hardly visible.

to leading order in N.

Still, I stress that there is a clear hierarchy of the energies of the three states to subleading order in N: $|\Phi_{\rm MF}(\ell_0)\rangle$ has the highest energy, $|\Phi_{\rm ex}(L_0)\rangle$ has a lower energy, and $|\Phi(\ell_0)\rangle$ has the lowest. The first inequality has been analysed in Ref. [88, 89], while the second is due to the simple reason stated earlier [see Eq. (4.17)].

In Fig. (4.3) I plot the dispersion relation, which is evaluated within the mean-field approximation, the energy of the corresponding eigenstates of the many-body Hamiltonian, and the energy of $|\Phi(\ell_0)\rangle$ that I have evaluated. In the middle curve L on the x-axis is the eigenvalue of the angular momentum operator $\hat{L}$, while in the other two curves L is the expectation value of the angular momentum operator $\hat{L}$. These results provide full support of the arguments we made about the hierarchy of the energies. I should also mention that according to Bloch's theorem [49], the total energy spectrum (i.e., for higher values of ℓ) is the one shown in Fig. (3.7), on top of a parabola.

Turning to the question of fragmentation, the single-particle density matrix of $|\Phi(\ell_0)\rangle$, $\rho_{ij} = \langle\Phi(\ell_0)|a_i^\dagger a_j|\Phi(\ell_0)\rangle = c_i c_j$. This result generalizes the one I found earlier for the case of two modes only. This matrix has one eigenvalue which is equal to unity, while all the other eigenvalues vanish and indeed $|\Phi(\ell_0)\rangle$ is not fragmented. The eigenvector that corresponds to the nonzero eigenvalue is the expected one, i.e., $\sum c_m \phi_m$.

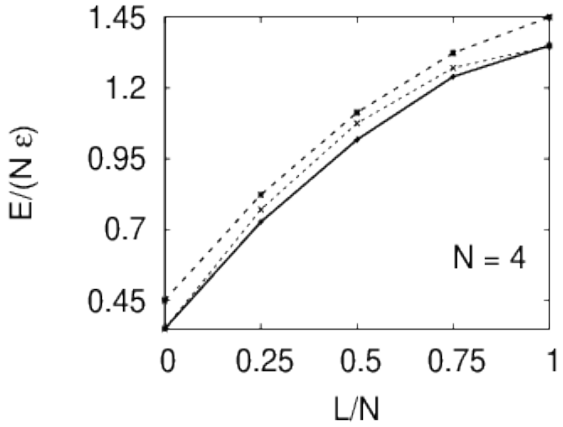

FIGURE 4.3: The energy per particle as function of the angular momentum per particle for $N = 4$ atoms, $\gamma = (N-1)g/e_0 = 0.9$, and $\ell = L/N = 0.50, 0.75$, and 1.00, within the space of states with $m = -2, \ldots, 3$. The lowest data corresponds to the expectation value of the energy of $|\Phi(\ell)\rangle$, the middle to the eigenvalues of the yrast states $|\Phi_{\rm ex}(L)\rangle$, and the top to the energy of the mean-field state $|\Phi_{\rm MF}(\ell)\rangle$. I stress that in the middle curve L on the x-axis is the eigenvalue of $\hat{L}$, while in the other two curves L is the expectation value of $\hat{L}$.

4.7 Experimental relevance

In order to make contact with experiment, the first question is the extent that under typical conditions the motion of the atoms is quasi-one-dimensional, as I have assumed here. If we consider the experiment of Ref. [35] as an example, the system is far from this limit. In this experiment, where $N \approx 4 \times 10^5$ ^{23}Na atoms were used, their chemical potential $\mu/\hbar \approx 2\pi \times 1.7$ kHz, was much larger than the frequencies of the (annular-like) trapping potential, $\omega_1 \approx 472$ Hz and $\omega_2 \approx 188$ Hz. The dimensionless quantity that describes the transition to the one-dimensional limit may also be expressed in terms of Na/R, which has to be $\ll 1$ in this limit. Here $R \approx 19.5$ μm is the mean radius of the torus/annulus and $a \approx 28$ Å is the s-wave scattering length for atom-atom collisions. Since Na/r is $\approx 5 \times 10^2$, the system is not in the limit of quasi-one-dimensional motion.

In addition, the dimensionless parameter $\gamma = 2NaR/S$, where S is the cross section of the torus/annulus, for the parameters of this experiment is on the order of 1500 [34]. As a result, this experiment is in the Thomas-Fermi regime (see Sec. 4.5), where $1 \ll \gamma \ll N^2$, and the solitary waves will resemble the well-known ones of an infinite system.

According to the results of this chapter three conditions have to be satisfied in order for the corrections that we have predicted to be substantial. First of all, N should not exceed ~ 10, since otherwise the corrections will be suppressed. Also the interaction energy has to be sufficiently strong, i.e., γ should be at least of order unity, since otherwise the system is in the limit of weak interactions, where the deviations we have found are also suppressed. Finally, Na/R has to be $\ll 1$.

If one simply reduces N under the conditions of the experiment of Ref. [35], by e.g., a factor of order 10^5, so that N will become equal to 4, then $Na/R \sim 5 \times 10^{-3}$,

i.e., indeed it will be $\ll 1$, however $\gamma \sim 1.5 \times 10^{-2}$, i.e., γ will also become $\ll 1$, which will bring the system to the limit of weak interactions. Therefore, in addition to reducing N by a large factor, one should also decrease $S \propto 1/\sqrt{\omega_1\omega_2}$ (by, e.g., increasing the trapping frequencies in the transverse direction), in order to make $\gamma \sim 1$.

4.8 Summary and conclusions

To summarize the results of this chapter, the general problem that I investigated is the relationship between the mean-field approximation and the method of diagonalization of the many-body Hamiltonian, in connection with the spontaneous breaking of the symmetry of the Hamiltonian (assumed to be axially symmetric). While the mean-field states break the symmetry of the Hamiltonian by construction, the eigenstates of the Hamiltonian respect this symmetry, thus giving rise to a single-particle density distribution which is always axially symmetric. Still, in a real system the axial symmetry is broken, even under very weak symmetry-breaking mechanisms (if one is interested in the solutions which do not break the symmetry, these are the eigenstates of the Hamiltonian.)

One of the main goals of this project was to investigate how one breaks the symmetry, going also beyond the mean-field approximation. To achieve this goal, I made use of the mean-field approximation and then constructed a linear superposition of the eigenstates of the many-body Hamiltonian. This state breaks the symmetry and is not a product state, i.e., it goes beyond the mean-field approximation. I stress that the method that I have developed is general and may be applied to other problems, as well.

Another main result of this project is the actual problem where I have applied this method, namely the finite-N corrections of the well-known solitary-wave solutions which result within the (one-dimensional) nonlinear Schrödinger equation in a finite ring. Interestingly, the state that I have used is one of "minimum-uncertainty" and in a sense it is the mostly "classical". According to the results, for low interaction strengths, where the two-state model is a good approximation, the finite-N corrections are negligible and one gets back to the ordinary Jacobi solutions of the nonlinear Schrödinger equation (which are sinusoidal in this limit). For larger interaction strengths and/or small atom numbers, where more than two single-particle states need to be considered, these corrections become non-negligible and there are significant deviations between our many-body state and the mean-field state.

While I have not proven that the many-body state that I have constructed provides the absolute minimum of the energy, what I do know is that it has the same energy to leading order in N, and a lower energy to subleading order in N, as compared the mean-field state, and the corresponding eigenstate of the Hamiltonian. In other words, this many-body state lowers the energy bound. One subtle point in these arguments is of course that in this comparison the yrast state is an eigenstate of the operator of the angular momentum $\hat{L}$, and thus "L" is the corresponding eigenvalue. Within the other two states, since they break the symmetry, "L" is the expectation value of $\hat{L}$.

When the angular momentum is an integer multiple of $\hbar$ within the mean-field approximation the density of the cloud is predicted to be homogeneous. According to

my results, the single-particle density distribution remains homogeneous even for a small atom number. When the angular momentum per particle is equal to a half integer within the mean-field approximation the “dark" solitary wave forms, which has a node in its density. According to the presented analysis in a system with a small atom number the single-particle density distribution still has a node, with the main effect of the finiteness appearing at the “edges" of the wave. Interestingly, a “universal" feature of the dark solitary wave is its velocity of propagation, which turns out to be $\hbar/(2MR)$ (for any interaction strength, or any atom number N), as I have found numerically, essentially due to Bloch's theorem [49]. Last but not least, deviations in the density between the two states are also present in the intermediate values of the angular momentum (between 0.5 and 1). These corrections vanish in the appropriate limit of large N. My suggested many-body state is not a “solitary-wave state" in the strict sense of a travelling-wave solution and for this reason I have not used this terminology here.

The interaction strengths that I have considered keep us away from the correlated, Tonks-Girardeau limit. It would be interesting to try to push this calculation to this regime [85, 91]. In the spirit of density functional theory, one may develop a mean-field description [92] and then use the present approach, which may still provide an accurate description of the system. It would be interesting to study this problem and get some quantitative answers.

Chapter 5

Mixtures of two Bose gases

In this chapter I study the rotational properties of a two-component Bose-Einstein condensed gas of distinguishable atoms which are confined in a ring potential using both the mean-field approximation, as well as the method of diagonalization of the many-body Hamiltonian. I demonstrate that the angular momentum may be given to the system either via single-particle, or "collective" excitation. Furthermore, despite the complexity of this problem, under rather typical conditions the dispersion relation takes a remarkably simple and regular form. Finally, I argue that under certain conditions the dispersion relation is determined via collective excitation. The corresponding many-body state, which, in addition to the interaction energy minimizes also the kinetic energy, is dictated by elementary number theory.

5.1 Introduction

I have already mentioned in the previous chapters that experimentalists have managed to trap atoms in toroidal/annular traps and have even created persistent currents in them [58, 59, 60, 61, 62, 63, 64, 70]. Going one step further, the addition of an extra, distinguishable, component may also be considered. This problem is even more interesting. The extra degrees of freedom associated with this extra component introduce novel and highly non-trivial effects. Interestingly enough, this has also become possible experimentally [65].

On the theoretical side [51, 95, 96, 97, 98, 99, 100, 101, 102], the general problem of a Bose-Einstein condensate with two distinguishable components – which I label as "A" and "B" – that is confined in a ring potential may be attacked at various levels of complication/difficulty. Assuming equal masses M for the two components, there are two cases that one may distinguish. The first is the "symmetric" one, where the scattering lengths a_{AA}, a_{BB}, and a_{AB} for elastic atom-atom collisions between AA, BB, and AB atoms respectively are all equal to each other. The second (and more realistic) is the "asymmetric" one, where at least two of the scattering lengths are not equal to each other.

In the symmetric case the dispersion relation is exactly linear within the mean-field approximation [51] for $0 \leq L \leq N_B$ and $N_A \leq L \leq N = N_A + N_B$, where $L\hbar$ is the total angular momentum of the system, and N_A, N_B are the numbers of particles in each component (here I assume without loss of generality that $N_B < N_A$). In the asymmetric case, the linearity of the spectrum disappears [101, 102], while for $N_B \leq L \leq N_A$ in both the symmetric and the asymmetric case the dispersion relation is more complex.

In the present project I focus on the asymmetric case and use both the mean-field approximation, as well as the method of diagonalization of the many-body Hamiltonian to study the rotational properties of this system. Two crucial assumptions are made throughout the present chapter. The first is that the inter- and intra-component effective interaction is repulsive. The second is that the two components coexist spatially. The condition for phase coexistence in a finite ring has been derived in Ref. [51] and we make sure we do not violate it with any set of parameters that we use. Roughly speaking this condition demands that the repulsion within the same species is stronger than that of the different ones.

In a real experiment there is also of course the question of dynamic instability. As shown in Ref. [51] the condition of energetic stability coincides with the one of dynamic stability of the system. I should also mention that in spinor condensates realistic dynamic simulations show that the spatial separation of the two components is possible, and this may affect significantly the rotational behaviour of the system, see, e.g., Ref. [97].

According to the results which are described below, under rather typical conditions, the minority component carries the majority of the angular momentum in the whole interval $0 < L \leq N_B$. One of the novel results of this project is that under certain conditions the whole excitation spectrum is quasi-periodic (in addition to the periodicity dictated by the Bloch theorem [49], which holds also in a two-component system [51]) and may be derived from the one for $0 < L \leq N_B$ by exciting the center of mass motion, either of the A component, of the B component, or both.

Furthermore, in the limit of "strong" interactions there is a very simple candidate state that minimizes the interaction energy of the system (under the assumption that there is no phase separation). This is the one where the density is homogeneous in each component separately, i.e., the one where the two order parameters (Ψ_A, Ψ_B) of the two components are in the plane-wave states (ϕ_m, ϕ_n). Here $\phi_m(\theta) = e^{im\theta}/\sqrt{2\pi R}$ are the eigenstates of the non-interacting problem, where R is the radius of the ring, which have an angular momentum $m\hbar$. The corresponding total angular momentum in the pair of states (ϕ_m, ϕ_n) is $L\hbar$, with $L = mN_A + nN_B$. A suitable choice of the integers m and n allows us to give any value to L, provided that N_A and N_B are relatively prime. Clearly, among all the possible values of m and n that satisfy the constraint of the angular momentum, one has to choose the pair of (ϕ_m, ϕ_n) that minimize the kinetic energy.

The number-theoretic arguments presented above hold for any atom number. For large atom numbers the mean-field approximation provides an excellent description of the state of the system. Still, within the mean-field approximation one fixes the population imbalance $x_i = N_i/N$, treating x_i as a continuous variable. Even though the number-theoretic behaviour that results from the analysis presented above still applies, it has more dramatic effects in the limit of small atom numbers. To explore these finite-N effects, I use the method of numerical diagonalization of the many-body Hamiltonian.

In what follows below I describe in Sec. 5.2 the model that I use and the two approaches, namely the mean-field approximation and the diagonalization of the many-body Hamiltonian. In Sec. 5.3 I study the excitation spectrum, starting with the limit of long-wavelength excitation. In the same section I then focus on the mean-field approximation and show how one can derive the whole excitation spectrum starting from the one for $0 \leq L \leq N_B$. Then, in Sec. 5.4 I investigate the excitation spectrum

beyond the mean-field approximation, diagonalizing the many-body Hamiltonian. I first present an alternative way of exciting the system collectively and present an approximate generalization of Bloch's theorem. Finally, I compare the results that I get from the diagonalization with the ones of the mean-field approximation. In Sec. 5.5 I present a conjecture about the form of the many-body state that is expected to be the state of lowest energy under some conditions that are analysed. Finally, in Sec. 5.6 I give a summary and an overview of the results of this chapter. Section 5.7 has the form of an appendix. There, I present a specific example of the diagonalization of the many-body problem.

5.2 Model and approach

The Hamiltonian that I consider is the one already discussed in Chap. 2, Eq. (2.50),

$$\begin{aligned} H = \frac{\hbar^2}{2MR^2} \sum_{m=m_{\min}}^{m_{\max}} m^2 (a_m^\dagger a_m + b_m^\dagger b_m) + \frac{g_{AA}}{2} \sum_{m,n,k,l} a_m^\dagger a_n^\dagger a_k a_l \, \delta_{m+n,k+l} \\ + \frac{g_{BB}}{2} \sum_{m,n,k,l} b_m^\dagger b_n^\dagger b_k b_l \, \delta_{m+n,k+l} + g_{AB} \sum_{m,n,k,l} a_m^\dagger b_n^\dagger a_k b_l \, \delta_{m+n,k+l}, \end{aligned} \tag{5.1}$$

Here $\hbar^2 m^2/(2MR^2)$ is the eigenenergy of the single-particle eigenstates $\phi_m(\theta)$. The mass M is assumed to be the same for the two species, while g_{ij} being the matrix elements for zero-energy elastic collisions between the AA, BB, and AB components. Also, a_m and b_m are the operators which destroy an A, or a B atom with angular momentum $m\hbar$, respectively. In what follows below I set $E_m = m^2 e_0$, where $e_0 = \hbar^2/(2MR^2)$ and also $\hbar = 2M = R = 1$.

In the case of a single component this problem has been attacked by Lieb and Liniger [103, 104] with use of the Bethe ansatz. The case of two species with equal scattering lengths has also been considered, see, e.g., Refs. [105, 106, 107, 108, 109, 110, 111].

In the present project I attack this problem in two ways. The first is within the mean-field approximation, introducing the two order parameters Ψ_A and Ψ_B of the two components, thus solving the corresponding coupled, Gross-Pitaevskii-like equations, as described also in Eq. (2.42) (with Ψ_A and Ψ_B normalized to unity),

$$\begin{aligned} -\frac{\partial^2 \Psi_A}{\partial \theta^2} + 2\pi (g_{AA} N_A |\Psi_A|^2 + g_{AB} N_B |\Psi_B|^2) \Psi_A &= \mu_A \Psi_A \\ -\frac{\partial^2 \Psi_B}{\partial \theta^2} + 2\pi (g_{BB} N_B |\Psi_B|^2 + g_{AB} N_A |\Psi_A|^2) \Psi_B &= \mu_B \Psi_B, \end{aligned} \tag{5.2}$$

where μ_A and μ_B is the chemical potential, and N_A and N_B is the number of atoms in each component. I find the solutions of lowest energy of the above equations imposing the constraint of some fixed angular momentum, as described in detail in Ref. [102].

Alternatively I solve this problem by diagonalizing the many-body Hamiltonian. Within this scheme I choose a set of single-particle states $\phi_m(\theta)$, with $m_{\min} \leq m \leq$

$m_{\max}$. As before, in this subspace of basis states I impose the constraints of a fixed number of atoms A and B, N_A and N_B, respectively. I also impose the constraint of some fixed angular momentum L (which can be shared between the two components), see, e.g., [51]. Finally I diagonalize the resulting Hamiltonian matrix in this subspace, thus deriving the eigenstates and the corresponding eigenenergies.

Finally, I stress that the problem of fixing the angular momentum is intimately connected with the one where the angular velocity of the trap is fixed, instead.

5.3 Excitation spectrum – Mean-field approximation

5.3.1 Elementary excitations

I start with the mean-field approximation. When the system has zero angular momentum, $L = 0$, it is in the state

$$|L = 0\rangle = |0^{N_A}\rangle_A \bigotimes |0^{N_B}\rangle_B, \tag{5.3}$$

where in this notation I have N_A and N_B atoms in the single-particle state with $m = 0$. The total energy of the system is

$$E_0 = \frac{1}{2} g_{AA} N_A (N_A - 1) + g_{AB} N_A N_B + \frac{1}{2} g_{BB} N_B (N_B - 1). \tag{5.4}$$

Giving one unit of angular momentum via single-particle excitation to, e.g., the B component, then

$$|L = 1\rangle = |0^{N_A}\rangle_A \bigotimes |0^{N_B - 1}, 1^1\rangle_B, \tag{5.5}$$

and correspondingly for the species A. The total energy of this state is

$$E' = 1 + \frac{1}{2} g_{AA} N_A (N_A - 1) + g_{AB} N_A N_B + \frac{1}{2} g_{BB} [(N_B - 1)(N_B - 2) + 4(N_B - 1)]. \tag{5.6}$$

Therefore,

$$E' - E_0 = 1 + g_{BB}(N_B - 1), \tag{5.7}$$

where the last term comes from the exchange interaction. From the above equation it follows that it is the ratio

$$r = \frac{g_{BB}(N_B - 1)}{g_{AA}(N_A - 1)}, \tag{5.8}$$

which determines whether the angular momentum goes to the one, or the other component.

In what follows below I set $g_{AA} = g_{BB} = g$, and thus as Eq. (5.8) implies, with the assumption $N_A > N_B$ that I have made, I conclude that it is the B (minority) component that carries the angular momentum, for $L = 1$. By the way, Eq. (5.7) may be identified as the speed of sound c of the B component, or equivalently as the slope

of the dispersion relation for $L \to 0^+$ for exciting it. More specifically,

$$c = 1 + g(N_B - 1). \tag{5.9}$$

5.3.2 Distribution of the angular momentum between the two components

While the above result holds for $L = 1$, it turns out that more generally, under "typical" conditions (which will be analysed below) the minority component carries the largest part of the angular momentum, all the way up to $L = N_B$.

The two order parameters may be expanded in the basis of plane-wave states,

$$\Psi_A = \sum_{m=m_{\min}}^{m_{\max}} c_m \phi_m, \quad \Psi_B = \sum_{m=m_{\min}}^{m_{\max}} d_m \phi_m. \tag{5.10}$$

The corresponding energy per atom is

$$\begin{aligned} \frac{E}{N} &= \sum_{m=m_{\min}}^{m_{\max}} m^2 (x_A c_m^2 + x_B d_m^2) \\ &+ x_A^2 \pi N g \int \left| \sum_{m=m_{\min}}^{m_{\max}} c_m \phi_m \right|^4 d\theta \\ &+ x_B^2 \pi N g \int \left| \sum_{m=m_{\min}}^{m_{\max}} d_m \phi_m \right|^4 d\theta \\ &+ x_A x_B \pi N g_{AB} \int \left| \sum_{m=m_{\min}}^{m_{\max}} c_m \phi_m \right|^2 \left| \sum_{m=m_{\min}}^{m_{\max}} d_m \phi_m \right|^2 d\theta, \end{aligned} \tag{5.11}$$

where $x_i = N_i/N$.

Considering the limit of weak interactions, in the interval $0 \leq \ell \leq 1$ one may work with the states with $m = 0$ and $m = 1$, only,

$$\Psi_A = c_0 \phi_0 + c_1 \phi_1, \quad \Psi_B = d_0 \phi_0 + d_1 \phi_1, \tag{5.12}$$

where $\ell = L/N = x_A c_1^2 + x_B d_1^2$ is the angular momentum per particle. In the "symmetric" case ($g = g_{AB}$) it turns out that for $0 \leq \ell \leq x_B$ [95],

$$c_0^2 = \frac{(x_A - \ell)(1 - \ell)}{x_A(1 - 2\ell)}, \quad c_1^2 = \frac{(x_B - \ell)\ell}{x_A(1 - 2\ell)} \tag{5.13}$$

and

$$d_0^2 = \frac{(x_B - \ell)(1 - \ell)}{x_B(1 - 2\ell)}, \quad d_1^2 = \frac{(x_A - \ell)\ell}{x_B(1 - 2\ell)}, \tag{5.14}$$

with $c_0 c_1 d_0 d_1$ negative (as minimization of the energy implies). In this symmetric case the maximum value of the angular momentum carried by the majority component in the interval $0 \leq \ell \leq x_B$ is of order $x_B^2/4$, for $\ell \approx x_B/2$ (for relatively small x_B). Figure (5.1) shows c_0^2, c_1^2, d_0^2, and d_1^2 for $x_A = 0.8$ and $x_B = 0.2$. I have seen numerically that in the asymmetric model ($g > g_{AB}$) the angular momentum of the

majority component decreases as g/g_{AB} increases. This is expected, since in the limit of $g_{AB} \to 0$, the two components decouple. Thus, from the above expressions we can get an upper bound on the angular momentum carried by the majority component, which is $\approx x_B^2/4$, at least for reasonably small values of $x_B \leq 0.3$.

For stronger interactions (and still in the asymmetric case), as we have seen in the numerical results, the angular momentum carried by the majority component for $0 \leq \ell \leq x_B$ is still very small, on the order of 1%, at least up to $x_B \leq 0.3$ and $g/g_{AB} = 5/3$.

Actually, I argue that this is a very general result, due to energetic reasons. There are four energy scales in the problem [see, e.g., Eq. (5.11)], namely the kinetic energy (which is set equal to unity), the interaction energy among the A particles, $\sim x_A^2 gN$, among the B particles, $\sim x_B^2 gN$, and the interaction energy between the A and the B particles, $x_A x_B g_{AB} N$. There are thus three dimensionless parameters, namely the coupling g, the interaction asymmetry g/g_{AB}, and the population imbalance x_A/x_B. Clearly, for large values of g/g_{AB} and/or large values of x_A/x_B, there is a clear hierarchy in the three energy scales of the interaction energy, which makes it energetically favorable for the system to carry its angular momentum by the one component (i.e., the B component in this case).

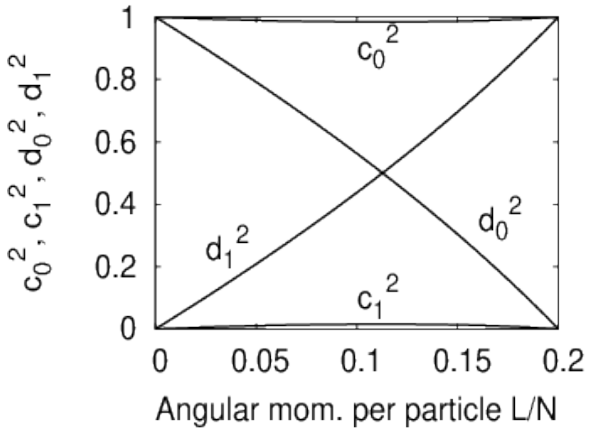

FIGURE 5.1: The occupancy of the four states, c_0^2, c_1^2, d_0^2, and d_1^2, for $x_A = 0.8$ and $x_B = 0.2$ from Eqs. (5.13) and (5.14). One can hardly distinguish the coefficients c_0^2 and c_1^2 from 1 and 0, respectively.

5.3.3 Quasi-periodic structure of the dispersion relation and a specific example

As shown in Ref. [102], for $x_A = 0.8$, $x_B = 0.2$, $Ng/e_0 = 1250/\pi^2$, and $Ng_{AB}/e_0 = 750/\pi^2$, to high accuracy the energy spectrum is given by the formula

$$E(\ell) = E_{\text{int}} + P_0(\ell) + e_p(\ell). \tag{5.15}$$

Here E_{int} is the interaction energy of the homogeneous system, $e_p(\ell)$ is a periodic function of ℓ, and

$$P_0(\ell) = [\ell]^2 x_A + (\ell - x_A[\ell])^2/x_B, \tag{5.16}$$

where $[\ell]$ denotes the nearest-integer function.

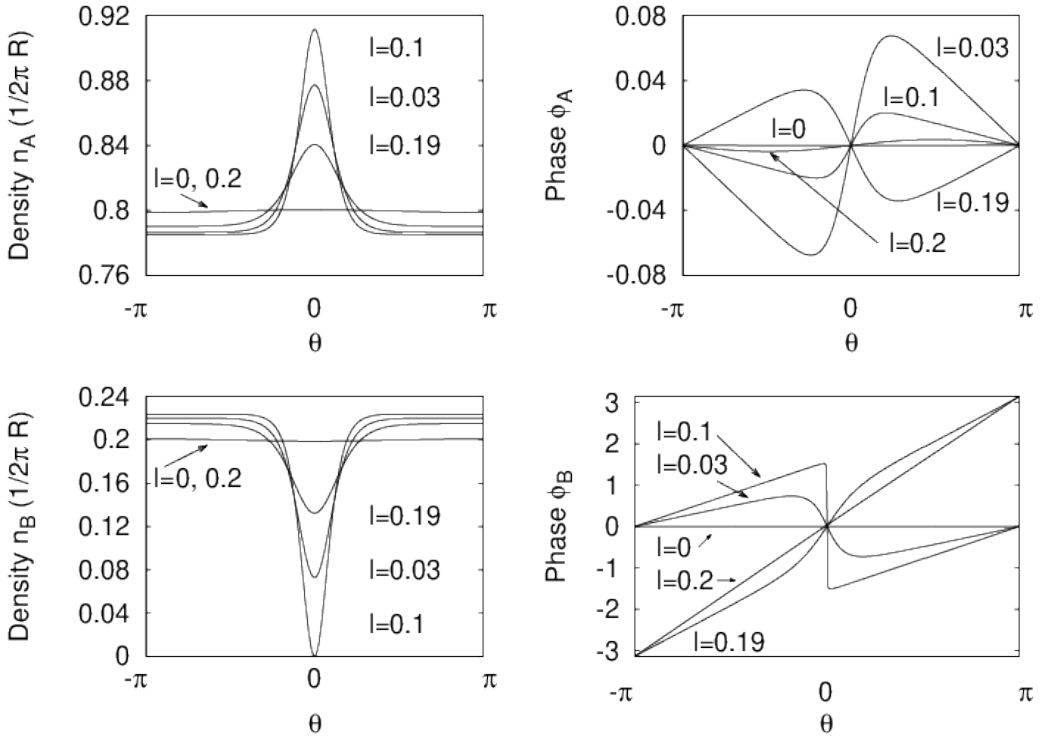

FIGURE 5.2: Density and phase of the order parameters $\Psi_k = \sqrt{n_k}\, e^{i\phi_k}$ of the two components A and B, for $x_A = 0.8$, $x_B = 0.2$ and for $\ell = 0, 0.03, 0.1, 0.19$, and 0.2. Here $Ng/e_0 = 1250/\pi^2$ and $Ng_{AB}/e_0 = 750/\pi^2$.

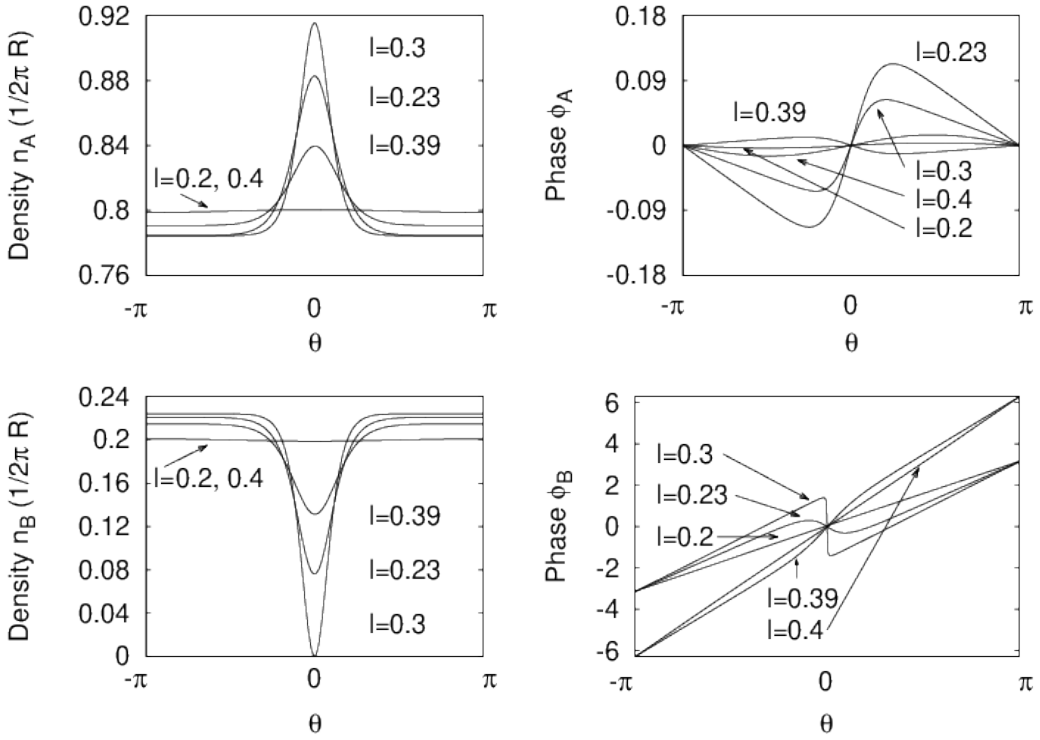

FIGURE 5.3: Density and phase of the order parameters $\Psi_k = \sqrt{n_k}\, e^{i\phi_k}$ of the two components A and B, for $x_A = 0.8$, $x_B = 0.2$ and for $\ell = 0.2, 0.23, 0.3, 0.39$, and 0.4. Here $Ng/e_0 = 1250/\pi^2$ and $Ng_{AB}/e_0 = 750/\pi^2$.

In Figs. (5.2) and (5.3) I show the density and the phase of the two order parameters Ψ_A and Ψ_B, in the two intervals $0 \leq \ell \leq 0.2$ and $0.2 \leq \ell \leq 0.4$. Comparing the density of the same species for values of ℓ which differ by $x_B = 0.2$ we observe that the difference is hardly visible. On the other hand, the phases of the two order parameters do change. These observations are explained in the analysis that follows below. Finally, the angular momentum carried by the majority component in the interval $0 \leq \ell \leq 0.2$ is very small, smaller than 1%, as I argued also above.

The above results follow from the facts that (i) at the interval $0 \leq \ell \leq x_B$ the minority component carries essentially all the angular momentum, and (ii) if one starts from the order parameters in the interval $0 \leq \ell \leq x_B$, the rest of the spectrum results by exciting the center of mass motion of each component separately. This operation changes the kinetic energy only, leaving the interaction energy unaffected. I thus essentially show below that Eqs. (5.15) and (5.16) follow from these two facts.

In order for the above procedure to give the yrast states, for a fixed population imbalance and a fixed interaction asymmetry, g has to be sufficiently large. Considering, for example, $\ell = 0.4$, the yrast state – which has to be $(\Psi_A, \Psi_B) = (\phi_0, \phi_2)$, as the quasi-periodic behaviour implies – is indeed the expected one for a sufficiently strong interaction, as analysed in Ref. [101]. For a fixed interaction asymmetry and a fixed g, the population imbalance has to be sufficiently large. Finally, for a fixed g and a fixed population imbalance the interaction asymmetry has to be sufficiently large.

To see the above arguments it is instructive to consider the specific example $x_A = 0.8$, $x_B = 0.2$. First of all, the possible values of the angular momentum carried by (purely) plane-wave states is a multiple of 0.2 in this case, since $\ell = mx_A + nx_B = 0.2(4m + n)$. It is also important to notice that the condition for a state (Ψ_m, Ψ_n) to become an yrast state, depends only on $|m - n|$ [101]. Thus, when, e.g., the state $(\Psi_m, \Psi_n) = (\phi_0, \phi_2)$ with $\ell = 2x_B = 0.4$, becomes the yrast state, also the state $(\Psi_m, \Psi_n) = (\phi_1, \phi_{-1})$ with $\ell = 3x_B = 0.6$, becomes the yrast state, as well. (This also follows from Bloch's theorem, however it is a more general result).

Having solved the yrast problem in the interval $0 \leq \ell \leq x_B = 0.2$, one may construct solutions at the interval $0.2 = x_B \leq \ell \leq 2x_B = 0.4$, etc., all the way up to $4x_B \leq \ell \leq 5x_B = 1$ keeping the correlations unaffected and putting all the energy in the form of kinetic energy, by exciting the center of mass motion. In other words, the spectrum will "repeat" itself in a quasi-periodic way (explained below) all the way up to $\ell = 1$. Beyond this point Bloch's theorem determines the rest of the excitation spectrum [51].

Let me thus assume that in the interval $0 \leq \ell \leq x_B = 0.2$ the two order parameters are

$$(\Psi_A, \Psi_B) = (\Psi_A^0, \Psi_B^0). \tag{5.17}$$

One should keep in mind that Ψ_A^0 carries a very small amount of angular momentum, and I will assume that it is zero. The angular momentum per particle of the above pair of states is

$$\ell = x_A \sum m c_m^2 + x_B \sum m d_m^2 = x_B \sum m d_m^2. \tag{5.18}$$

The kinetic energy per particle is

$$K^0(\ell) = x_A \sum m^2 c_m^2 + x_B \sum m^2 d_m^2, \tag{5.19}$$

and the total energy per particle is

$$E(\ell)/N = K^0(\ell) + V(\ell)/N, \tag{5.20}$$

where $V(\ell)$ is the total interaction energy. Finally, for the kinetic energy $K^0(\ell = 0) = 0$ and $K^0(\ell = x_B) = x_B = 0.2$.

For $0.2 = x_B \leq \ell \leq 2x_B = 0.4$ the order parameters are

$$(\Psi_A, \Psi_B) = (\Psi_A^0, e^{i\theta}\Psi_B^0). \tag{5.21}$$

The factor that multiplies Ψ_B^0 does not affect the interaction energy and thus the interaction energy is identical to the one in the interval $0 \leq \ell \leq x_B$, $V(\ell) = V(\ell - x_B)$. The interesting part is the kinetic energy, which is

$$K(\ell) = K^0(\ell - x_B) + 2\ell - x_B, \tag{5.22}$$

with $K(\ell = x_B) = x_B = 0.2$ and $K(\ell = 2x_B) = 4x_B = 0.8$.

For $0.4 = 2x_B \leq \ell \leq 3x_B = 0.6$ we have two competing solutions around $\ell = 1/2$. For values of ℓ smaller than $1/2$,

$$(\Psi_A, \Psi_B) = (\Psi_A^0, e^{2i\theta}\Psi_B^0). \tag{5.23}$$

The kinetic energy is

$$K(\ell) = K^0(\ell - 2x_B) + 4\ell - 4x_B, \tag{5.24}$$

with $K(\ell = 2x_B) = 4x_B = 0.8$ and $K(\ell = 3x_B) = 9x_B = 1.8$.

For larger values than $\ell = 1/2$,

$$(\Psi_A, \Psi_B) = (e^{i\theta}\Psi_A^0, e^{-2i\theta}\Psi_B^0). \tag{5.25}$$

The kinetic energy is

$$K(\ell) = K^0(\ell - x_A + 2x_B) + 5 - 4\ell - 9x_B, \tag{5.26}$$

with $K(\ell = 2x_B) = 5 - 17x_B = 1.6$ and $K(\ell = 3x_B) = 5 - 20x_B = 1$. Comparing the energies one sees that they cross at $\ell = 5x_A/8 = 1/2$. This gives rise to a discontinuity in the derivative of the dispersion relation at $\ell = 1/2$. I have evaluated the slope to be $1/x_B$ as $\ell \to (1/2)^-$ and $(1 - 2x_A)/x_B$ for $\ell \to (1/2)^+$, and therefore the difference between the right and the left slopes is $-2x_A/x_B$.

I stress that this discontinuous transition at $\ell = 1/2$ is also experimentally relevant, since the slope of the dispersion relation gives the velocity of propagation of the corresponding solitary waves. Interestingly, at this point the sign of the slope changes and thus the velocity of propagation also changes sign.

For $0.6 = 3x_B \leq \ell \leq 4x_B = 0.8$,

$$(\Psi_A, \Psi_B) = (e^{i\theta}\Psi_A^0, e^{-i\theta}\Psi_B^0). \tag{5.27}$$

The kinetic energy is

$$K(\ell) = K^0(\ell - x_A + x_B) + 1 - 2\ell + 2x_A - 2x_B, \tag{5.28}$$

with $K(\ell = 3x_B) = 1$ and $K(\ell = 4x_B) = 0.8$.

Finally, for $0.8 = 4x_B \leq \ell \leq 1$,

$$(\Psi_A, \Psi_B) = (e^{i\theta}\Psi_A^0, \Psi_B^0). \tag{5.29}$$

The kinetic energy is

$$K = K^0(\ell - x_A) + x_A, \tag{5.30}$$

with $K(\ell = 4x_B) = x_A = 0.8$ and $K(\ell = 1) = 1$. Figure (5.4) shows the result of this calculation for $x_A = 0.8$ and $x_B = 0.2$.

The results presented above imply Eqs.(5.15) and (5.16), which were motivated numerically [102], as mentioned also earlier. They are also consistent with the numerical results of Figs. (5.2) and (5.3). I also stress that, although the arguments were presented within the mean-field approximation, they do not rely in any way on the validity of the mean-field approximation, but rather they are much more general, as I also demonstrate in Sec. 5.4. As a final remark I mention that when N_A and N_B are relatively prime, e.g., $x_A = 0.7$ and $x_B = 0.3$, a similar picture develops.

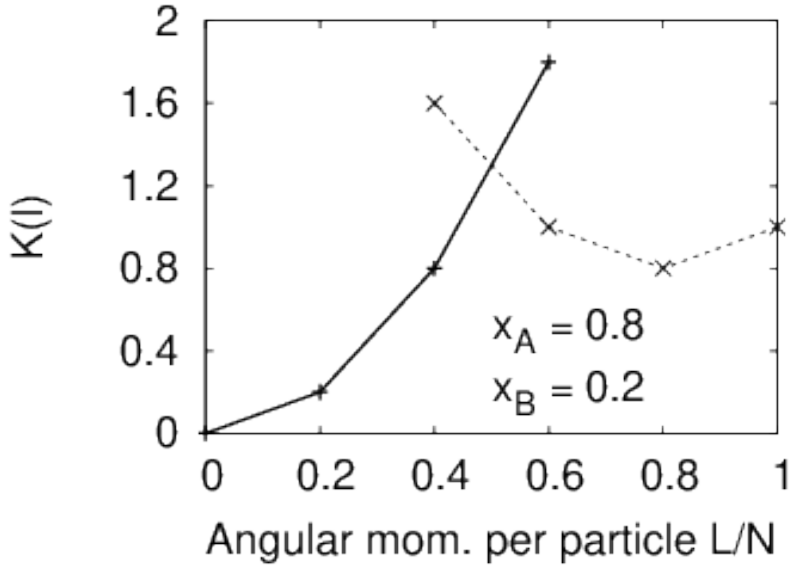

FIGURE 5.4: The kinetic energy $K(\ell)$, evaluated at $\ell = 0, 0.2, 0.4, 0.6, 0.8$, and 1.0, for $x_A = 0.8$, and $x_B = 0.2$, from Eqs. (5.22), (5.24), (5.26), (5.28), and (5.30). Knowing the energy at the interval $0 \leq \ell \leq x_B$, one may derive the rest of the spectrum using the transformations described in the text.

5.4 Excitation spectrum – many-body problem

5.4.1 "Collective" excitation of the system

Up to now we have seen how the yrast states progress with increasing angular momentum via essentially single-particle excitation of the system. In other words, as L increases, the additional momentum is carried by moving single particles to different single-particle states.

Still, there is another way to excite the system "collectively". By this term I mean that even an increase of the angular momentum by one unit requires a major rearrangement of the atoms in the single-particle states. Before we go to the many-body problem, we should recall the results of Ref. [101], where it was argued that for sufficiently strong interactions, the mean-field state $(\Psi_A, \Psi_B) = (\phi_m, \phi_n)$ becomes the yrast state, where obviously the angular momentum is $\ell = x_A m + x_B n$.

A way to argue about the state (ϕ_m, ϕ_n) becoming the yrast state for the specific value of ℓ and for sufficiently strong interactions is that any density variation costs interaction energy. If this is the dominant term in the Hamiltonian, it is minimized by these plane-wave states, which have a constant density distribution. The expense that one pays is the corresponding kinetic energy, which is $x_A m^2 + x_B n^2$, and has to be sufficiently small in order for the argument to be self-consistent; this argument is analysed further in Sec. 5.5. The details of this calculation (performed within the mean-field approximation), as well as the corresponding phase diagram are given in Ref. [101].

Let us thus consider a toy model which demonstrates the above arguments about the collective excitation. Assuming for convenience that $N_A - N_B = 1$, a state that

competes with the one of Eq. (5.5) is

$$|L=1\rangle = |1^{N_A}\rangle_A \bigotimes |(-1)^{N_B}\rangle_B. \tag{5.31}$$

The energy of this state $E^{''}$ is

$$E^{''} = N + \frac{1}{2}gN_A(N_A-1) + g_{AB}N_AN_B + \frac{1}{2}gN_B(N_B-1) = N + E_0, \tag{5.32}$$

or

$$E^{''} - E_0 = N. \tag{5.33}$$

Therefore

$$E^{''} - E' = (N-1) - g(N_B-1). \tag{5.34}$$

For values of g larger than the critical value which satisfies the equation

$$g = \frac{N-1}{N_B-1}, \tag{5.35}$$

it is energetically favourable to excite the system collectively. In the limit of large N and N_B, g is of order unity which is necessary in order for the system not to enter the highly-correlated Tonks-Girardeau regime. (One should not forget that for the low atom numbers that we have used, the system easily makes the transition to the Tonks-Girardeau limit, when g becomes of order N [54]).

I stress that the above calculation is just a toy model and should not in any way be trusted quantitatively. Besides, for g of order unity, the typical interaction energy per atom is of order N and thus (much) larger than the kinetic energy. Thus, the interaction energy will deplete the condensate significantly, while the depletion will also make the result dependent on g_{AB}; all these effect have been ignored here.

5.4.2 A “generalization" of Bloch’s theorem

The arguments presented above ignore the depletion of the condensate. However, the depletion lowers the energy to subleading order in the number of atoms N and, in particular for small systems, it may have a rather important effect. Below, I suggest a different way of constructing a many-body state, taking into account also the depletion. Essentially this ansatz state generalizes (in an approximate way) Bloch’s theorem, which also holds in a two-component system [51].

The ansatz many-body state that I introduce is based on the “exact" many-body state for $L=0$. The many-body state of each component will be a linear superposition of the “Fock" states of the form

$$|m_{\rm min}^{N^A_{m_{\rm min}}}, \ldots, m_{\rm max}^{N^A_{m_{\rm max}}}\rangle_A \bigotimes |m_{\rm min}^{N^B_{m_{\rm min}}}, \ldots, m_{\rm max}^{N^B_{m_{\rm max}}}\rangle_B \tag{5.36}$$

for some given truncation to the single-particle states with $m_{\min} \leq m \leq m_{\max}$, with the obvious constraints in each state

$$\sum_m N_m^i = N_i, \tag{5.37}$$

with $i = A, B$ and also with

$$\sum_{m,i} m N_m^i = 0. \tag{5.38}$$

Then, one may excite the center of mass coordinate using the same amplitudes, thus creating the state

$$\begin{aligned} &|(m_{\min}+m_A)^{N^A_{m_{\min}}}, \ldots, (m_{\max}+m_A)^{N^A_{m_{\max}}}\rangle_A \bigotimes \\ &\quad |(m_{\min}+m_B)^{N^B_{m_{\min}}}, \ldots, (m_{\max}+m_B)^{N^B_{m_{\max}}}\rangle_B. \end{aligned} \tag{5.39}$$

The resulting state has an angular momentum

$$L = N_A m_A + N_B m_B. \tag{5.40}$$

Also, this state has the same interaction energy as the one with $L = 0$, since the matrix elements do not depend on the angular momentum of the colliding particles. Its total energy is higher than the total energy of the many-body state with $L = 0$, $E(L = 0)$, due to its higher kinetic energy,

$$\begin{aligned} E''' &= V(L=0) + \sum_m (m+m_A)^2 N_m^A + \sum_m (m+m_B)^2 N_m^B \\ &= E(L=0) + N_A m_A^2 + N_B m_B^2 + 2(m_A L_A + m_B L_B). \end{aligned} \tag{5.41}$$

Here $V(L = 0)$ is the exact, total, interaction energy of the full many-body state with $L = 0$, and L_A, L_B is the angular momentum of the A and B components of the state with $L = 0$. In general, their sum has to vanish, $L_A + L_B = 0$, without each of them vanishing separately. Still, the states with the dominant amplitudes are the ones for which $L_A = 0$ and $L_B = 0$, separately, because of the condition $g > g_{AB}$, which is roughly the condition for phase co-existence. As a result,

$$E''' - E(L=0) \approx N_A m_A^2 + N_B m_B^2, \tag{5.42}$$

which becomes exact for $g_{AB} = 0$. Equation (5.42) is also exact within the mean-field approximation, since the terms with $L_A \neq 0$ and $L_B \neq 0$ appear due to the depletion. On the other hand, whether the resulting (mean-field, or many body) state is the yrast state, depends on the parameters. Finally, I also mention that Eq. (5.42) reduces to Eq. (5.33) when $m_A = 1$ and $m_B = -1$, as expected.

From Eqs. (5.40) and (5.41) if follows trivially that when L is an integer multiple of N, $L = qN$, then $m_A = m_B = q$, in which case Bloch's theorem [49] holds exactly, even in a two-component system [51], $E''' - E_0 = Nq^2$. In the case of the "traditional" Bloch theorem (i.e., in the case of one component) starting from the $L = 0$ state, by exciting the center of mass motion one gets (exactly) only the states with an additional angular momentum which is an integer multiple of the total number of particles N.

On the other hand, in the present case of a two-component system, this procedure allows us to give L any desired value, at least when the populations N_A and N_B

are relatively prime, otherwise the argument will hold for values of L which are integer multiples of their greatest common divisor. Still, the generated states are not necessarily the yrast states, but rather they are candidate yrast states.

5.4.3 Results of numerical diagonalization

I turn now to the results that I got from the diagonalization of the many-body Hamiltonian. I consider as a first example the case $N_A = 16, N_B = 4, g_{AA} = g_{BB} = g = 0.1, g_{AB} = 0.05$, with $m_{\min} = -1$, and $m_{\max} = 2$ and the results are shown in the Appendix. For $0 < L \leq 4 (= N_B)$ we see that indeed the angular momentum of the majority component, A, is less than 10% of the total, which is consistent with the results of Sec. 5.3. Partly this relatively large value is due to finite-N corrections; increasing N will make this number even smaller. For $5 \leq L \leq 9$ the dominant state of the B (minority) component is ϕ_1, carrying 4 units of angular momentum, while the additional angular momentum is carried by the A component. This is because exciting the B component costs kinetic energy. The state with $L = 10 (= N/2)$ is analysed in detail below, for $N = 10$ and $L = 5 (= N/2)$. The rest of the spectrum follows from Bloch's theorem.

In order to see the effects that I investigate in the present project I turn now to higher couplings using the above as a "reference" example. To achieve a decent convergence I expand the space of single-particle states to $m_{\min} = -2$, and $m_{\max} = 3$, which forces us to reduce the atom number, as otherwise the dimensionality of the Hamiltonian matrix explodes. I thus consider $N_A = 8, N_B = 2, g_{AA} = g_{BB} = g = 1.5, g_{AB} = 0.15$. Another example, where g and g_{AB} are closer to each other, follows below.

For $L = 0$ and in the space with $m_{\min} = -1$ and $m_{\max} = 1$ the dimensionality of the Hamiltonian matrix is 26, while the lowest eigenenergy is ≈ 38.5864. For $m_{\min} = -2$, and $m_{\max} = 2$ the dimensionality becomes 457 and the lowest eigenenergy reduces to ≈ 33.8139, i.e., there is a reduction of roughly 14%. For $m_{\min} = -2$, and $m_{\max} = 3$ the dimensionality becomes 1163 and the lowest eigenenergy reduces further to ≈ 32.8452, i.e., there is a further reduction of roughly 3%, indicating that although convergence has not been achieved, the results are relatively accurate.

A generic feature of the above problem is that there is a very rapid increase of the dimensionality of the Hilbert space as more single-particle states are included, as seen also in the numbers mentioned above. I should also mention that in order to satisfy Bloch's theorem for e.g., $0 \leq L \leq N$ the single-particle states have to be "symmetric" around $1/2$. This is the reason why I choose to work, for example, with $m_{\min} = -2$, and $m_{\max} = 3$. The fact that we have to increase the single-particle states in pairs makes it even more difficult to investigate the convergence of the results and to increase the Hilbert space. For example, going e.g., from $m_{\min} = -2$, and $m_{\max} = 3$ to $m_{\min} = -3$, and $m_{\max} = 4$ may result in a very large increase of the dimensionality of the Hamiltonian matrix (for some fixed N_A and N_B).

The lowest-energy eigenstate with $L = 0$ (and with an eigenenergy equal to ≈ 32.8452), consists of the following four Fock states (with the amplitudes with the largest absolute value)

	Comp. A						Comp. B					
Ampl.	ϕ_{-2}	ϕ_{-1}	ϕ_0	ϕ_1	ϕ_2	ϕ_3	ϕ_{-2}	ϕ_{-1}	ϕ_0	ϕ_1	ϕ_2	ϕ_3
-0.2559	1	0	6	0	1	0	0	0	2	0	0	0
-0.2650	0	0	8	0	0	0	0	1	0	1	0	0
-0.4326	0	1	6	1	0	0	0	0	2	0	0	0
0.6465	0	0	8	0	0	0	0	0	2	0	0	0

In the above notation, the Fock state with e.g., 8 "A" atoms in the single-particle state ϕ_0 and 2 "B" atoms in the single-particle state ϕ_0 has an amplitude 0.6465, etc.

To understand the arguments which follow, it is instructive to get some insight into the structure of the above many-body state. The Fock state with the largest amplitude has zero kinetic energy and it puts all 8 "A" atoms at the $m = 0$ state, as well as all 2 "B" atoms at the state with $m = 0$, also. The following three have a kinetic energy which is equal to 2, 2, and 8, respectively. The degeneracy between the first two is lifted by the interactions. More specifically, in the two specific states there are processes where atoms are transferred from the $m = 0$ state to the states with $m = \pm 1$, $m = \pm 2$, etc., which lower the energy (they are off-diagonal matrix elements which come from, e.g., $c_0^2 c_{-1}^\dagger c_1^\dagger$ [67]).

For $L = 1$, the lowest eigenenergy is ≈ 34.6431, while the states with the four largest amplitudes are

	Comp. A						Comp. B					
Ampl.	ϕ_{-2}	ϕ_{-1}	ϕ_0	ϕ_1	ϕ_2	ϕ_3	ϕ_{-2}	ϕ_{-1}	ϕ_0	ϕ_1	ϕ_2	ϕ_3
-0.2506	1	0	6	0	1	0	0	0	1	1	0	0
-0.2904	0	0	8	0	0	0	0	1	0	0	1	0
-0.4223	0	1	6	1	0	0	0	0	1	1	0	0
0.6323	0	0	8	0	0	0	0	0	1	1	0	0

Here we see that indeed it is the minority component that carries the angular momentum (in all four Fock states).

For $L = 2$, the lowest eigenenergy is ≈ 34.8276, with

	Comp. A						Comp. B					
Ampl.	ϕ_{-2}	ϕ_{-1}	ϕ_0	ϕ_1	ϕ_2	ϕ_3	ϕ_{-2}	ϕ_{-1}	ϕ_0	ϕ_1	ϕ_2	ϕ_3
-0.2557	1	0	6	0	1	0	0	0	0	2	0	0
-0.2644	1	0	6	0	1	0	0	0	1	0	1	0
-0.4322	0	1	6	1	0	0	0	0	0	2	0	0
0.6461	0	0	8	0	0	0	0	0	0	2	0	0

The minority, B, component still carries the angular momentum (in all four Fock states). The state with the largest amplitude is the one expected also from the mean-field approximation. Furthermore, this state does indeed result (to high accuracy) from the one with $L = 0$ by exciting the center of mass coordinate of the minority component, while the difference between the eigenenergy of this state and the one with $L = 0$ is ≈ 1.9814, i.e., very close to the value $2 (= N_B)$. These are in agreement with the results presented in Sec. 5.3.

For $L = 3$ the lowest eigenenergy is ≈ 38.7296, with

	Comp. A						Comp. B					
Ampl.	ϕ_{-2}	ϕ_{-1}	ϕ_0	ϕ_1	ϕ_2	ϕ_3	ϕ_{-2}	ϕ_{-1}	ϕ_0	ϕ_1	ϕ_2	ϕ_3
-0.2401	1	0	6	0	1	0	0	0	0	1	1	0
-0.3224	0	0	8	0	0	0	0	0	1	0	0	1
-0.4035	0	1	6	1	0	0	0	0	0	1	1	0
0.6057	0	0	8	0	0	0	0	0	0	1	1	0

In agreement with the results of Sec. 5.3, and contrary to the corresponding state with $L = 5$, the above state results to rather high accuracy from the one with $L = 1$ by exciting the center of mass of the minority component. The energy difference is ≈ 4.0865, while the one predicted by the results of Sec. 5.3 is $2L - N_B = 4$.

For $L = 4$ the lowest eigenenergy is ≈ 40.8526, with

	Comp. A						Comp. B					
Ampl.	ϕ_{-2}	ϕ_{-1}	ϕ_0	ϕ_1	ϕ_2	ϕ_3	ϕ_{-2}	ϕ_{-1}	ϕ_0	ϕ_1	ϕ_2	ϕ_3
-0.2494	1	0	6	0	1	0	0	0	0	0	2	0
-0.2970	0	0	8	0	0	0	0	0	0	1	0	1
-0.4218	0	1	6	1	0	0	0	0	0	0	2	0
0.6305	0	0	8	0	0	0	0	0	0	0	2	0

Here we observe that the Fock state with the dominant amplitude is the one where all 8 "A" atoms occupy the $m = 0$ state, as well as all 2 "B" atoms occupy the state with $m = 2$. Again, this state results approximately from the states with $L = 0$ and $L = 2$, by exciting the center of mass motion of the minority component. The energy difference between this state and the one with $L = 0$ is ≈ 8.0074, while the one that one gets from Sec. 5.3 is 8. I stress that for weaker interactions the many-body state does not have the structure seen above. For example, the state with $L = 8(= 2N_B)$, where the state with the largest amplitude is $0.6158\,|0, 12, 4, 0\rangle_A\,|0, 0, 4, 0\rangle_B$.

For $L = 5$ the lowest eigenenergy is ≈ 45.7010, with

	Comp. A						Comp. B					
Ampl.	ϕ_{-2}	ϕ_{-1}	ϕ_0	ϕ_1	ϕ_2	ϕ_3	ϕ_{-2}	ϕ_{-1}	ϕ_0	ϕ_1	ϕ_2	ϕ_3
0.3194	0	1	5	2	0	0	0	0	0	0	2	0
0.3194	0	0	2	5	1	0	0	2	0	0	0	0
-0.3516	0	0	7	1	0	0	0	0	0	0	2	0
-0.3516	0	0	1	7	0	0	0	2	0	0	0	0

Interestingly, this state with $L = N/2 = 5$ cannot in any way be linked to any other state and it does not result from exciting the center of mass motion [1]. This is seen by comparing this eigenstate with the ones with $L = 1$ and $L = 3$. The state that one would construct following this rule has an energy equal to ≈ 46.8276, which is higher than the actual eigenenergy. Therefore, the system manages to construct a state that lies lower in energy. We should recall here that within the mean-field approximation for $L = N/2$ one gets a "dark" solitary wave in the minority component, and the winding number changes.

[1] A state that resembles this one has been seen in Ref. [95], for $g = g_{AB}$, and for weak interactions.

Furthermore, this eigenstate has the peculiar feature that the Fock states go in pairs, having the same amplitudes (modulo signs). This can be seen by the fact that for every Fock state, there has to be another one, which is its mirror image that results from the transformation $m \to 1 - m$. The first state will have an angular momentum $\sum mN_m = N/2$, while the other one $\sum(1-m)N_m = N - L = N/2$. Furthermore, the kinetic energy of the first will be $K = \sum m^2 N_m$, while that of the other will be $\sum(1-m)^2 N_m = K + N - 2L = K$. Since the interaction energy will also be the same, that is the reason that these states go in pairs.

It is interesting that within the mean-field approximation and for $\ell = 1/2$ there are two degenerate solutions, with a very different structure in ϕ_A, i.e., the phase of the order parameter Ψ_A of the majority component. For $\ell \to (1/2)^{\pm}$ we get either the one, or the other solution (in practice depending, e.g., on the initial condition that we use in the algorithm). This is an example of spontaneous symmetry breaking. This symmetry is restored within the method of diagonalization, where, for $\ell = 1/2$, we get a superposition of these two states.

Returning to the results from numerical diagonalization, the rest of the spectrum, for $L = 6, \ldots, 10$, as well for $L > 10$, follows (exactly) from the above states, according to Bloch's theorem, as I have also checked numerically.

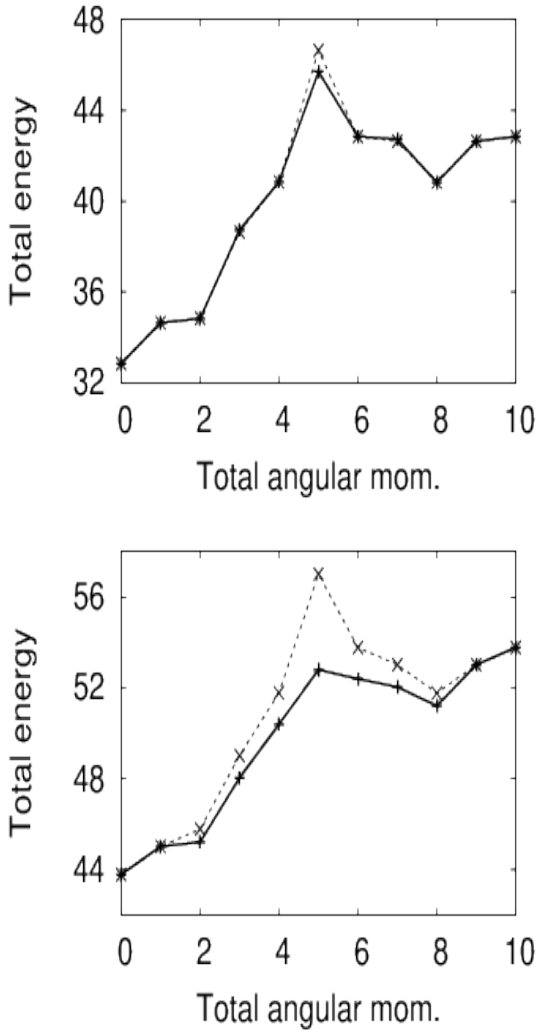

FIGURE 5.5: Top figure: The solid curve connects the lowest eigenenergies, for $N_A = 2$, $N_B = 8$, $g_{AA} = g_{BB} = 1.5$, and $g_{AB} = 0.15$, for $L = 0$ up to 10, in the truncated space $m_{\min} = -2$, $m_{\max} = 3$. The dashed curve connects the energies evaluated by the phase transformations described in Sec. 5.3, which result from the eigenenergies for $L = 0$ and $L = 1$. Bottom figure: Same as the top one, with $g_{AB} = 0.9$.

Another example that I show below has a larger value for g_{AB}, $g_{AB} = 9/10$, with $N_A = 8, N_B = 2, g_{AA} = g_{BB} = g = 3/2$ being the same as before. The ratio g/g_{AB} is the same as the one in the mean-field calculation of Ref. [102]. In this project the chosen couplings were rather strong, however here considering the same parameters would require inclusion of a large space of single-particle states and a correspondingly huge dimensionality of the resulting Hamiltonian matrix.

The lowest-energy eigenstate with $L = 0$ has an eigenenergy equal to ≈ 43.7724. The Fock states with the four largest amplitudes are

	Comp. A						Comp. B					
Ampl.	ϕ_{-2}	ϕ_{-1}	ϕ_0	ϕ_1	ϕ_2	ϕ_3	ϕ_{-2}	ϕ_{-1}	ϕ_0	ϕ_1	ϕ_2	ϕ_3
-0.2420	1	0	6	0	1	0	0	0	2	0	0	0
0.2422	0	0	8	0	0	0	0	1	0	1	0	0
-0.4146	0	1	6	1	0	0	0	0	2	0	0	0
0.6468	0	0	8	0	0	0	0	0	2	0	0	0

For $L = 1$, the lowest eigenenergy is ≈ 45.0110, while

	Comp. A						Comp. B					
Ampl.	ϕ_{-2}	ϕ_{-1}	ϕ_0	ϕ_1	ϕ_2	ϕ_3	ϕ_{-2}	ϕ_{-1}	ϕ_0	ϕ_1	ϕ_2	ϕ_3
-0.2312	0	0	8	0	0	0	0	1	0	0	1	0
-0.2370	1	0	6	0	1	0	0	0	1	1	0	0
-0.3676	0	1	6	1	0	0	0	0	1	1	0	0
0.6135	0	0	8	0	0	0	0	0	1	1	0	0

Again, we observe that the angular momentum is carried by the minority component. For $L = 2$, the lowest eigenenergy is ≈ 45.2024, with

	Comp. A						Comp. B					
Ampl.	ϕ_{-2}	ϕ_{-1}	ϕ_0	ϕ_1	ϕ_2	ϕ_3	ϕ_{-2}	ϕ_{-1}	ϕ_0	ϕ_1	ϕ_2	ϕ_3
-0.2205	0	0	8	0	0	0	0	0	1	0	1	0
-0.2369	1	0	6	0	1	0	0	0	0	2	0	0
-0.4035	0	1	6	1	0	0	0	0	0	2	0	0
0.6351	0	0	8	0	0	0	0	0	0	2	0	0

This state is linked with $|L = 0\rangle$ the way we discussed above. The only difference is that the Fock states with the two smallest amplitudes are reversed. For $L = 3$ the lowest eigenenergy is ≈ 48.0354, with

	Comp. A						Comp. B					
Ampl.	ϕ_{-2}	ϕ_{-1}	ϕ_0	ϕ_1	ϕ_2	ϕ_3	ϕ_{-2}	ϕ_{-1}	ϕ_0	ϕ_1	ϕ_2	ϕ_3
-0.2857	0	1	6	1	0	0	0		0	1	1	0
0.3043	0	1	5	2	0	0	0	0	0	2	0	0
-0.3555	0	0	7	1	0	0	0	0	0	2	0	0
0.4900	0	0	8	0	0	0	0	0	0	1	1	0

The difference between this state and $|L = 1\rangle$ is more pronounced (in the second and the third lines). In these two Fock states we observe that there are 2 units of angular momentum, as compared to the first and the fourth lines, where there are 3 units of angular momentum, as a result of the increase of g_{AB}. Still, the Fock state with the largest amplitude is the one expected from the earlier discussion.

For the state with $L = 4$ the lowest eigenenergy is ≈ 50.3904, with

	Comp. A						Comp. B					
Ampl.	ϕ_{-2}	ϕ_{-1}	ϕ_0	ϕ_1	ϕ_2	ϕ_3	ϕ_{-2}	ϕ_{-1}	ϕ_0	ϕ_1	ϕ_2	ϕ_3
-0.2058	1	0	6	0	1	0	0	0	0	0	2	0
-0.2074	0	0	7	1	0	0	0	0	0	1	1	0
-0.3488	0	1	6	1	0	0	0	0	0	0	2	0
0.5529	0	0	8	0	0	0	0	0	0	0	2	0

Again, this state is linked with the states $|L = 0\rangle$ and $|L = 2\rangle$, with the main difference in the third Fock state, which has 3 units of angular momentum, while the other ones have 4 units. Finally, for $L = 5$ the lowest eigenenergy is ≈ 52.7947, with

	Comp. A						Comp. B					
Ampl.	ϕ_{-2}	ϕ_{-1}	ϕ_0	ϕ_1	ϕ_2	ϕ_3	ϕ_{-2}	ϕ_{-1}	ϕ_0	ϕ_1	ϕ_2	ϕ_3
-0.1817	0	1	4	3	0	0	0	0	0	1	1	0
-0.1817	0	0	3	4	1	0	0	1	1	0	0	0
0.1920	0	0	4	4	0	0	0	0	1	1	0	0
0.2038	0	0	6	2	0	0	0	0	0	1	1	0
0.2038	0	0	2	6	0	0	0	1	1	0	0	0

which still is not linked with the other states.

Figure (5.5) shows the eigenenergies for $0 \leq L \leq 10$ for the two values of g_{AB}. In the same figure I have also used the eigenenergies for $L = 0$ and $L = 1$ and evaluated the other ones using the arguments presented in Sec. 5.3. The agreement for the lower value of g_{AB} is better. With increasing g_{AB} the two systems become more coupled and as a result there are processes like, e.g., $c_0 c_1^\dagger d_0^\dagger d_1$, which lower the energy and become more important. These processes make the amplitudes of the Fock states which constitute the $L = 0$ yrast state and have $L_A \neq 0$ and $L_B \neq 0$ (with $L_A + L_B = 0$) larger. These states are responsible for the observed deviations [see Eq. (5.41)]. We also observe the relatively large deviation that appears for $L = 5 = N/2$. This deviation is due to the fact that this eigenstate does not result from the other ones via excitation of the center of mass motion.

To conclude, interestingly enough, essentially the whole excitation spectrum (with the exception of the distinct values of $L = N/2 + Nq$, with q being an integer), can thus be derived by the states $L = 0$ and $L = 1$ only – at least approximately – very much the same way that we saw in Sec. 5.3.

5.5 A conjecture: Dispersion relation based on the minimization of the kinetic energy

As I argued in Sec. 5.4, starting from the many-body state of a system with $L = 0$ it is possible to create a many-body state with some nonzero value of L at the expense of kinetic energy only, which is of order N (in the total energy of the system). Alternatively the many-body state may result from single-particle excitation with an energy expense in the interaction energy which is of order Ng (still in the total energy of the system), for $g_{AA} \approx g_{BB} \approx g_{AB}$, and equal to g. Furthermore, for sufficiently strong interactions, i.e., when g becomes of order N, the system enters the Tonks-Girardeau regime, where the energy does not depend on g, which is not desirable.

Therefore, provided that

$$N \ll Ng \ll N^2, \tag{5.43}$$

it may be energetically favorable for the system to carry its angular momentum via the collective excitation described above. In this case, provided that N_A and N_B are relatively prime one may achieve any value of $L = mN_A + nN_B$. The integers (m, n) are the ones which minimize the kinetic energy per particle

$$K = m^2 N_A + n^2 N_B, \tag{5.44}$$

under the obvious constraint

$$L = mN_A + nN_B. \tag{5.45}$$

Self-consistency requires that the resulting integers m and n have to be of order unity.

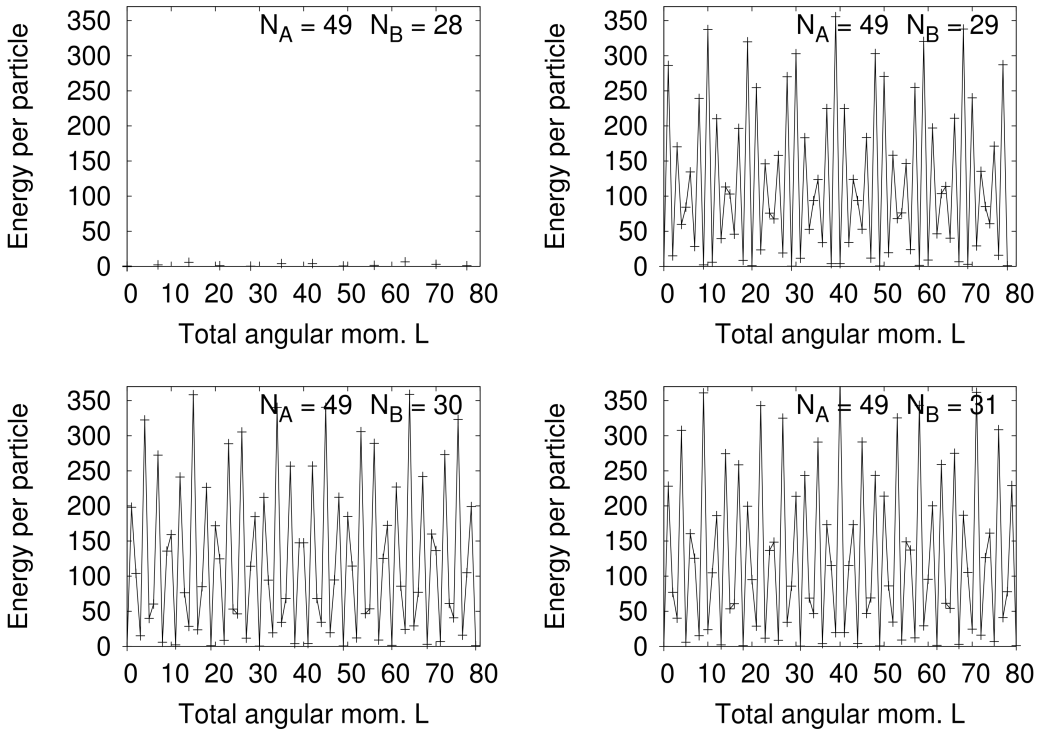

FIGURE 5.6: The dispersion relation (i.e., the kinetic energy) evaluated from the minimization of Eq. (5.44) under the constraint of Eq. (5.45), for the numbers of N_A and N_B shown in each plot.

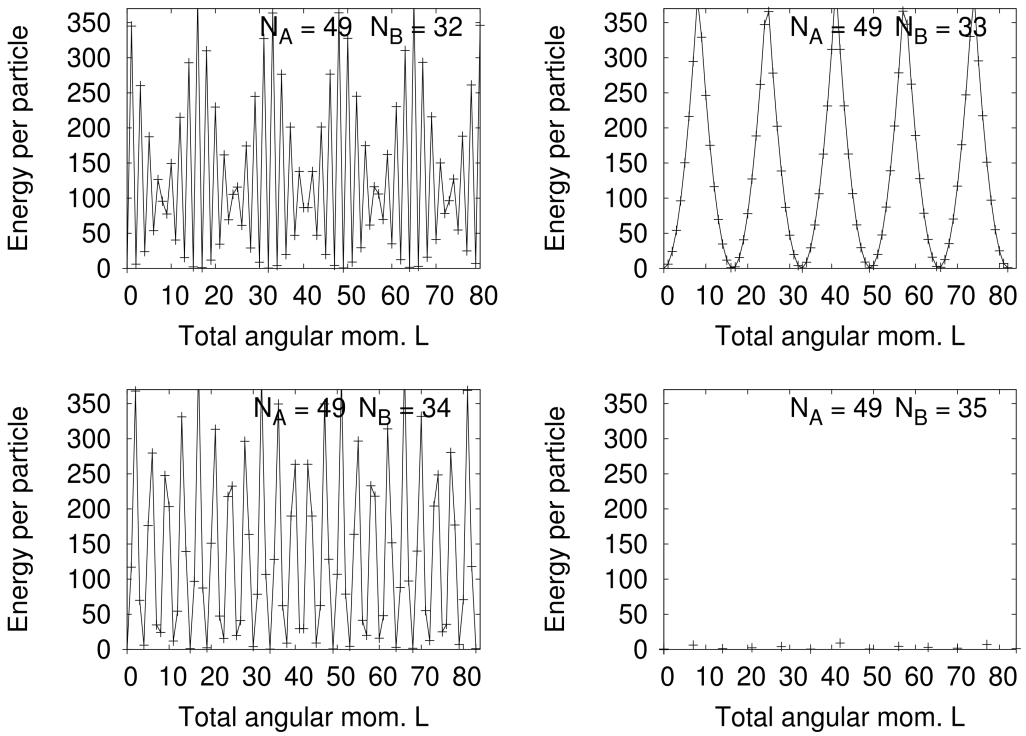

FIGURE 5.7: Same as in Fig. (5.6).

It is important to point out that Eq. (5.44) and (5.45) are linear in N_A and N_B. Thus, scaling N_A and N_B the same way will leave the resulting integers m and n unaffected. On the other hand, Eq. (5.43) will always be satisfied for a sufficiently large value of $N = N_A + N_B$, for some fixed g.

The inequality of Eq. (5.43) implies that in order for each term to differ by, e.g., one order of magnitude, g has to be at least 10, while N has to be at least 100. This introduces a very serious problem in the method of numerical diagonalization that we use. Convergence of the results requires that the space that one should work with is $|m_{\min}| \approx m_{\max} \approx \sqrt{Ng} \approx 30$. This implies that the dimensionality of the resulting matrices is too large and certainly beyond the capability of current technology.

Still, if one could reach these parameters – which is certainly possible experimentally – there is an interesting behaviour, which I investigate below. The most interesting aspect is that under the conditions presented above, the yrast spectrum is determined from the minimization of the kinetic energy and thus becomes trivial. In addition to the simplicity of the spectrum, even more interesting is that the dispersion relation may become very sensitive to N_A and N_B, due to number-theoretic reasons.

In Figs. (5.6) and (5.7), instead of diagonalizing the many-body Hamiltonian, I minimize Eq. (5.44) under the constraint of Eq. (5.45) and plot the dispersion relation [measuring the energy from $E(L = 0)$]. As an example, I have chosen $N_A = 49$ and N_B from 28 up to 35. For $N_B = 28$, the greatest common divisor of N_A and N_B is 7 and for this reason we find a solution for the values of L which are integer multiples of 7, i.e., 0, 7, 14, 21, 28, 35, 42, 49, 56, 63, 70, and 77.

For all other values of L the energy will be much higher, so the predicted dispersion relation will have minima at these values of L. Increasing the population of N_B by

one unit, i.e., for $N_B = 29$, the greatest common divisor of N_A and N_B is 1. This has dramatic consequences on the dispersion relation, since it is now possible to find a solution for all values of L between 0 and $N_A + N_B = 78$. Various interesting patterns show up as N_B continues to increase by one unit, until N_B increases by seven units, $N_B = 35$, in which case the greatest common divisor of N_A and N_B is again equal to 7, in which case the dispersion shows a similar structure as in the case $N_B = 28$.

A remarkable observation that follows from these results is that even if the population changes by one particle, this may change the dispersion dramatically. This is a direct consequence of the number-theoretic nature of the problem, much like shell-effects for fermions, due to the Pauli exclusion principle.

5.6 Summary and conclusions

In the project investigated in this chapter I examined the dispersion relation of a two-component Bose-Einstein condensed gas that is confined in a ring potential. The structure of the derived excitation spectrum and the corresponding states have immediate consequences on the rotational properties of the system that I have examined and thus they have a very interesting physical interpretation.

To name just the most important ones, we need to recall that the local minima of the dispersion relation correspond to non-decaying states, i.e., persistent currents. Furthermore, the states that I have evaluated correspond to “vector" solitary-wave solutions, i.e., density disturbances in both components (see Figs. (5.2) and (5.3)) which propagate together around the ring without change in their shape. In addition, the slope of the dispersion relation gives the velocity of propagation of these waves. Finally, the dispersion relation may be used to predict the behaviour of the system as it is driven by some external rotation of the trap and also it allows us to extract the hysteretic behaviour.

Turning to the more specific properties I have derived, I have shown that, quite generally (and not only within the mean-field approximation) under certain and rather typical conditions the whole energy spectrum repeats itself in a quasi-periodic way. More specifically, if one knows the spectrum in the range of the angular momentum between $L = 0$ and $L = N_B$, i.e., the population of the minority component, the rest may be derived by exciting the center of mass motion of the two components.

An interesting result that is directly related with the above is the fact that in this range of angular momentum the majority of the angular momentum is carried by the minority component, which is a definite experimental prediction. Another interesting physical consequence of these results is that, within the mean-field approximation – when the “dark" soliton appears (in the minority component), the velocity of propagation of the solitary waves changes discontinuously. Furthermore, within the many-body scheme the state with this value of the angular momentum has some peculiar properties.

One important observation in the problem I have studied is the fact that the matrix elements that determine the interaction do not depend on the angular momentum of the colliding particles. As a result, one may start from the non-rotating many-body state and use these correlations to build many-body states with some nonzero angular momentum. In the limit of relatively strong interactions these are possible yrast

states. The reason is that the energy expense that one pays to give the angular momentum is purely kinetic energy and for sufficiently strong interatomic interactions this kind of excitation provides an energetically inexpensive way for the system to carry its angular momentum (since the correlations are unaffected).

As a result in this limit it is the kinetic energy that has to be minimized, with the interesting consequence that the energy spectrum is trivial to calculate. Furthermore, much like non-interacting fermions, due to number-theoretic reasons the energy spectrum also becomes very sensitive to the population of the two components, as well as the angular momentum carried by the system. In a sense, this is an indication of "quantum chaos", where even infinitesimally small changes in the number of atoms (i.e., of order unity) have very significant changes in the dispersion relation, and as a result in the rotational properties of the system. While I cannot demonstrate this conjecture numerically because of the huge dimensionality of the resulting matrices, there are definite predictions, which may be tested experimentally.

5.7 A specific example

Below I give the result for $N_A = 16, N_B = 4, g_{AA} = g_{BB} = g = 0.1, g_{AB} = 0.05$ in the space with $-1 \leq m \leq 2$.

The lowest-energy eigenstate with $L = 0$ has an eigenenergy equal to ≈ 15.1799. Furthermore, the dimensionality of the matrix is 846. The states with the four largest amplitudes are

	Comp. A				Comp. B			
Ampl.	ϕ_{-1}	ϕ_0	ϕ_1	ϕ_2	ϕ_{-1}	ϕ_0	ϕ_1	ϕ_2
0.0944	2	12	2	0	0	4	0	0
-0.1139	0	16	0	0	1	2	1	0
-0.3122	1	14	1	0	0	4	0	0
0.9301	0	16	0	0	0	4	0	0

For $L = 1$, the lowest eigenenergy is ≈ 16.3549, while

	Comp. A				Comp. B			
Ampl.	ϕ_{-1}	ϕ_0	ϕ_1	ϕ_2	ϕ_{-1}	ϕ_0	ϕ_1	ϕ_2
0.1221	1	13	2	0	0	4	0	0
-0.2695	0	15	1	0	0	4	0	0
-0.2811	1	14	1	0	0	3	1	0
0.8893	0	16	0	0	0	3	1	0

For $L = 2$, the lowest eigenenergy is ≈ 17.4151, with

	Comp. A				Comp. B			
Ampl.	ϕ_{-1}	ϕ_0	ϕ_1	ϕ_2	ϕ_{-1}	ϕ_0	ϕ_1	ϕ_2
0.1245	1	13	2	0	0	3	1	0
-0.2742	1	14	1	0	0	2	2	0
-0.2814	0	15	1	0	0	3	1	0
0.8840	0	16	0	0	0	2	2	0

For $L = 3$ the lowest eigenenergy is ≈ 18.3432, with

	Comp. A				Comp. B			
Ampl.	ϕ_{-1}	ϕ_0	ϕ_1	ϕ_2	ϕ_{-1}	ϕ_0	ϕ_1	ϕ_2
0.1086	1	13	2	0	0	2	2	0
-0.2461	0	15	1	0	0	2	2	0
-0.2826	1	14	1	0	0	1	3	0
0.8960	0	16	0	0	0	1	3	0

For $L = 4$ the lowest eigenenergy is ≈ 19.1274, with

	Comp. A				Comp. B			
Ampl.	ϕ_{-1}	ϕ_0	ϕ_1	ϕ_2	ϕ_{-1}	ϕ_0	ϕ_1	ϕ_2
-0.1025	0	16	0	0	0	1	2	1
-0.1791	0	15	1	0	0	1	3	0
-0.3017	1	14	1	0	0	0	4	0
0.9153	0	16	0	0	0	0	4	0

For $L = 5$ the lowest eigenenergy is ≈ 21.0242, with

	Comp. A				Comp. B			
Ampl.	ϕ_{-1}	ϕ_0	ϕ_1	ϕ_2	ϕ_{-1}	ϕ_0	ϕ_1	ϕ_2
-0.1791	0	16	0	0	0	0	3	1
-0.2520	0	14	2	0	0	1	3	0
-0.3693	1	13	2	0	0	0	4	0
0.8354	0	15	1	0	0	0	4	0

For $L = 6$ the lowest eigenenergy is ≈ 22.8034, with

	Comp. A				Comp. B			
Ampl.	ϕ_{-1}	ϕ_0	ϕ_1	ϕ_2	ϕ_{-1}	ϕ_0	ϕ_1	ϕ_2
-0.2058	0	15	1	0	0	0	3	1
-0.3104	0	13	3	0	0	1	3	0
-0.3910	1	12	3	0	0	0	4	0
0.7640	0	14	2	0	0	0	4	0

For $L = 7$ the lowest eigenenergy is ≈ 24.4524, with

	Comp. A				Comp. B			
Ampl.	ϕ_{-1}	ϕ_0	ϕ_1	ϕ_2	ϕ_{-1}	ϕ_0	ϕ_1	ϕ_2
0.2136	1	10	5	0	0	1	3	0
-0.3627	0	12	4	0	0	1	3	0
-0.3855	1	11	4	0	0	0	4	0
0.6938	0	13	3	0	0	0	4	0

For $L = 8$ the lowest eigenenergy is ≈ 25.9611, with

	Comp. A				Comp. B			
Ampl.	ϕ_{-1}	ϕ_0	ϕ_1	ϕ_2	ϕ_{-1}	ϕ_0	ϕ_1	ϕ_2
0.2451	1	9	6	0	0	1	3	0
-0.3568	1	10	5	0	0	0	4	0
-0.4100	0	11	5	0	0	1	3	0
0.6158	0	12	4	0	0	0	4	0

For $L = 9$ the lowest eigenenergy is ≈ 27.3137, with

	Comp. A				Comp. B			
Ampl.	ϕ_{-1}	ϕ_0	ϕ_1	ϕ_2	ϕ_{-1}	ϕ_0	ϕ_1	ϕ_2
0.2956	1	9	6	0	0	0	4	0
0.2957	0	9	7	0	0	2	2	0
-0.4401	0	10	6	0	0	1	3	0
0.5067	0	11	5	0	0	0	4	0

Finally, for $L = 10$ the lowest eigenenergy is ≈ 28.4570, with

	Comp. A				Comp. B			
Ampl.	ϕ_{-1}	ϕ_0	ϕ_1	ϕ_2	ϕ_{-1}	ϕ_0	ϕ_1	ϕ_2
-0.2882	0	6	10	0	0	4	0	0
-0.2882	0	10	6	0	0	0	4	0
0.3625	0	7	9	0	0	3	1	0
0.3625	0	9	7	0	0	1	3	0
-0.3784	0	8	8	0	0	2	2	0

Chapter 6

Conclusions and Outlook

The problems that I have investigated in my thesis are all related with the behavior of bosonic atoms which are confined in a ring potential, at zero temperature. Furthermore, one of the main questions that I have posed is the effect of a finite atom number, where the usual mean-field approximation is expected to either fail (to some extent), or at least not provide a very accurate description of the system. According to the results of my thesis such ”small" systems have a lot of novel and interesting physics.

The method that I have used to overcome this difficulty is the diagonalization of the many-body Hamiltonian. Within this approach the many-body state is not assumed to have a product form, and thus it allows for correlations between the atoms to develop, which are expected to be enhanced in the limit of a small atom number.

At zero temperature the atoms form a Bose-Einstein condensate, where in the absence of interactions all of them occupy the lowest-energy state of the ring potential. While the non-interacting problem is trivial, the interesting and non-trivial question is the effect of interactions.

6.1 Project 1

In the first project that I have analyzed in Chap. 3 , I studied the phenomenon of hysteresis in a rotating Bose-Einstein condensate that is confined in a ring potential, as well the stability of persistent currents in this system.

Based on trivial arguments one may see that the dispersion relation in the absence of interactions consists of straight lines with different slopes. In this case no hysteresis effects are present, nor stable persistent currents are possible. Both effects show up due to the assumed repulsive interatomic interactions, which give a negative curvature to these straight lines. The crucial quantity that appears in both effects is the slope of the dispersion relation as the angular momentum tends to zero. Both the critical rotational frequencies, which appear in the problem of hysteresis, as well the critical value for stability of persistent currents may be linked to this slope, as Bloch’s theorem implies.

The results that I have derived within the mean-field approximation and the diagonalization of the Hamiltonian agree and provide a unified description of the system, all the way from the limit of small atom numbers, up to the thermodynamic limit of large atom numbers. From the fitting I have done, I have also extracted the corrections of the critical frequencies due to the finiteness of the atom number.

The second question that I have investigated within this project is the stability of persistent currents in a ring with a finite number of atoms. While the critical coupling has been evaluated with use of the mean-field approximation, my study was the one which provided the corrections on the critical coupling due to the finite number of atoms. Again, to do that, I used the method of diagonalization of the Hamiltonian, and I focused on the slope of the dispersion relation as the angular momentum tends to zero.

The fitting that I performed gave an asymptotic value for the critical coupling which agrees with the one derived from the mean-field approximation. In addition, the finiteness of the atom number works against the stability of the currents, forcing it to have a higher value than its asymptotic, mean-field, value.

Finally, an implicit assumption that is made in the arguments for the stability of the persistent currents is that the matrix element of any single-particle operator that connects the current-carrying state with the non-rotating state is suppressed. To confirm this I introduced a delta-function single-particle operator and evaluated this matrix element, thus demonstrating that indeed it decays rapidly with increasing atom number. Again, I saw that decreasing the atom number works against the stability of the persistent currents.

6.2 Project 2

The second project that I worked on is described in Chap. 4 of my thesis. Under the conditions that the mean-field approximation is valid (which is basically the diluteness condition, in combination with the condition of a large atom number), the system is very well described by the Gross-Pitaevskii equation, which is a nonlinear Schrödinger equation.

In the absence of an external potential this nonlinear equation supports travelling, solitary-wave solutions (which are given by Jacobi elliptic functions for the periodic boundary conditions imposed by the ring geometry).

A natural question that arises is whether these solutions persist in the case of a system of a small atom number. As mentioned also above the mean-field approximation itself becomes questionable in this limit, and so does the validity of these solutions.

In order to attack this problem a crucial observation is that the mathematical problem of solitary-wave solutions is equivalent to the minimization of the energy of the system for some fixed value of the angular momentum (see Chap. 2).

Thus, in the limit of small atom numbers, I have used the method of diagonalization of the Hamiltonian in order to evaluate the state of the system for some value of the angular momentum. Still, this is an eigenstate of the Hamiltonian, which has axial symmetry. To overcome this difficulty, I had to consider a linear superposition of these eigenstates with amplitudes which are taken from the mean-field solutions.

The resulting many-body state is thus a state that breaks the rotational invariance (as the mean-field solutions). Furthermore, by construction has an energy which lower that the mean-field. As I have demonstrated this correction is to sub-leading order in the number of atoms.

In addition to the fact that I have constructed a many-body state of lower energy than the mean-field solution, the arguments that I have developed in this project are of more general value. The question of spontaneous symmetry breaking is of great importance and my study provides insight into it. Furthermore, the method that I have introduced is of more general importance, since it may be used in other similar problems which are related with the breaking of the symmetry of the Hamiltonian.

6.3 Project 3

The third and last project of my thesis is described in Chap. 5. There I have investigated the effect of a second component. Quite generally, the problem of mixtures is interesting, since the extra degrees of freedom due to the second component introduce novel effects.

One of the main results of this project is that under rather typical conditions the dispersion relation develops a regularity which goes way beyond the one imposed by the periodic boundary conditions, i.e., by Bloch's theorem.

Furthermore, despite the complexity of this problem the dispersion relation shows a remarkable simplicity. The main reason for this is that at an "initial" interval the angular momentum is not shared by the two components, but rather it is carried by the minority component.

The above results are valid both within the mean-field approximation, as well as within the diagonalization of the Hamiltonian, for a low atom number. The combination of these two approaches provides a complete description of the system, starting from the limit of very small systems (in the atom number), and extending all the way up to (realistically) large numbers.

Furthermore, the derived dispersion relation has a very rich structure, with a correspondingly rich collection of consequences on physical observables. First of all, the local minima which form under certain conditions correspond to persistent currents. These are highly sensitive to the populations of the two components and have a remarkable dependence on elementary number theory. The states of lowest energy for some fixed value of the angular momentum correspond to "vector solitons", i.e., bound states of solitons in the two components. Finally, the slope of the dispersion relation corresponds to the velocity of propagation of these solitons, which has also an interesting structure.

6.4 Some last, more general, thoughts

In this interesting field, which has been expanding with an impressive rate in roughly the last three decades, one of its more recent ambitious goals is the realization of correlated, non-mean-field states. Various different directions have been followed in order to achieve this goal.

For example, experimentalists have tried to reach the limit of rapid rotation in a harmonically-trapped Bose-Einstein condensate and realize the so-called (correlated) bosonic Laughlin state. Another possibility is the increase of the scattering length, in order to violate the diluteness condition. Also, interesting experiments have been

performed in optical lattices, i.e., periodic potentials, where tuning the lattice constant, the interatomic interaction, or the lattice depth leads to non-mean-field states and to interesting quantum phase transitions. Tuning the effective dimensionality of these gases has also attracted a lot of attention, where quasi-one-dimensional, as well as quasi-two-dimensional confining potentials give rise to novel phases.

My own studies, presented in my thesis, contribute to the above variety of possible correlated states, where decreasing the atom number introduces correlations in the many-body state of the atoms which go beyond the mean-field approximation. While the experimental realization of such states may be tricky (due to the low signal resulting from the low atom number), still this possibility is within current experimental reach and certainly it will become even easier in the following years. Therefore, the results presented here are not only valuable from a theoretical point of view, but also are of experimental relevance.

Bibliography

[1] A. Einstein, Sitzungsberichte der Preussischen Akademie der Wissenschaften, Physikalisch-mathematische Klasse p. 261 (1924), p. 3 (1925)

[2] S. N. Bose, Zeitschrift für Physik **26**, 178 (1924)

[3] *Bose-Einstein Condensation*, ed. A. Griffin, D. W. Snoke, and S. Stringari (Cambridge University Press, Cambridge) (1995)

[4] *Bose-Einstein Condensation*, ed. L. Pitaevskii, and S. Stringari (Oxford Science Publications) (2003)

[5] *Bose-Einstein Condensation in Dilute Gases*, ed. C. J. Pethick, and H. Smith (Cambridge University Press) (2008)

[6] A. J. Leggett, Rev. Mod. Phys. **73**, 307 (2001)

[7] Lucy Walton, "States of Matter Liquids and Solids Changes of State", *https://slideplayer.com/slide/7865297/*

[8] H. Kamerlingh Onnes, KNAW, Proceedings **11**, 168, Amsterdam (1909)

[9] P. Kapitza, Nature **141**, 74 (1938)

[10] J.F. Allen and A.D. Misener, Nature **141**, 75 (1938)

[11] Balibar, Sébastien, Journal of Low Temperature Physics **146**, 441 (2007)

[12] F. London, Nature **141**, 643 (1938); Phys. Rev. **54**, 947 (1938)

[13] Dirk van Delft and Peter Kes, Physics Today **63**, 38 (September 2010)

[14] H. Kamerlingh Onnes, Comm. Phys. Lab. Univ. Leiden, No. **120b, 122b, 124c** (1911)

[15] J. G. Bednorz and K. A. Müller, Zeitschrift für Physik B **64**, 189 (1986)

[16] G. Baym, C. J. Pethick, and D. Pines, Nature **224**, 673 (1969)

[17] A. Bohr, and B. R. Mottelson, World Scientific, Nuclear Structure, Vol. **I** & **II** (1975)

[18] A. J. Leggett, Rev. Mod. Phys. **47**, 331 (1975)

[19] P. Noziéres and D. Pines, *The Theory of Quantum Liquids*, Vol. **II** (Addison-Wesley, Reading, Mass., 1990)

[20] A. J. Leggett, *Quantum liquids: Bose condensation and Cooper pairing in condensed-matter systems* (Oxford University Press, Oxford) (2006)

[21] David Snoke and G. M. Kavoulakis, Rep. Prog. Phys. **77**, 116501 (2014)

[22] K. v. Klitzing, G. Dorda and M. Pepper, Phys. Rev. Lett. **45**, 494 (1980)

[23] J. M. Kosterlitz and D. J. Thouless, Journal of Physics C: Solid State Physics **6**, 1181 (1973)

[24] Z. Hadzibabic, P. Krüger, M. Cheneau, B. Battelier, J. Dalibard, Nature **41**, 1118 (2006)

[25] M.H. Anderson, J.R. Ensher, M.R. Matthews, C.E. Wieman and E.A. Cornell, Science, **269**, 5221, 198 (1995)

[26] K. B. Davis, M. -O. Mewes, M. R. Andrews, N. J. van Druten, D. S. Durfee, D. M. Kurn, and W. Ketterle, Phys. Rev. Lett. **75**, 3969 (1995)

[27] C. C. Bradley, C. A. Sackett, J. J. Tollett, and R. G. Hulet, Phys. Rev. Lett. **75**, 1687 (1995)

[28] E. Cornell, W. Ketterle, and C. Weiman, Nobel Lectures, Rev. Mod. Phys. **74** (2002)

[29] W. D. Phillips and H. J. Metcalf, Scientific American **36** (1987)

[30] C. N. Cohen-Tannoudji and W. D. Phillips, Physics Today **33** (1990)

[31] S. Chu, Scientific American **33** (1992)

[32] A. Aspect and J. Dalibard, La Recherche **30** (1994)

[33] AN. Wenz, G. Zürn, S. Murmann, I. Brouzos, T. Lompe, S. Jochim, Science **342**, 457 (2013)

[34] A. Roussou, G. D. Tsibidis, J. Smyrnakis, M. Magiropoulos, Nikolaos K. Efremidis, A. D. Jackson, G. M. Kavoulakis, Phys. Rev. A **91**, 023613 (2015)

[35] S. Eckel, J. G. Lee, F. Jendrzejewski, N. Murray, C. W. Clark, C. J. Lobb, W. D. Phillips, M. Edwards, and G. K. Campbell, Nature **506**, 200 (London 2014)

[36] A. Roussou, J. Smyrnakis, M. Magiropoulos, Nikolaos K. Efremidis, G. M. Kavoulakis, Phys. Rev. A **95**, 033606 (2017)

[37] E. P. Gross, Nuovo Cimento **20**, 454 (1961)

[38] L. P. Pitaevskii, Zh. Eksp. Teor. Fiz. **40**, 646 (1961) [Sov. Phys. JETP **13**, 451 (1961)]

[39] A. Roussou, J. Smyrnakis, M. Magiropoulos, Nikolaos K. Efremidis, G. M. Kavoulakis, P. Sandin, M. Ögren, M. Gulliksson, New J. Phys. **20**, 045006 (2018)

[40] O. Penrose and L. Onsager, Phys. Rev. **104**, 576 (1956)

[41] Wolfgang Ketterle and N. J. van Druten, Phys. Rev. A **54**, 656 (1996)

[42] V. Bagnato and D. Kleppner, Phys. Rev. A **44**, 7439 (1991)

[43] A. Görlitz, J. M. Vogels, A. E. Leanhardt, C. Raman, T. L. Gustavson, J. R. Abo-Shaeer, A. P. Chikkatur, S. Gupta, S. Inouye, T. Rosenband, and W. Ketterle, Phys. Rev. Lett. **87**, 130402 (2001)

[44] L. D. Carr, C. W. Clark, and W. P. Reinhardt, Phys. Rev. A **62**, 063610 (2000)

[45] J. Smyrnakis, M. Magiropoulos, G. M. Kavoulakis, and A. D. Jackson, Phys. Rev. A **82**, 023604 (2010)

[46] A. D. Jackson and G. M. Kavoulakis, Phys. Rev. Lett. **89**, 070403 (2002)

[47] T. Tsuzuki, J. Low Temp. Phys. **4**, 441 (1971)

[48] V. E. Zakharov and A. B. Shabat, Zh. Eksp. Teor. Fiz. **64**, 1627 (1973) [Sov. Phys. JETP **37**, 823 (1973)]

[49] F. Bloch, Phys. Rev. A **7**, 2187 (1973)

[50] A. D. Jackson, J. Smyrnakis, M. Magiropoulos, G. M. Kavoulakis, Europhys. Lett. **95**, 30002 (2011)

[51] J. Smyrnakis, S. Bargi, G. M. Kavoulakis, M. Magiropoulos, K. Kärkkäinen, and S. M. Reimann, Phys. Rev. Lett. **103**, 100404 (2009)

[52] J. Smyrnakis, M. Magiropoulos, G. M. Kavoulakis, and A. D. Jackson, Phys. Rev. A **87**, 013603 (2013)

[53] Erich J. Mueller, Phys. Rev. A **66**, 063603 (2002)

[54] G. M. Kavoulakis, Y. Yu, M. Ögren, and S. M. Reimann, Europhys. Lett. **76**, 215 (2006)

[55] R. Kanamoto, L. D. Carr, and M. Ueda, Phys. Rev. A **79**, 063616 (2009)

[56] R. Kanamoto, L. D. Carr, and M. Ueda, Phys. Rev. A **81**, 023625 (2010)

[57] S. Baharian and G. Baym, Phys. Rev. A **87**, 013619 (2013)

[58] S. Gupta, K. W. Murch, K. L. Moore, T. P. Purdy, and D. M. Stamper-Kurn, Phys. Rev. Lett. **95**, 143201 (2005)

[59] S. E. Olson, M. L. Terraciano, M. Bashkansky, and F. K. Fatemi, Phys. Rev. A **76**, 061404(R) (2007)

[60] C. Ryu, M. F. Andersen, P. Cladé, V. Natarajan, K. Helmerson, and W. D. Phillips, Phys. Rev. Lett. **99**, 260401 (2007)

[61] B. E. Sherlock, M. Gildemeister, E. Owen, E. Nugent, and C. J. Foot, Phys. Rev. A **83**, 043408 (2011)

[62] A. Ramanathan, K. C. Wright, S. R. Muniz, M. Zelan, W. T. Hill, C. J. Lobb, K. Helmerson, W. D. Phillips, and G. K. Campbell, Phys. Rev. Lett. **106**, 130401 (2011)

[63] S. Moulder, S. Beattie, R. P. Smith, N. Tammuz, and Z. Hadzibabic, Phys. Rev. A **86**, 013629 (2012)

[64] C. Ryu, K. C. Henderson and M. G. Boshier, New J. Phys. **16**, 013046 (2014)

[65] S. Beattie, S.Moulder, R. J. Fletcher, and Z. Hadzibabic, Phys. Rev. Lett. **110**, 025301 (2013)

[66] A. I. Yakimenko, S. I. Vilchinskii, Y. M. Bidasyuk, Y. I. Kuriatnikov, K. O. Isaieva, and M. Weyrauch, e-print arXiv:1411.3490

[67] G. M. Kavoulakis, B. Mottelson, and C. J. Pethick, Phys. Rev. A **62**, 063605 (2000)

[68] M. Ögren and G. M. Kavoulakis, J. Low Temp. Phys. **149**, 176 (2007)

[69] A. D. Jackson, J. Smyrnakis, M. Magiropoulos, and G. M. Kavoulakis, Europh. Lett. **95**, 30002 (2011)

[70] P. Navez, S. Pandey, H. Mas, K. Poulios, T. Fernholz, and W. von Klitzing, New Journal of Phys. **18**, 075014 (2016)

[71] A. C. Scott, F. Y. F. Chu, and D. W. McLaughlin, Proc. IEEE **61**, 1443 (1973)

[72] R. Rajaraman, *Solitons and Instantons* (North-Holland, Amsterdam, 1987)

[73] V. E. Zakharov and A. B. Shabat, Zh. Eksp. Teor. Fiz. **64**, 1627 (1973) [Sov. Phys. JETP **37**, 823 (1973)]

[74] A. D. Jackson, G. M. Kavoulakis, and C. J. Pethick, Phys. Rev. A, **58**, 2417 (1998)

[75] Constantine Yannouleas and Uzi Landman, Rep. Prog. Phys. 2067, **70** (2007)

[76] Constantine Yannouleas and Uzi Landman, Phys. Rev. B **84**, 165327 (2011)

[77] A. N. Wenz, G. Zürn, S. Murmann, I. Brouzos, T. Lompe, and S. Jochim, Science **342**, 457 (2013)

[78] Ugo Marzolino and Daniel Braun, Phys. Rev. A **88**, 063609 (2013)

[79] M. Wadati and M. Sakagami, J. Phys. Soc. Jpn. **53**, 1933 (1984)

[80] M. Wadati, A. Kuniba, and T. Konishi, J. Phys. Soc. Jpn. **54**, 1710 (1985)

[81] Jacek Dziarmaga, Zbyszek P. Karkuszewski, and Krzysztof Sacha, Phys. Rev. A **66**, 043615 (2002)

[82] Dominique Delande and Krzysztof Sacha, Phys. Rev. Lett. **112**, 040402 (2014)

[83] Andrzej Syrwid and Krzysztof Sacha, e-print ArXiv: 1505.06586

[84] Andrzej Syrwid, Mirosław Brewczyk, Mariusz Gajda, and Krzysztof Sacha, e-print: ArXiv: 1605.08211

[85] M. D. Girardeau and E. M. Wright, Phys. Rev. Lett. **84**, 5691 (2000)

[86] Jun Sato, Rina Kanamoto, Eriko Kaminishi, and Tetsuo Deguchi, Phys. Rev. Lett. **108**, 110401 (2012)

[87] Jun Sato, Rina Kanamoto, Eriko Kaminishi, and Tetsuo Deguchi, e-print ArXiv: 1602.08329

[88] A. D. Jackson, G. M. Kavoulakis, B. Mottelson, and S. M. Reimann, Phys. Rev. Lett. **86**, 945 (2001)

[89] J. C. Cremon, A. D. Jackson, E. Ö. Karabulut, G. M. Kavoulakis, B. R. Mottelson, and S. M. Reimann, Phys. Rev. A **91**, 033623 (2015)

[90] H. Saarikoski, S. M. Reimann, A. Harju, and M. Manninen Rev. Mod. Phys. **82**, 2785 (2010)

[91] Igor Romanovsky, Constantine Yannouleas, Leslie O. Baksmaty, and Uzi Landman, Phys. Rev. Lett. **97**, 090401 (2006)

[92] Eugene B. Kolomeisky, T. J. Newman, Joseph P. Straley, and Xiaoya Qi, Phys. Rev. Lett. **85**, 1146 (2000)

[93] A. J. Leggett, Rev. Mod. Phys. **71**, S318 (1998)

[94] P. Sandin, M. Ögren, M. Gulliksson, J. Smyrnakis, M. Magiropoulos, and G. M. Kavoulakis, Phys. Rev. E **95**, 012142 (2017)

[95] J. Smyrnakis, M. Magiropoulos, A. D. Jackson, and G. M. Kavoulakis, J. Phys. B: At. Mol. Opt. Phys. **45**, 235302 (2012)

[96] K. Anoshkin, Z. Wu, and E. Zaremba, Phys. Rev. A **88**, 013609 (2013)

[97] A. I. Yakimenko, K. O. Isaieva, S. I. Vilchinskii, and M. Weyrauch, Phys. Rev. A **88**, 051602(R) (2013)

[98] Zhigang Wu and Eugene Zaremba, Phys. Rev. A **88**, 063640 (2013)

[99] J. Smyrnakis, M. Magiropoulos, Nikolaos K. Efremidis, and G. M. Kavoulakis, J. Phys. B: At. Mol. Opt. Phys. **47**, 215302 (2014)

[100] M. Abad, A. Sartori, S. Finazzi, and A. Recati, Phys. Rev. A **89**, 053602 (2014)

[101] Z. Wu, E. Zaremba, J. Smyrnakis, M. Magiropoulos, Nikolaos K. Efremidis, G. M. Kavoulakis, Phys. Rev. A **92**, 033630 (2015)

[102] P. Sandin, M. Ögren, and M. Gulliksson, Phys. Rev. E **93**, 033301 (2016)

[103] E. H. Lieb and W. Liniger, Phys. Rev. **130**, 1605 (1963)

[104] E. H. Lieb, Phys. Rev. **130**, 1616 (1963)

[105] S. J. Gu, Y. Q. Li, and Z. J. Ying, J. Phys. A **34**, 8995 (2001)

[106] Y. Q. Li, S. J. Gu, Z. J. Ying, and U. Eckern, Europhys. Lett. **61**, 368 (2003)

[107] J. N. Fuchs, D. M. Gangardt, T. Keilmann, and G. V. Shlyapnikov, Phys. Rev. Lett. **95**, 150402 (2005)

[108] N. Oelkers, M. T. Batchelor, M. Bortz, and X.-W. Guan, J. Phys. A **39**, 1073 (2006)

[109] M. T. Batchelor, M. Bortz, X. W. Guan, and N. Oelkers, J. Stat. Mech. (2006) P03016

[110] X.-W. Guan, M. T. Batchelor, and M. Takahashi, Phys. Rev. A **76**, 043617 (2007)

[111] Yajiang Hao, Yunbo Zhang, Xi-Wen Guan, and Shu Chen, Phys. Rev. A **79**, 033607 (2009)

6.5 Publications

1. A. Roussou, G. D. Tsibidis, J. Smyrnakis, M. Magiropoulos, Nikolaos K. Efremidis, A. D. Jackson, G. M. Kavoulakis, Phys. Rev. A **91**, 023613 (2015)
2. A. Roussou, J. Smyrnakis, M. Magiropoulos, Nikolaos K. Efremidis, G. M. Kavoulakis, Phys. Rev. A **95**, 033606 (2017)
3. A. Roussou, J. Smyrnakis, M. Magiropoulos, Nikolaos K. Efremidis, G. M. Kavoulakis, P. Sandin, M. Ögren, M. Gulliksson, New J. Phys. **20**, 045006 (2018)
4. A. Roussou, J. Smyrnakis, M. Magiropoulos, N. K. Efremidis, W. von Klitzing, G. M. Kavoulakis, arXiv:1810.07609